A STUDY OF SOME CHARACTERISTICS OF ATMOSPHERIC REFRACTIVE INDEX DIFFERENCES

by

J. L. Dodd
A. W. Straiton
A. P. Deam

ANTENNAS AND PROPAGATION DIVISION
ELECTRICAL ENGINEERING RESEARCH LABORATORY
THE UNIVERSITY OF TEXAS
Austin, Texas

Report No. P-15
15 May 1967

Prepared Under
NASA Grant NGR 44-012-048

A STUDY OF SOME CHARACTERISTICS OF ATMOSPHERIC REFRACTIVE INDEX DIFFERENCES

by

J. L. Dodd
A. W. Straiton
A. P. Deam

ANTENNAS AND PROPAGATION DIVISION
ELECTRICAL ENGINEERING RESEARCH LABORATORY
THE UNIVERSITY OF TEXAS
Austin, Texas

Report No. P-15

15 May 1967

Prepared Under

NASA Grant NGR 44-012-048

PREFACE

This is the third technical report prepared under NASA Grant NGR 44-012-048. The first report was

> "Estimating Refractive Index Spectra in Regions of Clear Air Turbulence," J. J. Stephens and E. R. Reiter, Report No. P-12, Antennas and Propagation Division, Electrical Engineering Research Laboratory, The University of Texas, Austin, Texas, 5 October 1966.

The second was

> "Remote Detection of Clear Air Turbulence: Part I - Pulsed Microwave Radars," B. M. Fannin, Report No. P-13, Antennas and Propagation Division, Electrical Engineering Research Laboratory, The University of Texas, 1 November, 1966.

Under this grant, a study of low frequency refractive index variations was made at a height of 80 meters. The understanding of the physical processes that contribute to the low altitude variations of refractive index should be very helpful in clarifying the properties of the refractive index anomalies present at higher elevations where regions of clear air turbulence are encountered.

This report is the Dissertation submitted to the Graduate School of The University of Texas by J. L. Dodd in partial fulfillment of the requirements for the Ph. D. degree.

A. W. Straiton
Principal Investigator

ABSTRACT

Atmospheric refractive index differences were measured during the summer and fall of 1966 at The University of Texas Electrical Engineering Research Laboratory. These measurements were analyzed for spectra content and amplitude distributions by using an SDS-930 digital computer.

Variations of refractive index at a single point were also measured. The ratio of refractive index difference spectra to spectra at a single point was calculated. This ratio which is the filter function of the difference output of two refractometers was examined.

Two models for the refractive index filter function were proposed. The first model assumes a frozen structure of the atmosphere moving with a constant wind. This model is of the form $4 \sin^2(\pi fr/v)$, where r is the refractometer spacing in meters, v is the wind speed in meters/second, and f is the frequency in Hz. The second proposed filter function model assumes a well mixed atmosphere with a variable wind. The form for the second model is $2(1 - \sin(2\pi fr/v)/2\pi fr/v)$ where the parameters are the same as in the first model.

Amplitude distibutions were plotted on Gaussian probability paper and from these plots, along with observation of original difference data, an empirical probability density function is proposed. This proposed probability density function is the sum of three Gaussian functions. One of the Gaussian functions has a zero mean whereas the two other Gaussian functions have mean values of $\pm a$. The variance of the function with zero mean is about one-tenth that of the other two functions.

Refractive index structure function, $D_n(r)$, is defined as

$$D_n(r) = \overline{[n(r) - n(o)]^2},$$

where n(r) is the index of refraction at point r and n(o) is the index of refraction at the reference point o. The overbar denotes time average.

Measurements of refractive index difference suggest a duality in the mechanism causing the fluctuation of these data. The original difference data show spikes superimposed on a continuum of variations. These spikes are present but obscured in single unit refractive index data.

Examination of amplitude probability distribution indicates one set of characteristics between approximately 5% and 95% points and another set of characteristics outside of these limits. The spikes make a major contribution to the structure function for separations below four meters.

Some characteristics of refractive index difference data were noted by observing paper strip chart recordings of the original data. Single unit refractive index changes tend to vary predominantly in the direction of increasing index. This indicates an enhancement of water vapor content in the atmosphere since the refractive index changes are influenced more by water vapor changes than by temperature changes.

TABLE OF CONTENTS

LIST OF FIGURES

List of Figures (cont'd.)

List of Figures (cont'd.)

LIST OF TABLES

I. INTRODUCTION

A. General

The purpose of this investigation is to study some of the characteristics of atmospheric refractive index differences. Much effort has been expended in studying the variations of refractive index at a single point in the atmosphere. The longer wavelength variations which tend to obscure the characteristics of the fine scale variations may be filtered out by measuring differences in refractive index rather than the index variation itself.

Refractive index difference measurements were made over a period of three months starting in September, 1966. Most of the measurements were made during the daylight hours of 1000 to 1600 hours. In addition to the three refractive index differences, measurements of wind speed, azimuth angle, and elevation angle were also taken. Measurements of refractivity at a single point were also taken for comparison with the difference measurements.

B. Background

It is the purpose of this section to describe some fundamentals of atmospheric index of refraction. The discussion will be limited to the non-ionized portion of the atmosphere.

The refractive index of any material is made up of a real and an imaginary part. The real part determines the phase velocity of an

electromagnetic wave and the imaginary part determines the attenuation of the electromagnetic energy.

Under the assumption that conduction currents may be neglected, the atmosphere can be considered a lossless dielectric for all wavelengths longer than 3 cm. The atmosphere is essentially a non-magnetic medium and its permeability relative to a vacuum is very nearly unity. Its refractive index n may be related to its dielectric constant K (relative to a vacuum) as

$$n^2 = K. \tag{1-1}$$

Molecules of matter located in an electric field acquire an electric moment by the deformation of the system of charges which they contain. This deformation causes an internal field which is superimposed on the initial field. This process is called polarization.

Debye (1929) calculated the internal field and showed that the polarization of a medium can be related to the relative dielectric and to refractive index as

$$\frac{K-1}{K+2} = \frac{n^2-1}{n^2+2} = \frac{4\pi}{3}\frac{A\rho}{M}\left(\alpha_o + \frac{\mu^2}{3kT}\right), \tag{1-2}$$

where K is the dielectric constant in cgs units, ρ is the density in g/cc, M is the weight of a gram-mole in g, A is Avogrado's number ($A = 6.061 \times 10^{23}$), α_o the polarization factor, μ the permanent electric moment in cgs units, k is Boltzman's constant ($k = 1.372 \times 10^{-16}$ erg/deg.), and T is the absolute temperature in degrees Kelvin.

In air K has a value very near unity, and eq. (1-2) becomes

$$K - 1 \cong \frac{4\pi A\rho}{M}\left(a_o + \frac{\mu^2}{3kT}\right). \tag{1-3}$$

The ratio $\frac{\rho}{M}$ can be expressed as

$$\frac{\rho}{M} = \frac{p}{RT} \tag{1-4}$$

where p is the pressure in dyne/cm^2 and R is the molecular constant ($R = 8.314 \times 10^7$ erg/deg.).

In terms of index of refraction, the relative dielectric constant can be expressed as

$$K - 1 = n^2 - 1 = (n+1)(n-1) \cong 2(n-1). \tag{1-5}$$

Substituting (1-4) and (1-5) into (1-3) and solving for (n - 1) as

$$n - 1 = \frac{2\pi A p}{RT}\left(a_o + \frac{\mu^2}{3kT}\right). \tag{1-6}$$

Equation (1-6) may be written in the form (Du Castel, 1966, p. 57)

$$n - 1 = \frac{1}{2}\left[\frac{B}{T}(p - e) + \frac{C}{T}e\right] \tag{1-7}$$

where (p - e) is the partial pressure of dry air in mb, T is the temperature in °K, and e is the water vapor pressure in mb.

From a review of the experimental determinations by a number of groups, Smith and Weintraub (1960) have given

$$\left.\begin{aligned} B &= 155.2 \times 10^{-6} \text{ deg K/mb} \\ C &= 133.2 \times 10^{-6}\,(1 + 5582/T) \text{ deg K/mb,} \end{aligned}\right\} \tag{1-8}$$

where T is in °K.

Refractive index of the atmosphere differs from unity by only a few hundred parts per million. The change in index of refraction from units multiplied by 10^6 is called refractivity N and expressed as

$$N = (n - 1) \times 10^6. \tag{1-9}$$

Using the values of B and C from eq. (1-8), eq. (1-7) can be expressed as

$$N = \frac{77.6}{T}(p + 4810\, e/T), \tag{1-10}$$

where p is the pressure in millibars, e is the water vapor pressure in millibars, and T is the temperature in degrees Kelvin. The term containing e/T has been neglected since it is very small compared to the term containing e/T^2 for conditions normally encountered in the lower atmosphere.

This expression for refractivity is valid for all wavelengths greater than 3.0 cm. The phenomenon of absorption influences refractivity for shorter wavelengths (Du Castel, 1966, p. 20).

Refractive index varies with height because temperature and pressure change with height. Water vapor pressure also varies with height but not in a systematic manner such as the variations of temperature and pressure. The mean variation of index of refraction with height is given approximately by various models.

The Comite' Consultatif Internation des Radiocommunication (CCIR), 10th Plenary Assemble, Geneva, 1963, in Recommendation No. 369 suggests an exponentially varying model as

$$N = 289 \exp(0.136h), \tag{1-11}$$

where h is the height above sea level in kilometers.

This committee also suggests a linearly varying refractivity for the first 3.0 km of the atmosphere as

$$N = 289 - 39h, \tag{1-12}$$

where the units are the same as in eq. (1-11).

Superimposed on the mean variations of index of refraction with height are variations with time and distances. These variations primarily result from changes in water vapor density and temperature.

This study is concerned with changes in refractive index at a fixed height. The changes in refractive index with changes in temperature and water vapor pressure will now be considered.

Refractive index can be expressed as functions of pressure, temperature, and water vapor pressure as

$$N = N(p, T, e) = \frac{77.6}{T}(p + 4810\, e/T), \tag{1-13}$$

where the units are the same as for eq. (1-10).

The change in refractivity can be expressed as

$$dN = \frac{\partial N}{\partial p}\, dp + \frac{\partial N}{\partial T}\, dT + \frac{\partial N}{\partial e}\, de. \tag{1-14}$$

For constant height, the variations in p are very small and therefore the term containing dp can be neglected. Equation (1-14) then becomes

$$dN = \frac{\partial N}{\partial T}\, dT + \frac{\partial N}{\partial e}\, de. \tag{1-15}$$

Variations in refractivity due only to changes in temperature can be determined by taking the partial derivative of eq. (1-13) with respect to T.

$$\begin{aligned}\frac{\partial N}{\partial T} &= \frac{\partial}{\partial T}\left(\frac{77.6}{T}\left(p + \frac{4810\,e}{T}\right)\right) \\ &= -\frac{77.6}{T^2}\left(p + \frac{4810\,e}{T}\right) - \frac{2 \times 77.6 \times 4810\,e}{T^3} \\ &= -\frac{1}{T}\left[\frac{77.6}{T}\left(p + \frac{4810\,e}{T}\right) + \frac{7.46 \times 10^5 e}{T^2}\right] \\ &= -\frac{1}{T}\left[N + \frac{7.46 \times 10^5 e}{T^2}\right].\end{aligned} \tag{1-16}$$

Changes in refractivity caused by changes in water vapor pressure can be found by taking the partial derivative of eq. (1-13) with respect to e.

$$\begin{aligned}\frac{\partial N}{\partial e} &= \frac{\partial}{\partial e}\left(\frac{77.6}{T}\left(p + \frac{4810\,e}{T}\right)\right) \\ &= \frac{3.73 \times 10^5}{T^2}.\end{aligned} \tag{1-17}$$

Substituting eqs. (1-16) and (1-17) into eq. (1-15) variations in refractivity due to changes in both temperature and water vapor pressure can be determined as

$$dN = -\frac{1}{T}\left[N + \frac{7.46 \times 10^5 e}{T^2}\right] dT + \frac{3.73 \times 10^5}{T^2}\, de. \tag{1-18}$$

Equation (1-18) can also be expressed as incremental changes rather than as a total derivative.

$$\Delta N = -\frac{1}{T}\left[N + \frac{7.46 \times 10^5}{T^2}\right] \Delta T + \frac{3.73 \times 10^5}{T^2}\, \Delta e. \tag{1-19}$$

Using the following values of pressure, temperature, and water vapor pressure, changes in refractive index due to temperature and water vapor pressure changes were calculated.

$T = 300°K$

$p = 1000$ mb

$e = 17.9$ mb.

The value of 17.9 mb vapor pressure corresponds to a value of 50 per cent relative humidity for the given temperature.

Following are the calculations for a 1.0 unit change in N due to temperature variations alone and then calculations for a 1.0 unit change in N caused by water vapor pressure changes only.

$$N = \frac{77.6}{300}\left[1000 + \frac{4810 \times 17.9}{300}\right] = 332 \text{ N units.} \tag{1-20}$$

For $\Delta e = 0$,

$$\Delta N = \frac{\partial N}{\partial T}\Delta T, \tag{1-21}$$

or

$$\Delta T = \frac{\Delta N}{\left(\frac{\partial N}{\partial T}\right)} = \frac{\Delta N}{-\frac{1}{T}\left(N + \frac{7.46 \times 10^5 e}{T^2}\right)} = \frac{1}{\frac{1}{300}\left[332 + \frac{7.46 \times 10^5 \times 17.9}{300^2}\right]} \tag{1-22}$$

$$= -0.625 \text{ degree.}$$

For $\Delta T = 0$,

$$\Delta N = \frac{\partial N}{\partial e} \Delta e ,$$

or

$$\begin{aligned} \Delta e &= \frac{\Delta N}{(\frac{\partial N}{\partial e})} \\ &= \frac{\Delta N}{(\frac{3.73 \times 10^5}{T^2})} \\ &= \frac{1}{(\frac{3.73 \times 10^5}{300^2})} \\ &= 0.24 \text{ mb.} \end{aligned} \qquad (1\text{-}23)$$

For the given values of pressure, temperature, and water vapor pressure, a ± 1.0 N unit change in refractivity corresponds to approximately a $\pm 5/8$ degree change in temperature and a $\pm 1/4$ mb change in water vapor pressure.

Measurements of refractive index differences indicate incremental changes of refractivity that are caused by changes in temperature and water vapor pressure between the two measuring points.

In the next section advantages of refractive index difference measurements over single refractive index measurements will be discussed.

C. Previous Studies

Beginning in the early 1950's several groups undertook direct measurements of the radio refractive index of the atmosphere. Straiton (1964) has given a comprehensive review of the early history of refractometry and of various measuring techniques.

Lane (1964) reported on vertical, horizontal, and simultaneous vertical and horizontal differences for 0.1 to 1.0 meter spacings. These measurements were made using refractometers mounted on captive balloons. Measurements of peak refractive index variation and mean square refractive index variation were reported for different vertical and horizontal refractometer spacing.

Spectra of radio refractive index difference measurements were reported by Straiton, Deam, and Walker (1962). Measurements were made between ground level and 1500 meters by mounting refractometers on a small aircraft and on an 85 meter tower.

Measurements of refractive index and temperature by use of tethered balloons and aircraft were used to determine spectra of temperature, humidity, and refractive index (Gossard, 1960). In his paper, the refractive index spectra approached a "-5/3" power law at high wave numbers. The scattered fields as computed from intensity and scale size of refractive index as obtained from measured auto-covariance are unreliable. The mean square value of refractive index is greatly influenced by the power density in the lower frequencies, whereas the

scattered fields at microwave frequencies are affected by the power density at the higher frequencies.

Refractivity can be calculated from meteorological data or measured directly by use of refractometers. The slow response of humidity sensors limits the use of meteorological data to longer periods. The shape of spectra curves has been determined based on the mechanical energy aspects of temperature, humidity, and air pressure which can be regarded as conservative passive additives (Tatarski, 1961, p. 40). In general, most observers find that the refractive index spectra follow a "-5/3" power law as predicted in the inertial subrange by the universal equilibrium theory (Batchelor, 1953).

As pointed out by Straiton, Deam, and Walker (1962), the atmospheric refractive index variations do not have the properties of a statistically stationary process. Tatarski (1961, p. 9) suggests that in order to circumvent the problem of a time varying mean, one take the difference of a non-stationary random process at two points in time or space. The difference data will then have characteristics which are essentially those of stationary processes. (In the data presented in this study as difference functions, the mean value has been essentially reduced to zero).

Norton (1964) presents data that show the variance of refractivity as a function of sample length. In Fig. 1-1, spectra of long term refractive index variations are shown. Data is presented for

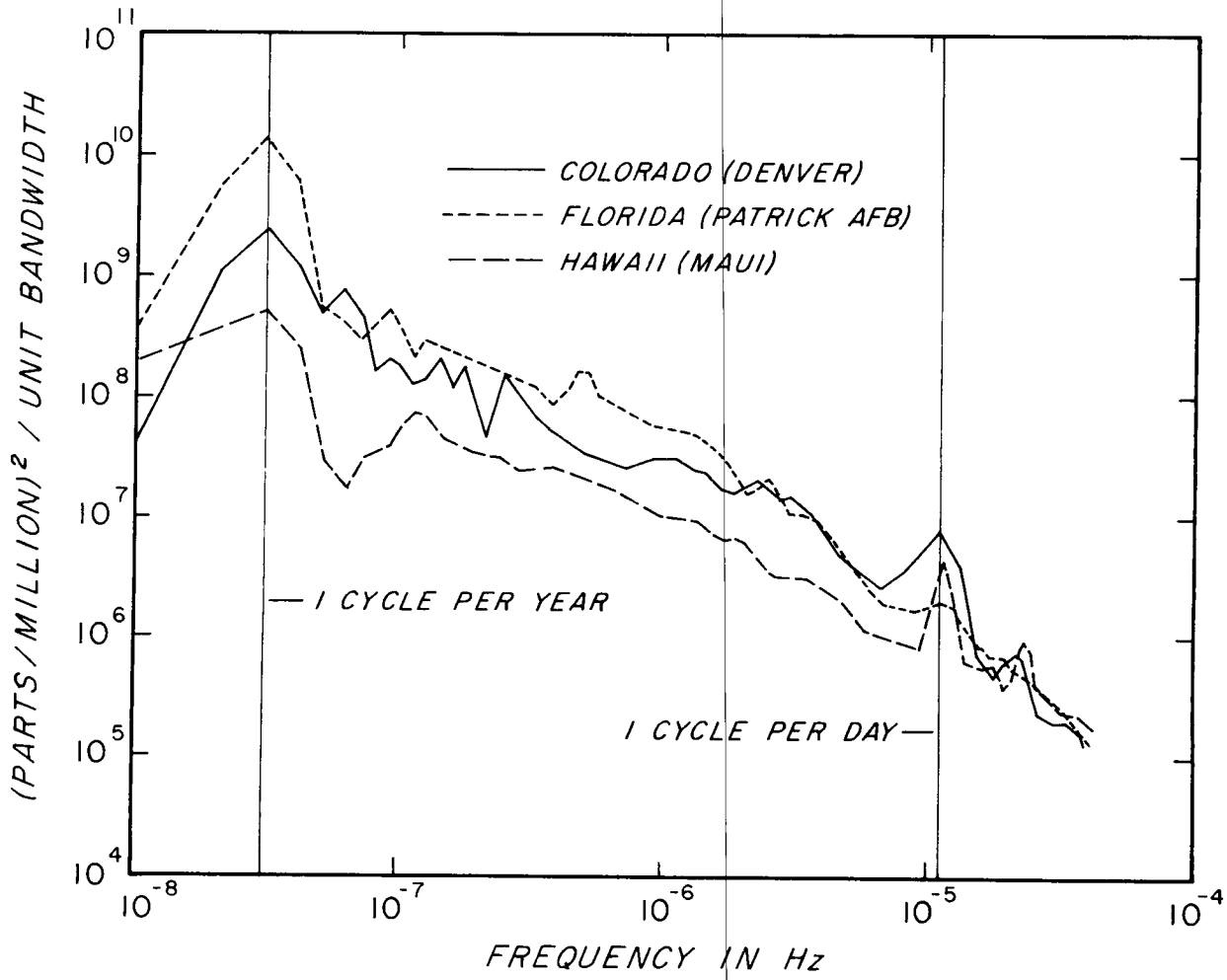

Figure 1-1. Power Spectra of Long Term Refractive Index Variations [Each Spectrum Based on Approximately 8 Years of U. S. Weather Bureau Data (from Norton, p. 1-174)]

frequencies with periods greater than one year. There are peaks in the spectra for daily and yearly periods. It is possible that the other peaks with periods longer than one year could correspond to effects caused by sunspot cycle activity, etc.

Spectra of eight years of meteorological data are shown in Fig. 1-2. Again the spectra show peaks for daily and yearly periods. The Cape Kennedy spectra show a peak for a period of approximately one lunar month. Peaks are not present in the Maui, Hawaii and Colorado data for this period.

Table 1-1 gives the standard deviation of surface refractivity, σ_{NST}, as a function of sample length, T. Figure 1-3 is plotted from data given in Table 1-1.

In order to get an estimate of how fast the standard deviation is changing, a rate of change per hour as a function of sample length is plotted in Fig. 1-4. As shown in this figure for a sample length of 24 hours, the standard deviation is changing at a rate of 0.5% per hour.

D. This Study

This investigation was made for the purpose of determining some of the characteristics of refractive index differences. In Section II the instrumentation used in making the refractive index difference measurements is presented with the main emphasis on the sampling cavity,

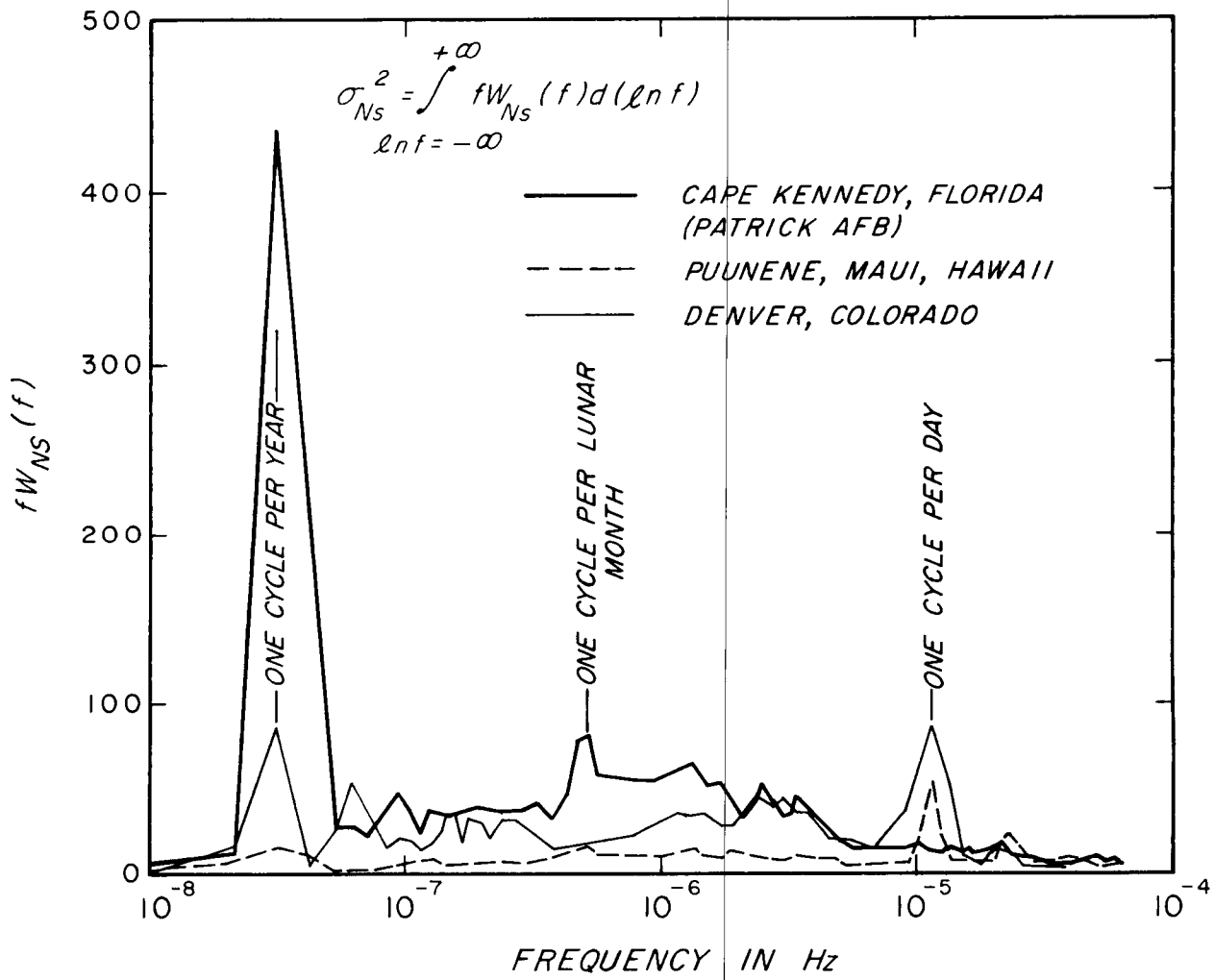

Figure 1-2. Approximately 8 Years of Weather Bureau Meteorological Data 1948-1956 (from Norton, p. 1-176)

Table 1-1

Standard Deviation σ_{NsT} of Surface Refractivity within Samples of Length T and Standard Deviations $\sigma_{\overline{Ns}}$ of the Mean Surface Refractivity for Samples of Length T

(From Norton, p. 1-155)

$$\sigma^2_{\overline{Ns}} = \sigma^2_{Ns} - \sigma^2_{NsT}$$

Sample Length, T			Puuene, Maui		Denver, Colorado		Cape Canaveral, Florida	
Hours	Days	Months	σ_{NsT}	$\sigma_{\overline{Ns}}$	σ_{NsT}	$\sigma_{\overline{Ns}}$	σ_{NsT}	$\sigma_{\overline{Ns}}$
4			4.34	8.91	4.16	13.78	4.71	21.59
8			4.92	8.60	5.99	13.09	5.70	21.35
16			5.84	8.11	7.71	12.16	6.66	21.07
32	1.33		6.32	7.63	8.65	11.51	7.98	20.61
64	2.67		6.90	7.11	9.61	10.72	9.64	19.88
128	5.33		7.47	6.51	10.50	9.84	11.15	19.07
256	10.66		7.96	5.90	11.26	8.97	12.80	18.00
512	21.33		8.24	5.50	11.82	8.21	14.01	17.08
1024		1.24	8.58	4.96	12.19	7.65	15.09	16.12
2048		2.8	8.75	4.65	12.78	6.62	16.34	14.86
4096		5.7	9.17	3.75	13.53	4.92	18.37	12.12
8192		11.4	9.44	3.01	14.30	1.65	21.46	5.19
16384		22.8	9.42	3.09	14.32	1.43	21.68	4.23
TOTAL: 8 Years σ_{Ns}			9.91		14.40		22.10	

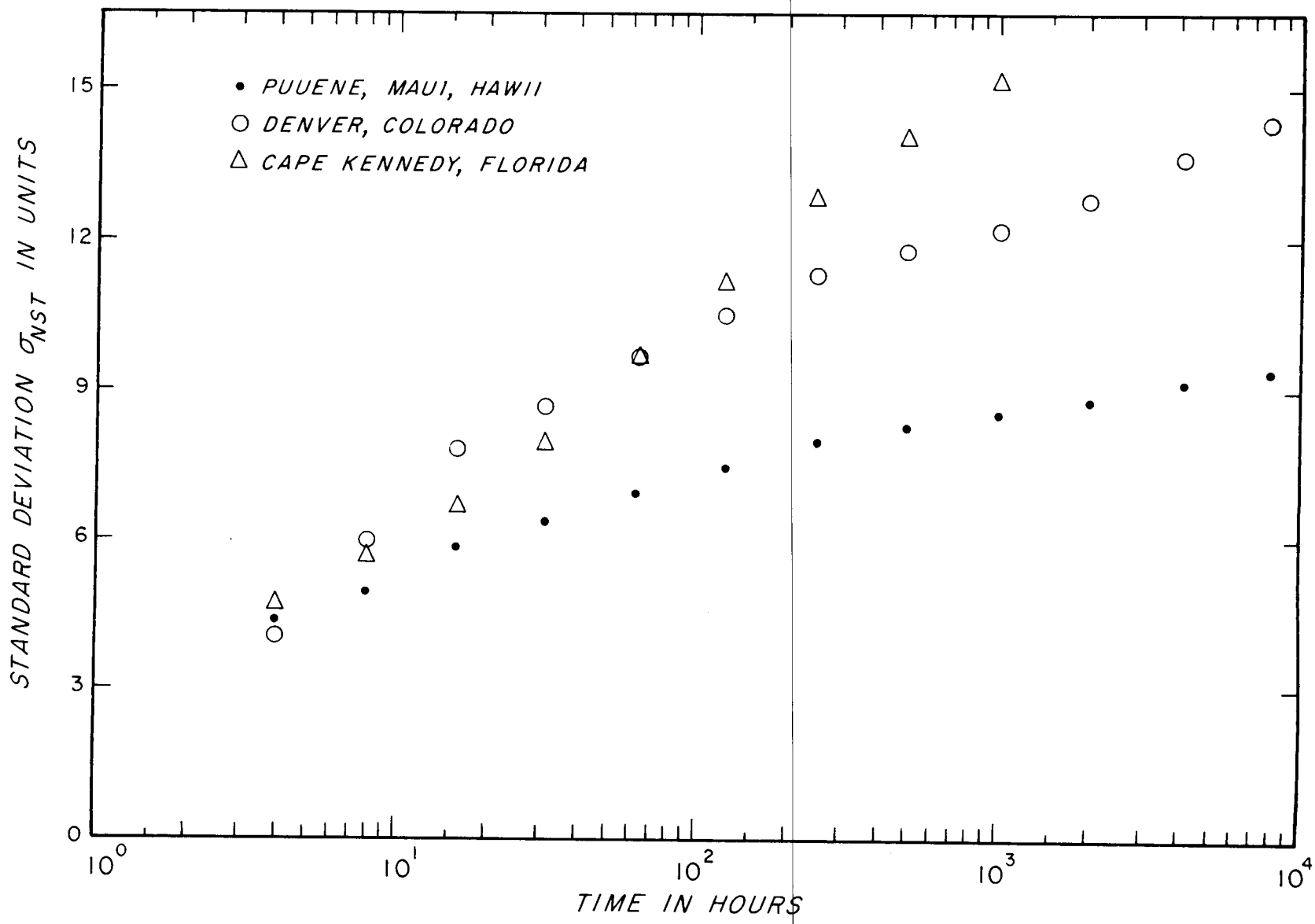

Figure 1-3. Plot of Standard Deviation of Surface Refractivity as a Function of Time

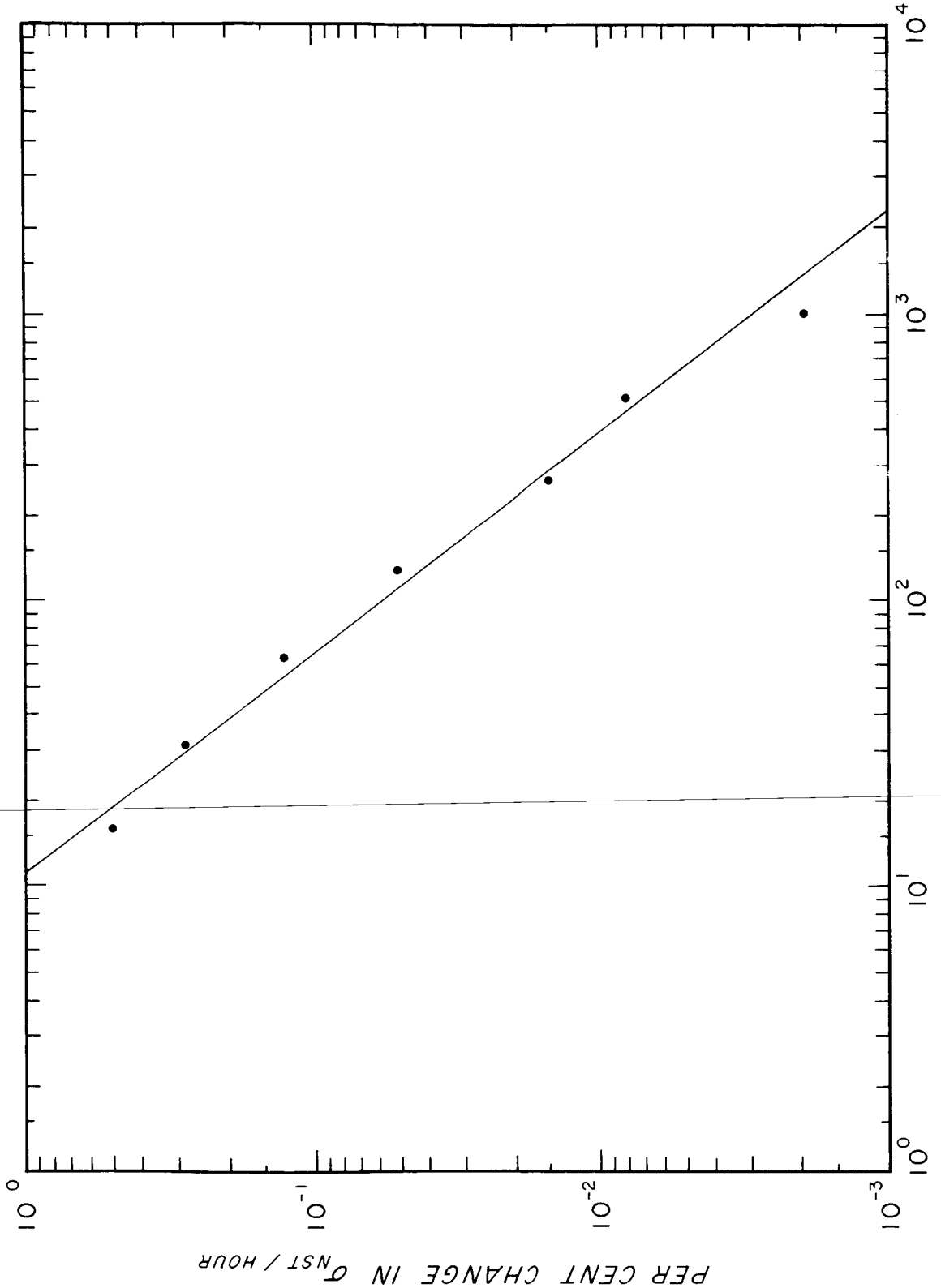

Figure 1-4. Plot of Per Cent Change in Standard Deviation of Surface Refractivity per Hour as a Function of Time

The technique used in determining spectra, amplitude distributions, and structure functions is described in Section III and the computer programs that were used are listed in the appendices.

In Section IV models for the filter function of the difference output of two spaced refractometers are proposed for various wind conditions. From the refractive index difference amplitude distribution plots and observation of original difference data, an empirical probability density function is proposed.

Results from the computer analysis of refractive index difference data are compared with the proposed models in Section V. The measured relative spectra are compared with the proposed filter function according to refractometer spacing and wind conditions.

In order to obtain a better understanding of the physical processes involved in refractive index variations, the interpretation of the original data is made by observing paper strip chart recordings. Comments are made in Section V concerning the effects of refractive index disturbances on a single unit refractometer output and the difference output of two spaced refractometers.

Relative index structure functions are discussed in Section V since these functions can be readily obtained from refractive index difference measurements.

A description of the device used to measure refractive index is given in the next section.

II. INSTRUMENTATION USED IN REFRACTIVE INDEX DIFFERENCE MEASUREMENTS

A. General

The method employed to make simultaneous measurements, at arbitrary points in space, of fluctuations in radio index of atmospheric refraction is indicated in the block diagram of Fig. 2-1. It works on the principle that the resonant frequency of a cavity resonator varies inversely with the index of refraction of the gas contained within the cavity. Since the index of refraction of the atmosphere is so near to unity, the variations in resonance frequency are directly analogous to variations in the index of refraction averaged over the cavity volume.

All cavities are exposed to the atmosphere and asperated at a rate of 0.3 to 0.4 cubic meter per minute. Each cavity is connected in an active circuit in order that variations in its resonant frequency may appear as variations in the frequency of an oscillator. The oscillator output is transmitted as a carrier and the signal may be monitored elsewhere. In this experiment, nominal carriers were 402.1, 402.55, 403.0 and 403.45 MHz. These particular frequencies were chosen to be compatible with the available receiving equipment.

B. Sensors

As indicated previously, the sensor is a cavity controlling the frequency of an oscillator. This combination is called a refractometer

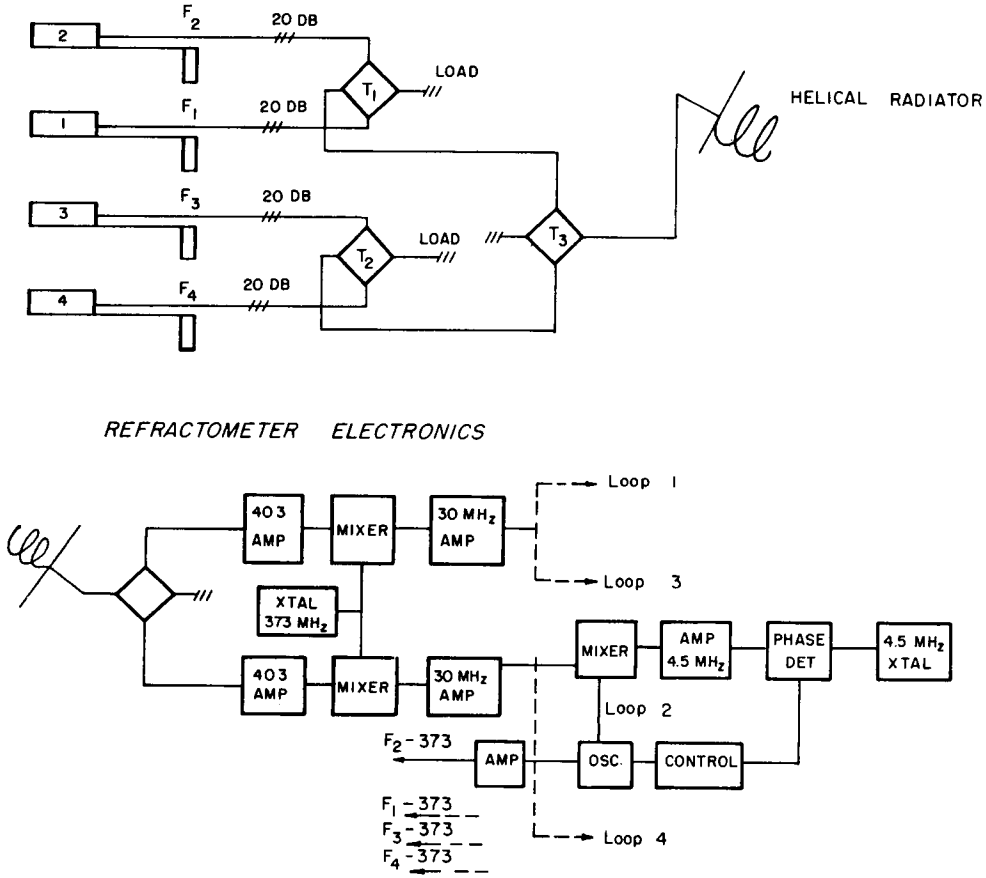

Figure 2-1. Block Diagram of System Electronics

and a total of four refractometers were used in the experiment. The refractometer used has been described adequately elsewhere (Deam, 1962) and this discussion is limited to certain facts about its application in this particular experiment. The cavity shown in this reference is, however, changed to a quarter wavelength invar cavity.

One cavity is shown drawn to scale in Fig. 2-2. It is constructed of silver plated invar which has a temperature coefficient of 1.5 parts per million and is a coaxial type. The unloaded or intrinsic Q of this cavity is measured and found to be near 2000. Air is drawn in through the slots in the outer conductor and exhausted at the blower end. The electric field distribution within this cavity causes it to be primarily responsive to fluctuations in refractivity occurring in the half of the cavity next to the open circuited end and as a result the effective sampling volume is about one-half of the total volume of the cavity.

The four refractometers were carried to an elevation of 80 meters on an elevator carriage operating on an 85 meter high tower. Clearances from the tower are indicated in Fig. 2-3. All refractometers were diplexed into one antenna through magic tees and attenuators as shown in Fig. 2-1.

Measurements are made with one refractometer($F_2 = 403.0$ MHz) being used as a reference. Frequency differences $F_2 - F_1$, $F_3 - F_2$, and $F_4 - F_2$ ultimately appear as time varying functions at the output of the receiving equipment.

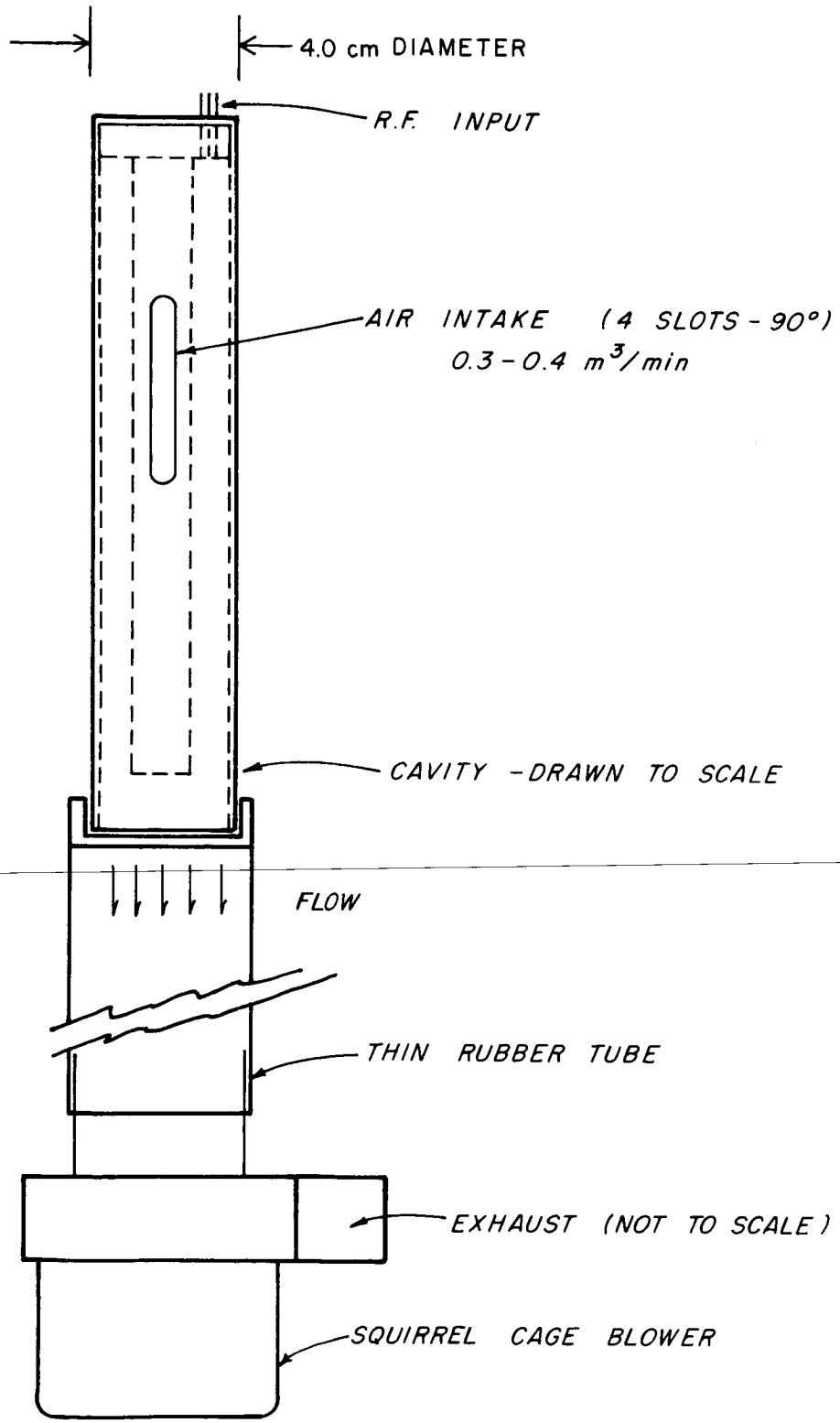

Figure 2-2. Cavity Sensor

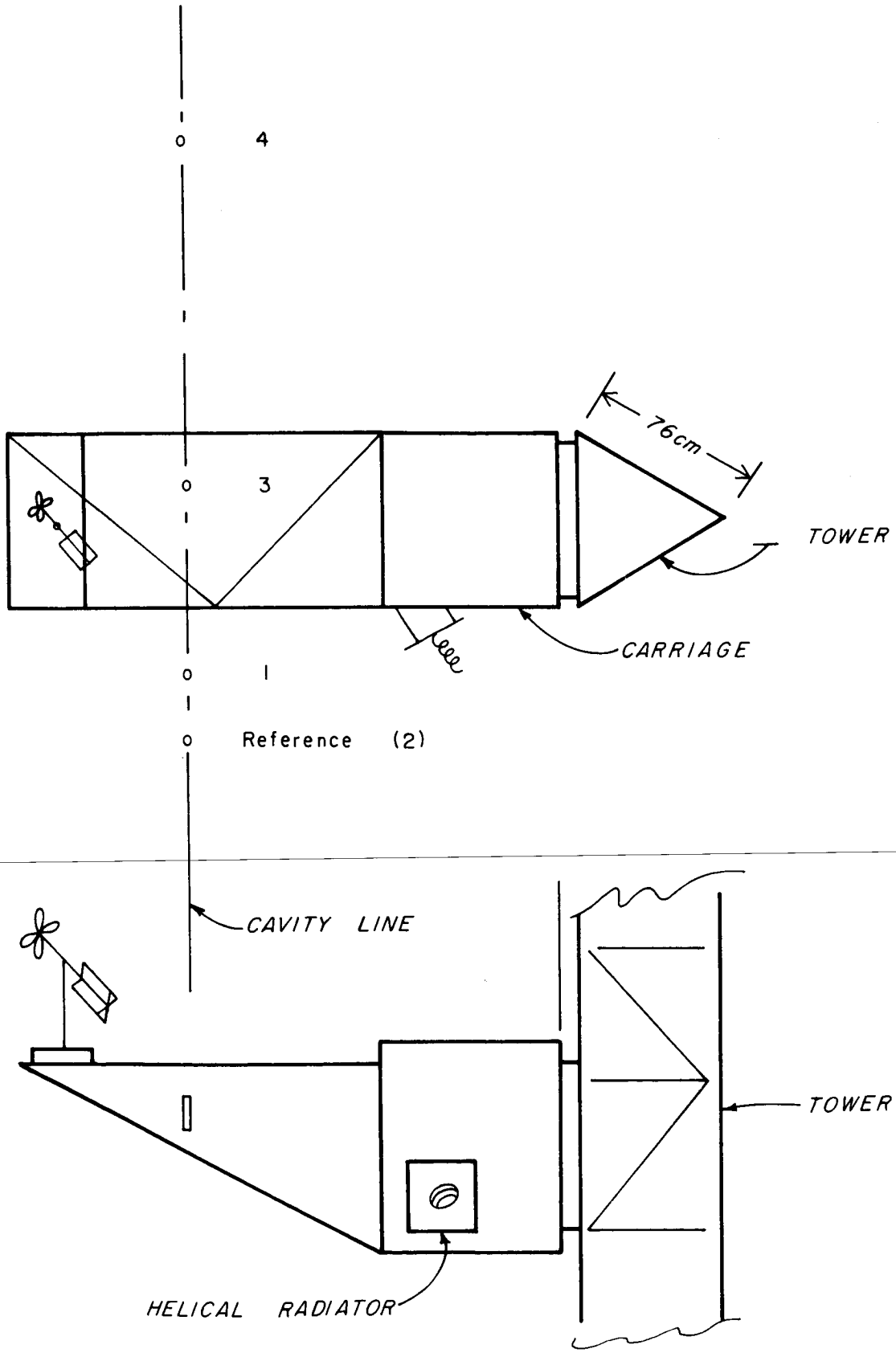

Figure 2-3. Cavity Locations on Tower

C. Receivers

Phase lock receivers (Fig. 2-1) are used to receive the refractometer emissions at the laboratory. These receivers have been reported elsewhere (EERL, 1960). Satisfactory operation is obtained at a signal level of -125 dBm. A single high frequency crystal local oscillator is common to the receivers and there is a separate phase lock channel for each refractometer. The loop frequency is 4.5 MHz and each loop controlled oscillator tracks the refractometer with which it is associated. The frequencies of these oscillators are processed as shown in Fig. 2-1 to give the desired differences.

Since each refractometer does change its mean frequency with temperature and since two refractometers do not track exactly with temperature, it is necessary to use a variable crystal controlled oscillator in the rate detectors to maintain proper operation of the detectors over extended time intervals. The rate detectors have a linear response with frequency and are designed for a nominal frequency of 5000 Hz.

Outputs from the rate detectors are continuously recorded on magnetic tape and/or, as desired, strip charts. Normally, components of frequency from 0 to 30 Hz are recorded and then filtered as desired at data reduction time.

In the next section, refractometer spacing and the method used to process the refractive index difference data are discussed.

III. METHOD OF PROCESSING DATA

A. Experimental Refractometer Arrangement

There were two refractometer arrangements used for this study which are described as follows:

1. Four units aligned horizontally with logarithmic separations from the reference end unit of 0.25 m, 1.0 m, and 4.0 m. For wide separations only two refractometers were used with spacing of 5 and 10 meters.

2. Four units arranged in a box formation with the reference unit at the origin of the rectangular coordinate system and three other units along the three axes at a distance of 0.75 m from the origin. An attempt was made to align one axis of the coordinate system with the wind direction. Another box formation with a separation of 1.8 meters was also used.

In addition to the refractive index measurements, the three outputs of a bi-vane anemometer were recorded for providing the wind speed, elevation angle, and azimuth angle.

B. Power Spectra

A block diagram of the method used to process the refractive index data to obtain power spectra is shown in Fig. 3-1.

The data were recorded using the FM mode of recording so that low frequency refractive index fluctuations would be preserved. The signal from the tape recorder was passed through a high pass filter with

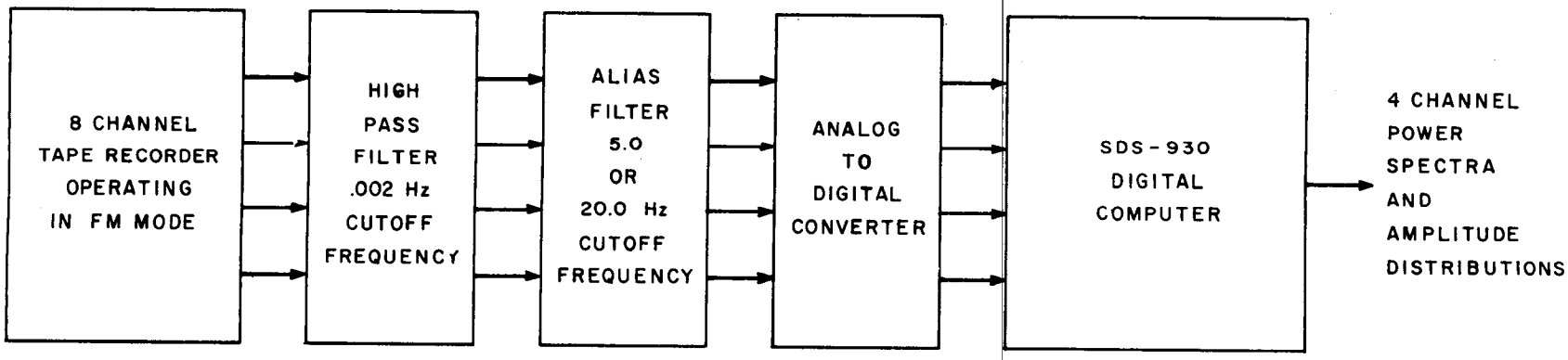

Figure 3-1. Block Diagram of Data Processing Method

a frequency cutoff of 0.002 Hz. This was done to minimize the slow variations in the data that are caused by differences in the temperature coefficients of the resonant cavities.

Before being digitized the analog signal from the high pass filter was passed through a low pass filter with a frequency cutoff of 5 Hz. The low pass filter was used to reduce aliasing errors and attenuate 60 Hz and other high frequency noise.

An SDS-930 digital computer with an analog-to-digital converter was programmed to digitize four channels of data at a rate of 16 samples per second per channel. A computer program for determining power spectra was written such that the data could be analyzed at the same speed at which it was recorded. Appendix A explains in detail how the spectra are determined.

C. Cumulative Amplitude Distributions

Three channels of difference data and one channel of single refractometer data were analyzed for cumulative amplitude distribution. The high pass filter with a 0.002 Hz cutoff frequency used is the same as used for determining power spectra. The aliasing filters were set at 20 Hz in order to include most of the high frequency variations in the refractive index data. A sampling rate of 120 samples per second was used for this program.

In addition to the cumulative amplitude distribution, the mean value and variance for each data channel were also determined.

Appendix B contains a listing of the program used for determining the amplitude distributions and describes the program.

D. Wind Data

Three channels of wind data were obtained from a bi-vane anemometer. Wind speed, azimuth angle, and elevation angle were recorded using the FM mode of recording to preserve the low frequencies contained in the wind data. Only aliasing filters were used in processing the wind data. The data were sampled at a rate of 120 samples per second after passing through aliasing filters of 2.5 Hz. Mean values and rms deviation from the mean values were determined for the three components of wind data.

In the next section, various models for spectra and amplitude distribution are proposed so that the measured data and its characteristics can be compared to the proposed models.

IV. PROPOSED MODELS FOR REFRACTIVE INDEX DIFFERENCE MEASUREMENTS

A. General

During this investigation, an attempt was made to fit measured spectra to some of the different models that apply to refractive index difference spectra under different atmospheric conditions. The models proposed here assume an isotropic medium. The difference measurements of refractive index will be assumed locally stationary and ergodic so that statistical averages may be set equal to time averages.

Two models of relative spectra for refractive index difference measurements are proposed. The first model is one that assumes a wind of constant speed, azimuth angle, and elevation angel. In addition, the refractive index difference is assumed to be taken at points that are in line with the wind direction. This condition is highly idealized, but measurements were made the night of September 19, 1966 in an atmosphere where the wind approached these conditions. The other measurements were made in conditions where the wind was quite variable. The second model proposed is for a variable wind.

The variations of the radio refractive index are very complex in nature and their theoretical treatment requires many assumptions whose limitations are frequently overlooked. A study of refractive index differences involves even more complications which do not lend themselves

to clear-cut explanations. A model of a frozen atmosphere moving with the wind will be assumed for the first model.

B. Refractive Index Difference Variations

The refractive index difference variations may be viewed as either deterministic signals when the atmosphere is relatively calm with constant wind speed and direction or as random signals when the atmosphere is in a disturbed condition with variable wind. Since in most instances the atmosphere is in the second condition, it is expedient to manipulate the measured quantities so that the assumption of stationarity in some sense will be valid. Thus, refractive index difference measurements appear to be favorable over single unit refractive index measurements.

Measurements of refractive index difference suggest a duality in the mechanism causing the fluctuation of these data. The original difference data show spikes superimposed on a continuum of variations. The spikes make a major contribution to the refractive index structure function.

It is suggested that the spikes on the difference data may be due to the clustering of water vapor with a preferential volume size of a few meters and with a gradient of refractive index from the edge to the center of a few N-units.

C. Refractive Index Amplitude Distributions

The refractive index difference data was analyzed as to amplitude distributions. From the shape of these distributions, a probability density model is proposed and some observations made concerning the parameters that contribute to refractive index variations.

The proposed model is examined in light of the original data and it is suggested that two different mechanisms may contribute to variations in refractive index.

D. Locally Isotropic Atmosphere with Constant Wind

The condition of locally isotropic atmosphere with constant wind may be examined in the same manner that Tatarski (1961, p. 21) examined a locally isotropic field along any line in space. The ratio H(k) of difference spectra, $E_d(k)$, to spectra of a single unit, $E_i(k)$, may be expressed as

$$\begin{aligned} H(k) &= E_d(k)/E_i(k) = 2(1-\cos kr)\,E_i(k)/E_i(k) \\ &= 2(1-\cos kr) \\ &= 4\sin^2(kr/2), \end{aligned} \tag{4-1}$$

where $k = 2\pi/\lambda$ and r is the separation distance for the difference spectra measurements. The wavelength λ can be expressed in terms of frequency f and wind speed v as

$$\lambda = \frac{v}{f}\,. \tag{4-2}$$

Rewriting H(k) in terms of frequency and wind speed, the ratio H(f) can be expressed as

$$H(f) = 4 \sin^2(\pi f r/v). \tag{4-3}$$

A deterministic approach to the same problem will be taken by considering a frozen atmosphere moving with constant speed. This is to say that continuous waves will be considered as moving with the atmosphere frozen in structure and with constant velocity. At a given point, the variational component at frequency f may be expressed by

$$\Delta N_1 = F(f) \sin 2\pi f t, \tag{4-4}$$

where ΔN_1 is the component of the change of the index of refraction at frequency f from an average value and F(f) is the amplitude of this variation at this frequency. The mean square value of ΔN_1 is given by

$$E_i(f) = \overline{(\Delta N_1)^2} = F^2(f)/2. \tag{4-5}$$

At a second point at the distance r downwind from the first point, the same events will occur delayed in time by the ratio of distance r to the wind velocity v.

The component of the difference in refractive index, δN, at frequency f is then given by

$$\delta N = \Delta N_1 - \Delta N_2 = F(f)\left(\sin(2\pi f t) - \sin 2\pi f\left(t - \frac{r}{v}\right)\right)$$

$$= 2F(f)\left(\sin \pi \frac{fr}{v} \cos 2\pi f\left(t - \frac{r}{2v}\right)\right). \tag{4-6}$$

The mean square value of this function is

$$\overline{\Delta N^2} = 4 \frac{F^2(f)}{2} \sin^2\left(\frac{\pi f r}{v}\right). \tag{4-7}$$

Since the mean square value of the single point variation is $F^2(f)/2$, substitute $E_i(f)$ for this value giving

$$E_d(f) = \overline{(\delta N)^2} = 4E_i(f) \sin^2(\frac{\pi f r}{v}), \qquad (4\text{-}8)$$

where $E_d(f)$ is the energy spectrum component of the difference function.

If the value of $E_d(f)$ is divided by $E_i(f)$, the form for the relative spectra H(f) becomes

$$H(f) = \frac{E_d(f)}{E_i(f)} = 4 \sin^2(\frac{\pi f r}{v}). \qquad (4\text{-}9)$$

This is essentially the filter function for the refractive index difference for this particular set of assumptions and the same result as derived by Tatarski.

Equation (4-8) and a "-5/3" power law spectra are plotted in Fig. 4-1.

The assumption of constant wind speed is one which is justified only under exceptional conditions. Therefore, it is necessary to investigate the case of variable wind condition.

E. Locally Isotropic Atmosphere with Variable Wind

Normally the wind varies over wide ranges. The nature of these variations is obviously complex and cannot be represented by a simple model. This development follows Tatarski (1961, pp. 14-21).

The difference between the values of refractive index at two points, r_1 and r_2, is chiefly affected only by inhomogeneities of refractive

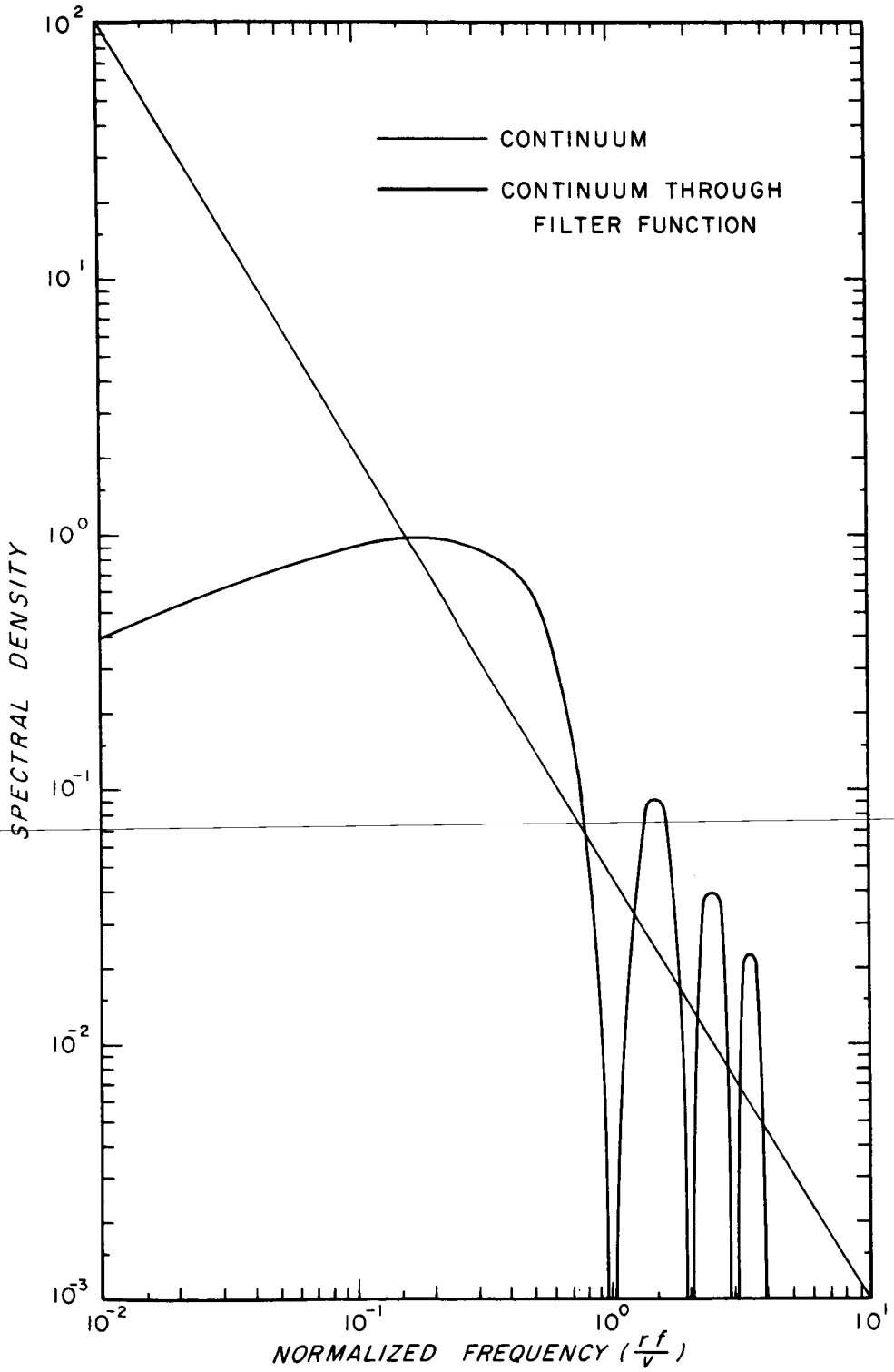

Figure 4-1. Calculated Spectral Shapes

index with dimensions which do not exceed the distance $(r_1 - r_2)$. If this distance is not too large, the largest inhomogeneities have no effect on $N(r_1) - N(r_2)$ and therefore the structure function

$$D_N(r_1, r_2) = \overline{[N(r_1) - N(r_2)]^2} \tag{4-10}$$

depends only on $(r_1 - r_2)$. The overbar denotes time average.

For an isotropic atmosphere, the correlation function $B_N(r_1, r_2)$ depends only on $(r_1 - r_2)$ and can be written as

$$B_N(r) = \iiint_{-\infty}^{\infty} \cos(\overline{k} \cdot \overline{r}) \, \Phi(k) \, d\overline{k} \tag{4-11}$$

where $\Phi(k)$ is the three dimensional energy spectral density function for refractive index and $r = (r_1 - r_2)$, and $k = |\overline{k}|$.

By introducing spherical coordinates in the space of vector $\overline{k}$ and carrying out angular integrations, the refractive index correlation function becomes

$$B_N(r) = 4\pi \int_0^{\infty} k^2 \, \Phi(k) \, \frac{\sin kr}{kr} \, dk, \tag{4-12}$$

$$= \overline{N(r) \, N(o)},$$

and

$$B_N(o) = 4\pi \int_0^{\infty} k^2 \, \Phi(k) \, dk \tag{4-13}$$

$$= \overline{[N(r)]^2},$$

where N(o) is the refractivity at point "o" and N(r) is the refractivity at a point separated from "o" by a distance r.

Expanding the expression of refractive index structure function for $r = (r_1 - r_2)$ as

$$D_N(r) = \overline{[N(r) - N(o)]^2}$$

$$= \overline{[N(r)]^2} - 2\overline{[N(r)\,N(o)]} + \overline{[N(o)]^2}. \qquad (4\text{-}14)$$

Substituting in terms of the correlation function

$$D_N(r) = B_N(o) - 2B_N(r) + B_N(o)$$

$$= 2[B_N(o) - B_N(r)]$$

$$= 4\pi\left[\int_o^\infty 2k^2\,\Phi(k)\,dk - \int_o^\infty 2k^2\,\Phi(k)\,\frac{\sin kr}{kr}\,dk\right]$$

$$= 4\pi\left[\int_o^\infty 2\left(1 - \frac{\sin kr}{kr}\right)k^2\,\Phi(k)\,dk\right]. \qquad (4\text{-}15)$$

The energy spectral density at a single point, $E_i(k)$, is thus multiplied by the function $2\left(1 - \frac{\sin kr}{kr}\right)$. The wave number k can be related to refractometer spacing, r, frequency, f, and mean wind speed, v, as

$$k = \frac{2\pi}{\lambda} = \frac{2\pi f}{v}. \qquad (4\text{-}16)$$

The filter function for refractive index difference variations can be expressed as

$$H(f) = \frac{E_d(f)}{E_i(f)} = 2\left[1 - \frac{\sin(2\pi fr/v)}{(2\pi fr/v)}\right]. \qquad (4\text{-}17)$$

This filter function has a high frequency asymptote of 2 which is expected as the frequency components become uncorrelated.

Another characteristic of refractive index differences is amplitude distribution. Amplitude distributions of refractive index differences are discussed in the next section and from the amplitude distributions a probability density model is proposed.

F. Refractive Index Difference Amplitude Probability Density Model

The proposed model is based on observations made from original data samples and from the cumulative amplitude distribution plots. When observing a strip chart recording of a single refractometer output, one notices that when a level is established over periods of minutes, large excursion spikes may be noted. These spikes seem to be predominately in the direction of increasing refractive index, although the large scale required for the swells partially obscures the spikes. These types of variations suggest the presence of discrete blobs of refractive index of considerably greater amplitude than the atmosphere surrounding these blobs.

Refractive index difference data contain both positive and negative spikes. This also suggests discrete blobs which may cause an increase in either refractometer response relative to the other.

The model proposed for the refractive index difference probability density is one that is represented by the sum of three Gaussian

functions. One of the Gaussian functions has a mean value of zero and the other two functions have mean values of the same amplitude but of opposite sign.

The cumulative amplitude distributions were plotted on probability paper on which a Gaussian distribution appears as a straight line. It is from the shape of these amplitude distribution plots that the following probability density function is proposed:

$$f(\Delta N) = \frac{K_2}{\sigma_2\sqrt{2\pi}} \exp\left[-\frac{(\Delta N+a)^2}{2\sigma_2^2}\right] + \frac{K_1}{\sigma_1\sqrt{2\pi}} \exp\left[-\frac{(\Delta N)^2}{2\sigma_1^2}\right] + \frac{K_2}{\sigma_2\sqrt{2\pi}} \exp\left[-\frac{(\Delta N-a)^2}{2\sigma_2^2}\right], \tag{4-18}$$

where K_1 and K_2 are normalizing constants that must satisfy the condition

$$K_1 + 2K_2 = 1, \tag{4-19}$$

and σ_1^2, σ_2^2 are the variances of the two difference components of the density function. The quantity a is the mean value of the component of the density function whose variance is σ_2^2.

The cumulative amplitude distribution function $F(\Delta N)$ is expressed as

$$F(\Delta N) = \int_{-\infty}^{\Delta N} f(u)\,du, \tag{4-20}$$

where $f(u)$ is given by eq. (4-18) with u substituted for ΔN.

The mean value $\overline{\Delta N}$ for this density function is determined by

$$\overline{\Delta N} = \int_{-\infty}^{\infty} uf(u)\,du$$

$$= -aK_2 + 0 + aK_2 = 0. \tag{4-21}$$

Since the mean value is zero, the variance σ^2 is found as follows:

$$\sigma^2 = \int_{-\infty}^{\infty} u^2 f(u)\,du$$

$$= K_1\sigma_1^2 + 2K_2(\sigma_2^2 + a^2). \tag{4-22}$$

A plot of eq. (4-18) is shown in Fig. 4-2 for $K_1 = 0.9$, $K_2 = 0.05$, $\sigma_1 = 0.05$, $\sigma_2 = 0.1$, and $a = 0.2$.

The refractive index structure function has been introduced earlier, and can be determined from the probability density of refractive index differences.

G. Structure Function for Refractive Index

Based on mechanical turbulence (Tatarski, 1961, p. 58), the refractive index structure function of two points separated by a distance r is expressed as

$$D_n(r) = C_n^2 r^{2/3} \tag{4-23}$$

where C_n^2 is a constant related to atmospheric conditions.

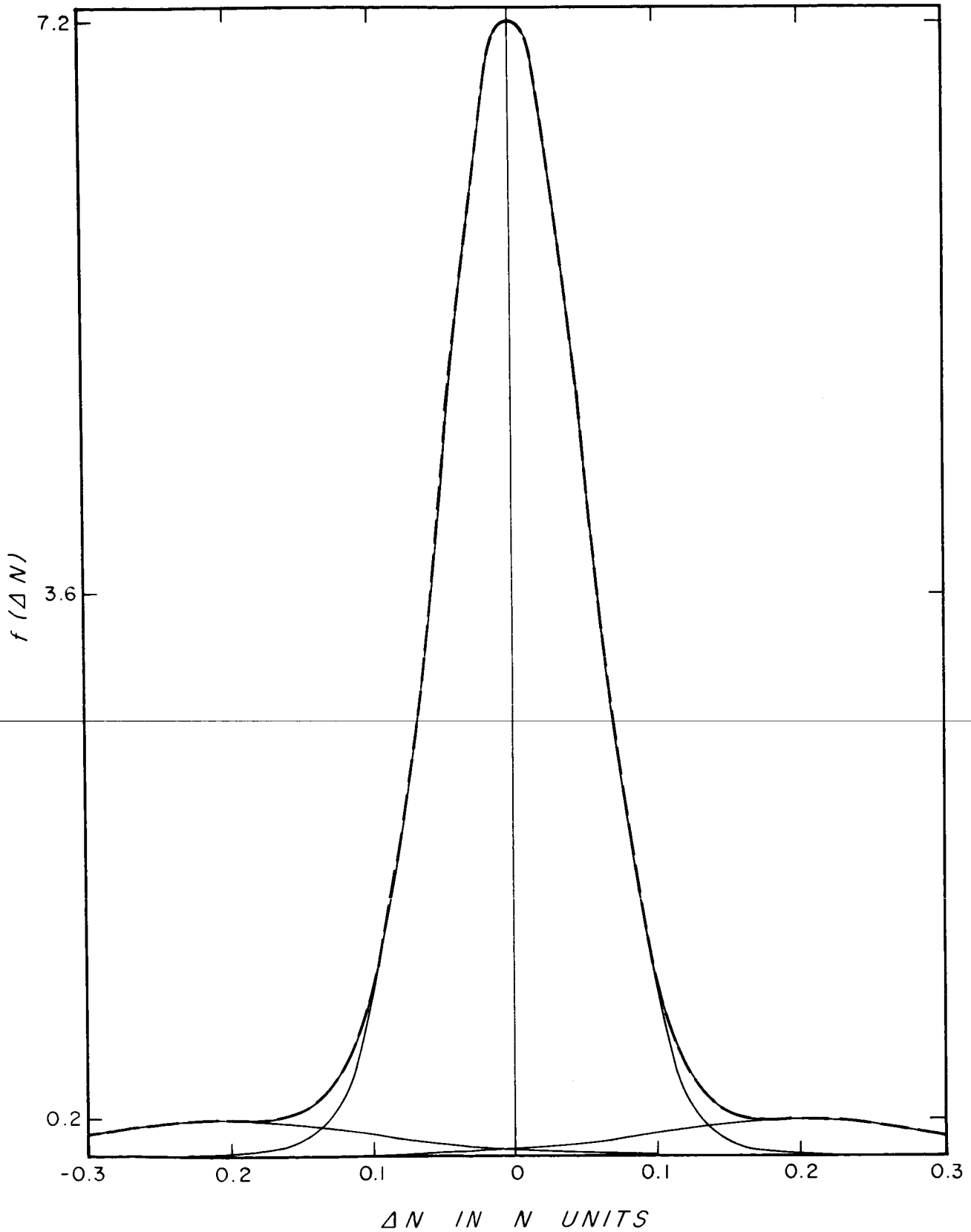

Figure 4-2. Plot of Proposed Density Function

In terms of readily measured quantities, the structure function for index of refraction can be expressed as

$$D_n(r) = \overline{[n(r) - n(o)]^2}, \qquad (4\text{-}24)$$

where n(o) is the index of refraction at reference point "o", n(r) is the index of refraction at a point separated from "o" by a distance r, and the bar over the bracket indicates the time average of the square of the difference. In this study, structure functions were determined for data samples of thirty minutes to one hour in duration.

The structure function for refractive index has been expressed by eq. (4-24), and by using the probability density function as expressed by eq. (4-18), the structure function becomes

$$D_n(r) = [K_1\sigma_1^2(r) + 2K_2(\sigma_2^2(r) + a^2(r))] \times 10^{-12}. \qquad (4\text{-}25)$$

The quantities K_1 and K_2 are assumed to be independent of r over the range of interest. The quantities $\sigma_1^2(r)$, $\sigma_2^2(r)$, and $a^2(r)$ are shown as functions of r.

Several models for refractive index differences have been proposed. In the next section data samples were analyzed and the results are compared with the proposed models.

V. INTERPRETATION OF DATA

A. General

The results of thirteen sets of measurements will be presented in this study. Wind speed, wind direction, date, and time of day are shown for each of the thirteen examples in Table 5-1. Figure 5-1 shows the legend for all plots shown for the different refractometer configurations. Also shown in Fig. 5-1 is the reference for the wind azimuth angle.

Examples 1, 2, 3. For these measurements, the four cavities were placed in a line at distances from the reference cavity of 0.25 m, 1.0 m, and 4.0 m. The changes in the difference in refractive index between the reference unit and each of the other refractometers were recorded. For these sets of data, the refractive index fluctuations of a single unit were not recorded.

Examples 4, 5. The refractometer arrangement for these cases was two units separated horizontally by 5.0 and 10.0 meters, respectively. Refractive index difference and single unit variations were measured.

Examples 6, 7, 8, 9, 10, 11, 12. These sets of data were taken with four sampling units arranged along the axes of a rectangular coordinate system with the reference cavity at the origin and the other three cavities along the three axes 0.75 meters from the origin. The

Table 5-1

The times and wind data for each of the 13 sets of data

Ex. No.	Date-Time	Wind Speed, M/S		Wind Direction, Degree		
		Mean Value	RMS Deviation	Mean Azimuth	RMS Azimuth Variation	RMS Vertical Deviation
1	19 Sept 66 1945-2045	4.0	0.2	22	4	-*
2	19 Sept 66 1845-1910	3.9	0.9	27	11	7
3	28 Sept 66 1130-1236	2.0	0.1	-	-	-
4	11 Nov 66 1052-1148	1.0	0.7	-	-	-
5	11 Nov 66 1526-1623	1.4	0.8	-	-	-
6	27 Sept 66 1300-1407	1.8	0.8	158	14	17
7	23 Sept 66 1400-1440	0.7	0.5	-10	43	-
8	24 Sept 66 0944-1015	1.0	0.5	154	32	-
9	24 Sept 66 1030-1140	1.4	0.7	160	23	17
10	26 Sept 66 1340-1445	2.0	0.9	158	17	20
11	26 Sept 66 1500-1605	2.0	0.5	101	12	13
12	27 Sept 66 0945-1055	3.2	0.9	176	10	14
13	11 Oct 66 1015-1115	1.4	0.8	-	-	-

* Indicates data not measured.

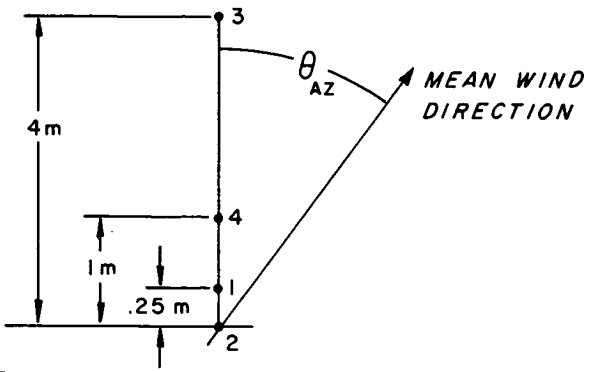

LEGEND FOR EXAMPLES 1, 2, and 3.

O — Difference between Refractometer Pair 2-1.
Δ — Difference between Refractometer Pair 2-4.
• — Difference between Refractometer Pair 2-3.

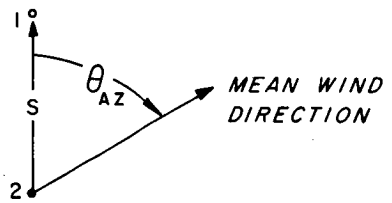

S = 5.0 meters for Example 4.
S = 10.0 meters for Example 5.

LEGEND FOR EXAMPLES 4 and 5.

• — Difference between Refractometer Pair 2-1.
x — Single unit number 2.

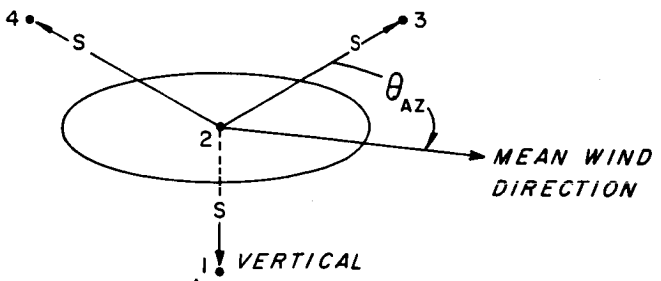

S = 0.75 meter for Examples 6 through 12.
S = 1.8 meter for Example 13.

LEGEND FOR BOX FORMATION EXAMPLES.

∘ — Vertical difference between Refractometer Pair 2-1.
O — Horizontal difference between Refractometer Pair 2-3
Δ — Horizontal difference between Refractometer Pair 2-4.
x — Single unit number 2.

Figure 5-1. Refractometer Spacing and Legend for Refractive Index Difference Measurements

refractive index changes of the reference cavity and the differences between the reference cavity and the other three cavities were recorded.

Example 13. This example had the same arrangement as the previous ones except that the spacing along each axis was 1.8 meters.

A sample of refractive index difference data for the in-line spacing of example 3 is shown in Fig. 5-2. The spikes in Fig. 5-2, as noted in segment "b", are in sharp contrast to the more continuous type of variations as shown by segment "c". The amplitudes of the spikes are consistently several times those of the continuous type variations.

The peak-to-peak variations of the refractive index differences increased as the spacing increased for the refractometer spacings used in this study. Also, the spikes which occur at approximately the same time on all three data channels increase in amplitude with increasing separations.

The general features of the original data for the 0.75 meter box formation are shown in Fig. 5-3 for example 6. The outer segments "A" and "C" of these data are taken at a slow chart speed (5 cm/min) and the middle segment "B" is taken at a speed five times that of the outer segments (25 cm/min).

The data seem to be made up of two distinct components. One is the continuum of variations and the other is a set of sharp spikes as seen on the slow speed segments of Fig. 5-3.

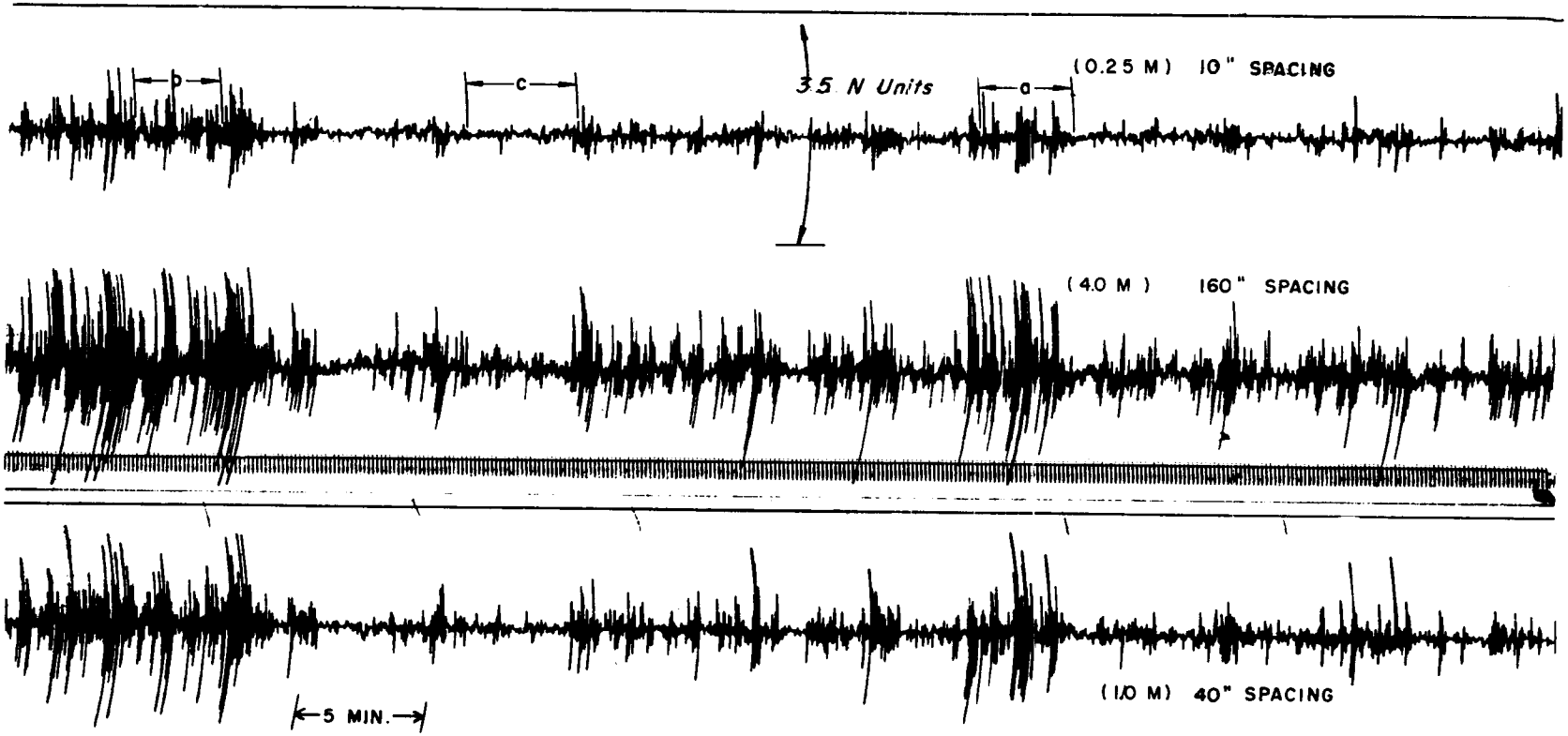

Figure 5-2. Typical Difference Outputs for Spaced Refractometers

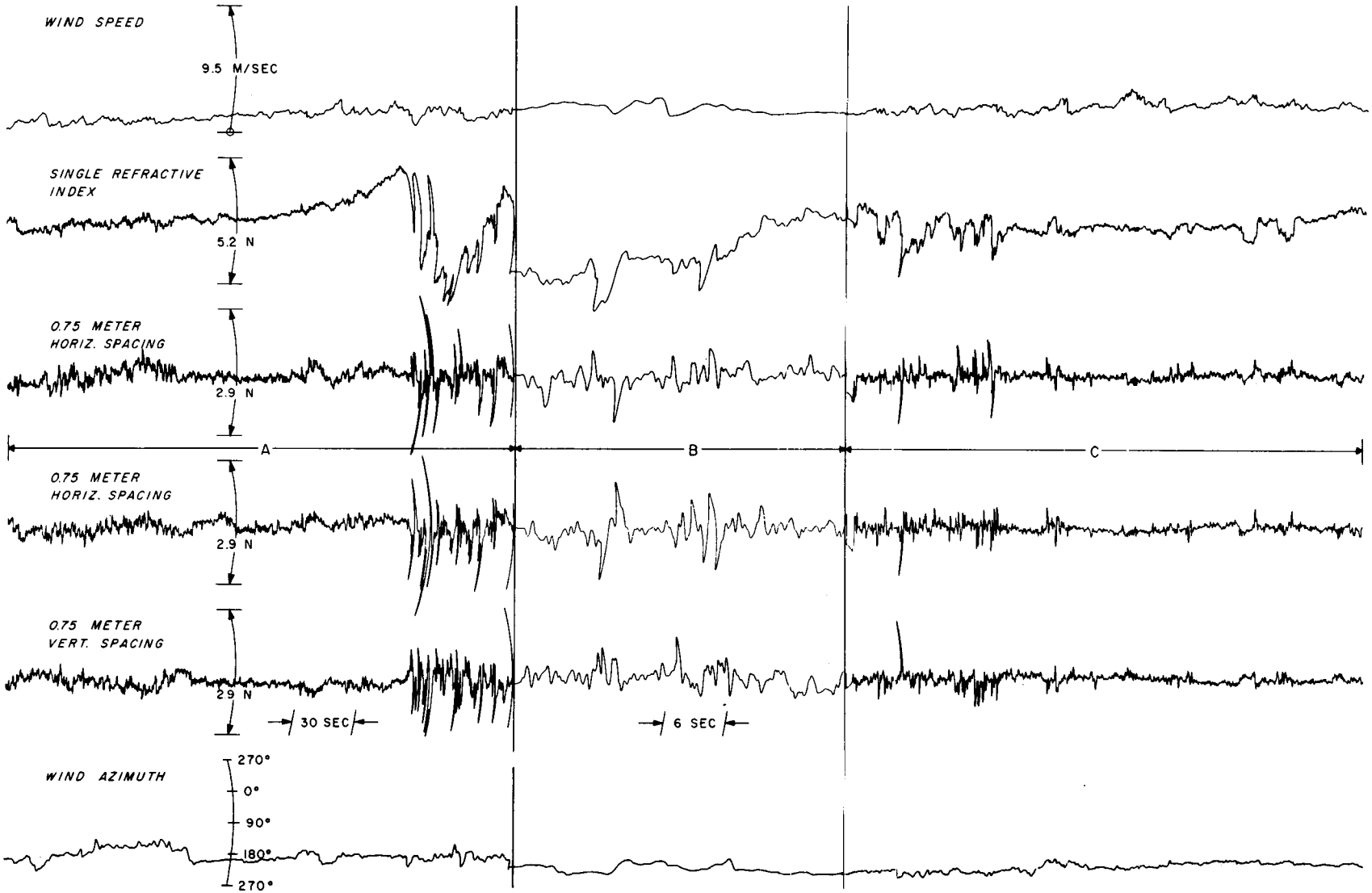

Figure 5-3. Original Data Sample of 0.75 Meter Box Formation with Slow and Fast Time Scale

In addition to difference data in Fig. 5-3, single unit refractive index variations, wind speed, and aximuth angle data are shown.

There is a waveform, approximately rectangular, of a single unit refractive index data in segment "B" of Fig. 5-3. Both horizontal differences show a spike at the beginning of the single unit rectangular waveform and another spike in the opposite direction at the end of the single unit waveform. The vertical differences also indicate a disturbance but not as pronounced as the horizontal ones.

Observation of the original difference data, before filtering, indicated frequency components from a few tenths to several Hz. In order to get a measure of frequency content of the data, a spectral analysis was made using a digital computer.

B. Spectral Analysis

1. In-Line Spacing

a. Nearly constant wind condition. The data for example 1 was taken at night during a period of nearly constant wind velocity. Log-log spectra for this example are shown in Fig. 5-4.

The interpretation of the spectra such as shown in Fig. 5-4 is aided by re-plotting on linear paper with the amplitudes of the difference spectra divided by the corresponding values of the amplitude of the single point index changes.

These relative spectra on a linear scale show the effect which the difference measurements have in filtering the fluctuations of

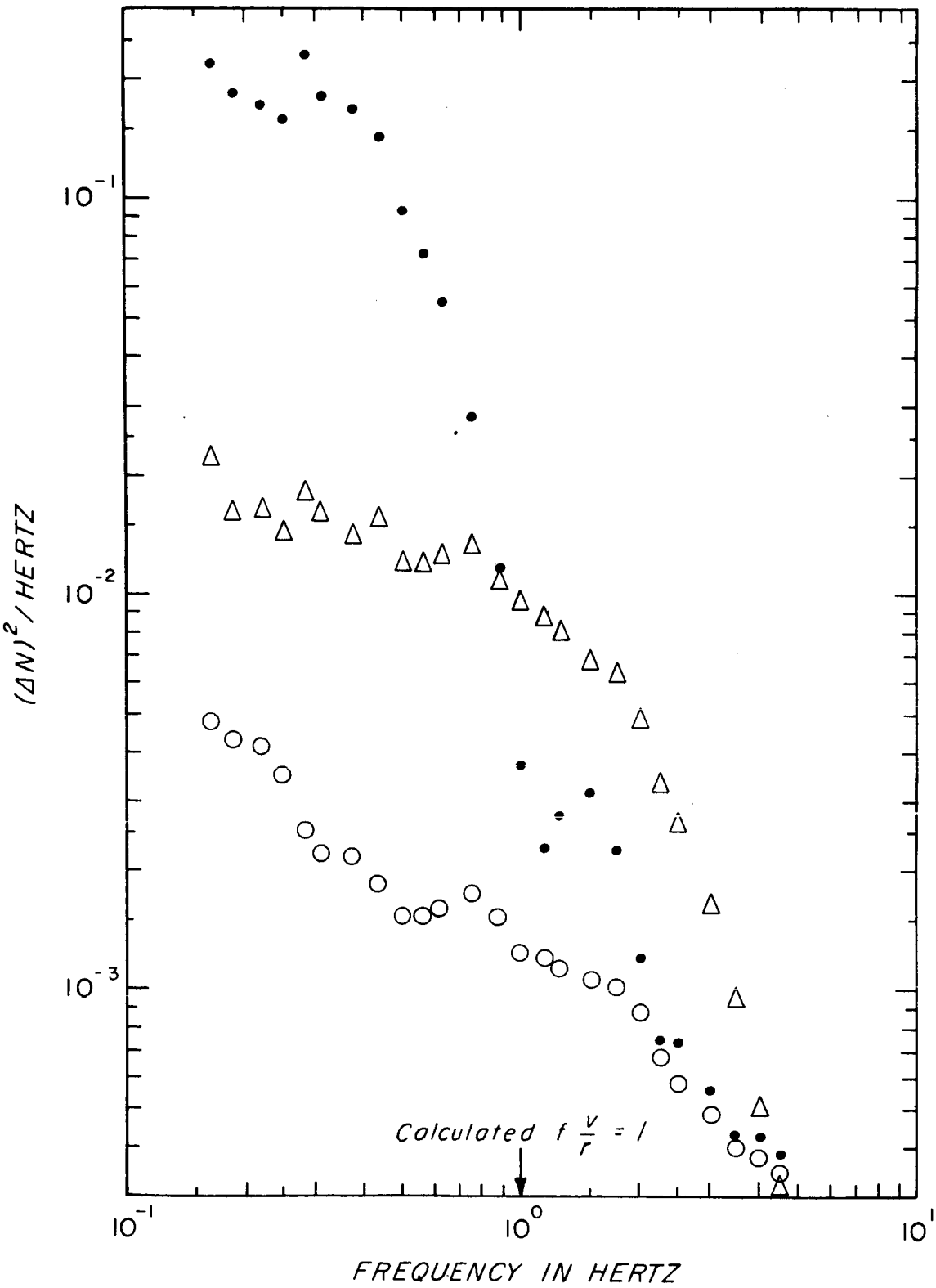

Figure 5-4 Spectra of In-Line Formation of Example 1
(Legend for this figure is on page 43)

the refractive index. The relative spectra will be referred to as the filter function for the difference output of the two refractometers.

Since the single point spectra were not available for this example, the relative spectra were obtained by multiplying the difference data by $Kf^{5/3}$ assuming a "-5/3" dependence of the single point variations as reported by several researchers, e.g., Gossard (1960) and Tatarski (1961, p. 58). A filter function of the form $2S^{1/2} \sin^2(x/2)$ is plotted along with the relative spectra in Fig. 5-5. The assumed filter function is shown as modified by the $S^{1/2}$ factor where S is the spacing between refractometers.

Since there is no justification for a spacing dependence for the filter function, the frequency variation of the single point index should be examined. By setting the maximum amplitudes of the relative spectra equal for the 4.0 and 1.0 meter spacing of example 1, the single point index variation was found to be of the form $Kf^{-2.16}$. The data and relative spectra for this assumed condition are shown in Fig. 5-6.

b. Variable wind condition. Examples 2 and 3 are for the 0.25, 1.0, and 4.0 meter in-line spacing. As in example 1, the spectra for a single point were not available so that the relative spectra were obtained by multiplying the difference spectra by $Kf^{5/3}$. Figure 5-7 shows the log-log spectra and Fig. 5-8 shows the relative spectra for example 2. Also the spectra for example 2 were obtained by multiplying the difference spectra by $Kf^{2.16}$ and are shown in Fig. 5-9. The

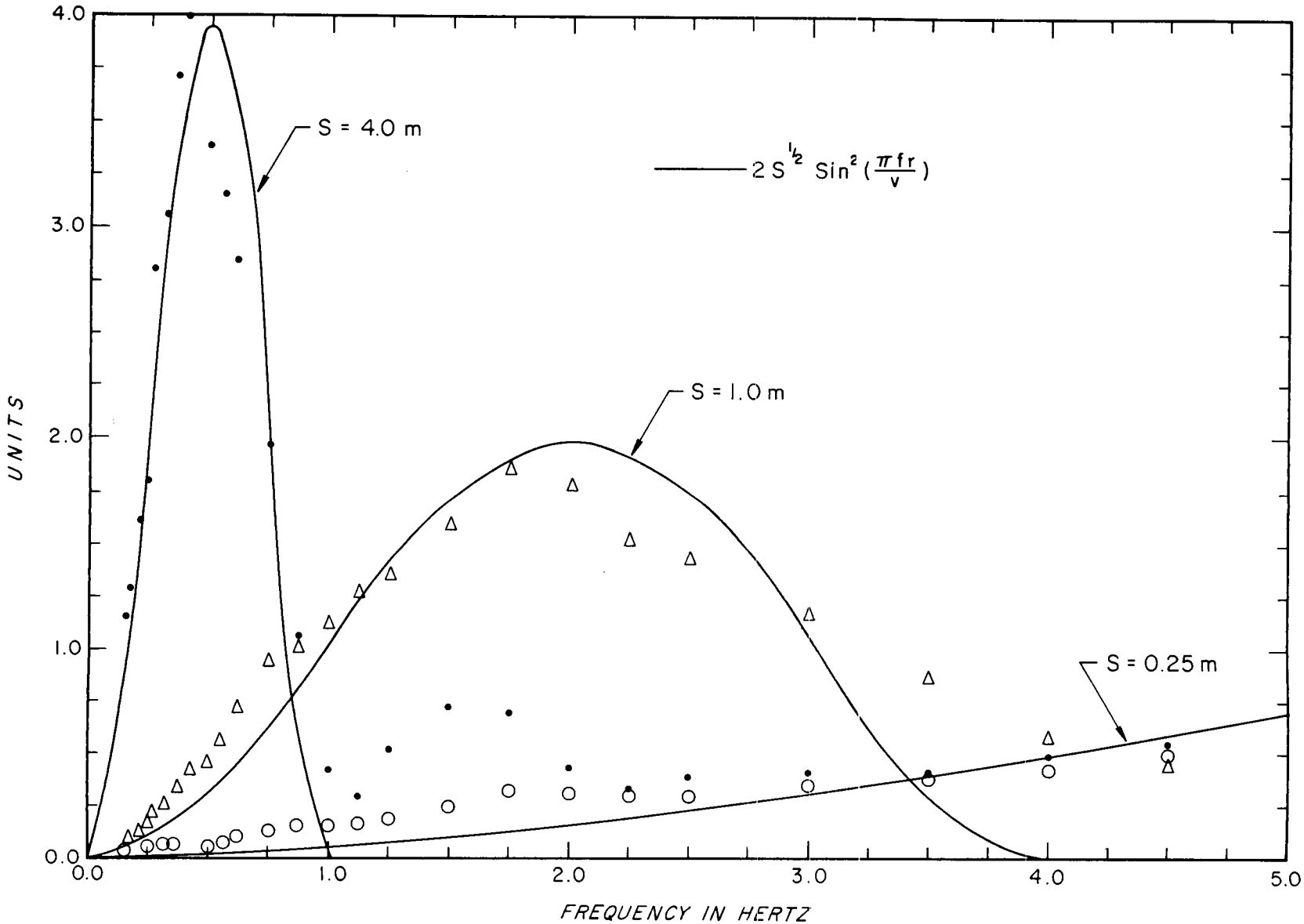

Figure 5-5. Difference Spectra of Example 1 Divided by $Kf^{-5/3}$
(Legend for this figure is on page 43)

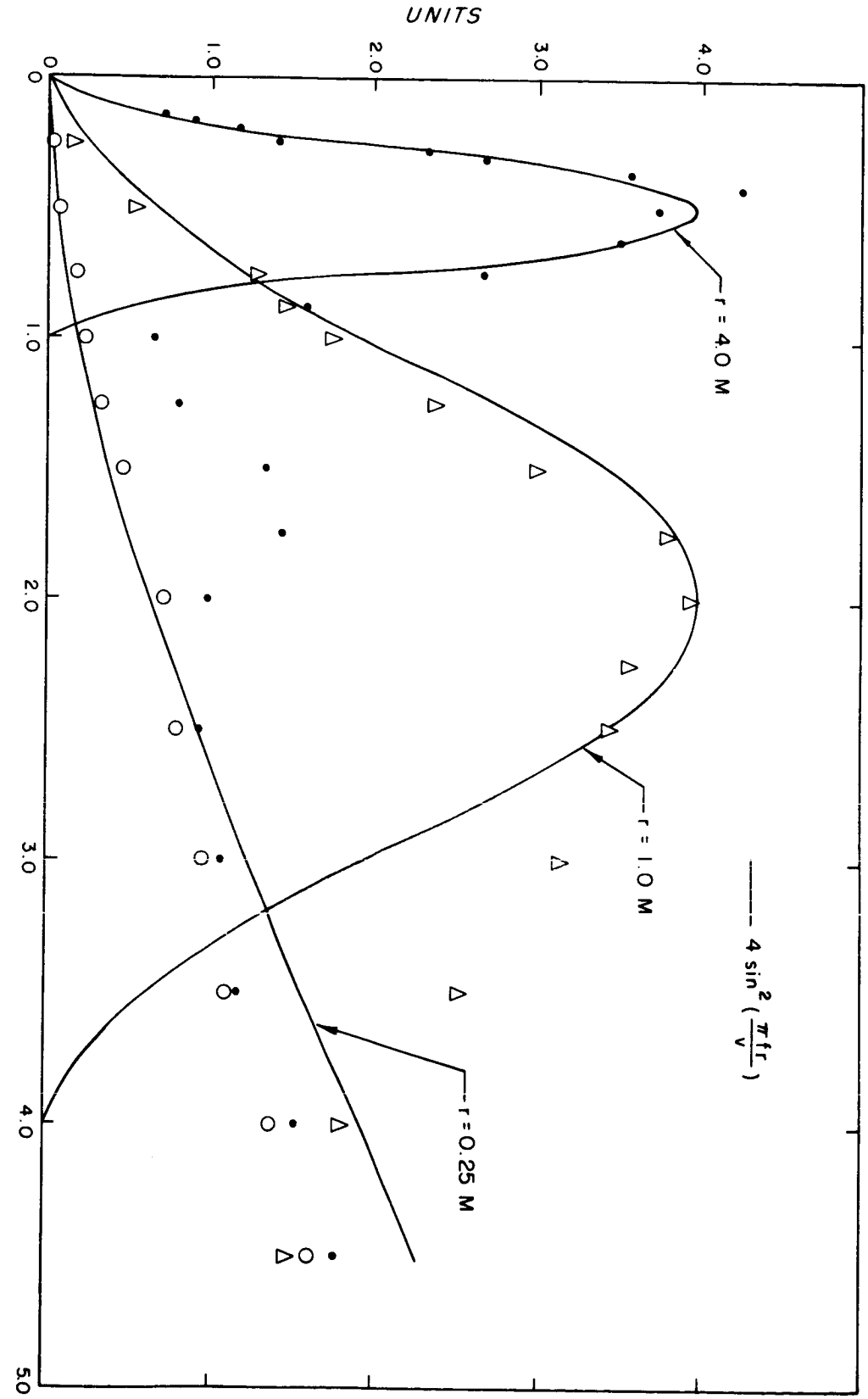

Figure 5-6. Difference Spectra of Example 1 divided by $Kf^{-2.16}$
(Legend for this figure is on page 43)

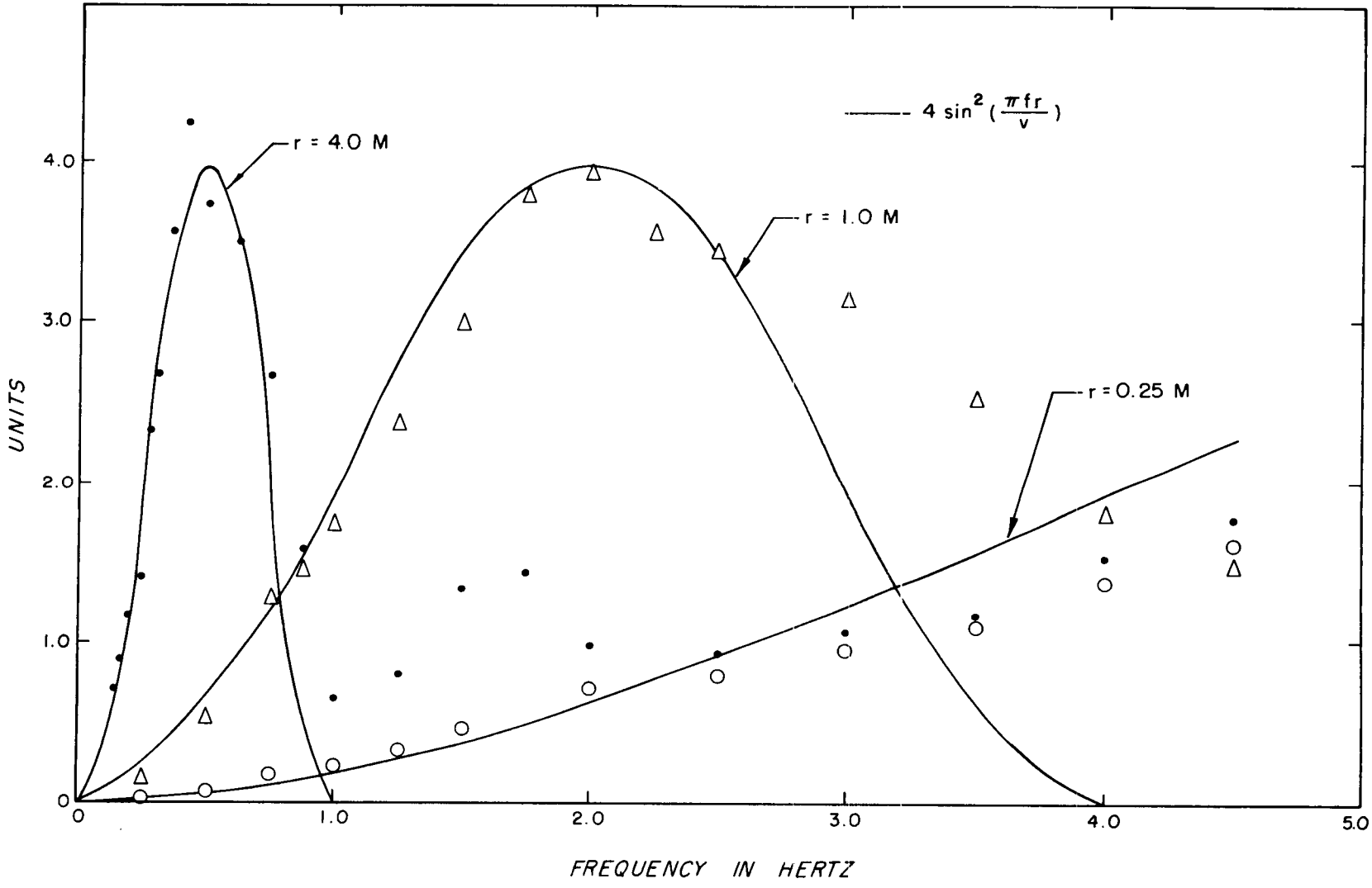

Figure 5-6. Difference Spectra of Example 1 Divided by $Kf^{-5/3}$
(Legend for this figure is on page 43)

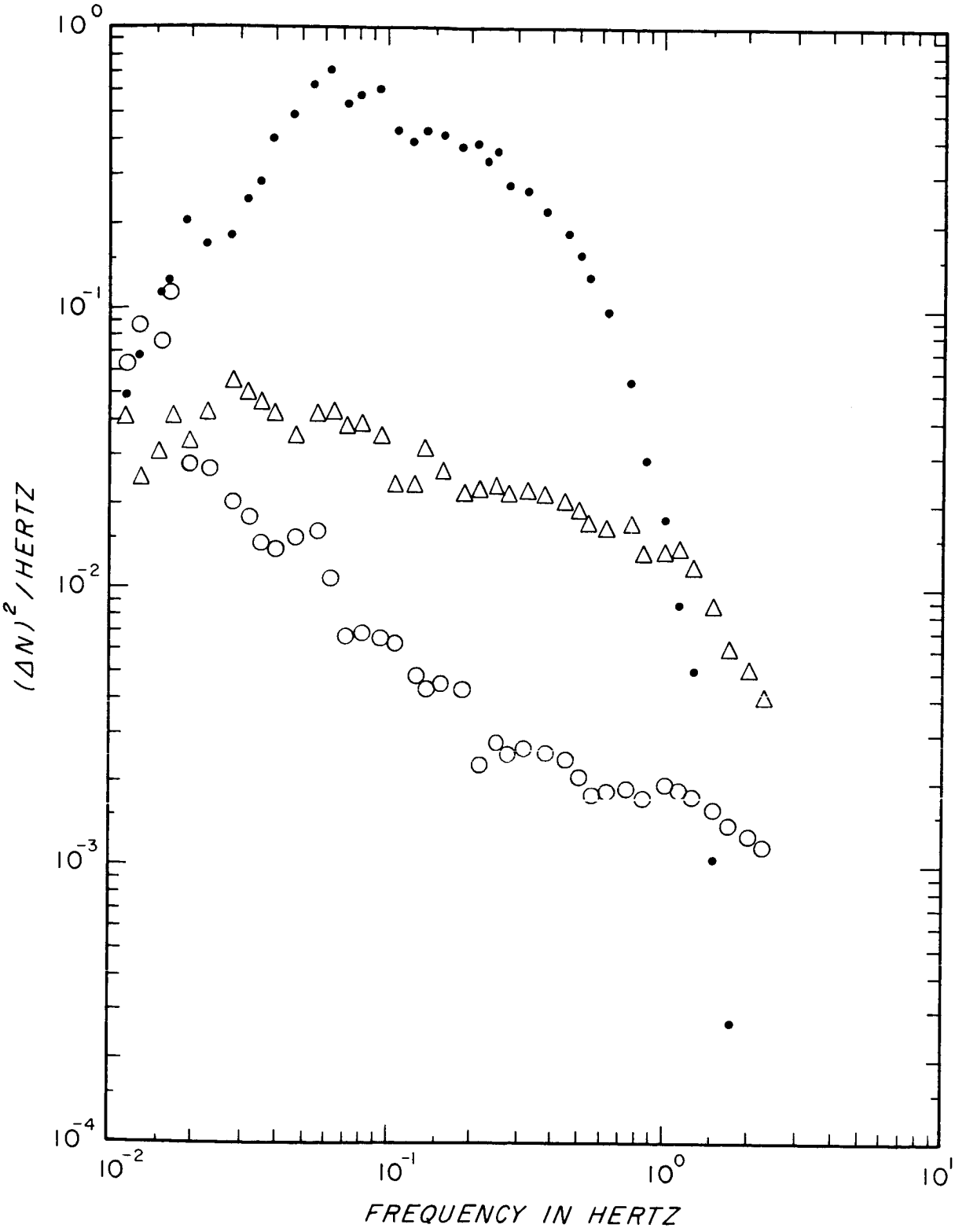

Figure 5-7. Spectra of In-Line Formation of Example 2
(Legend for this figure is on page 43)

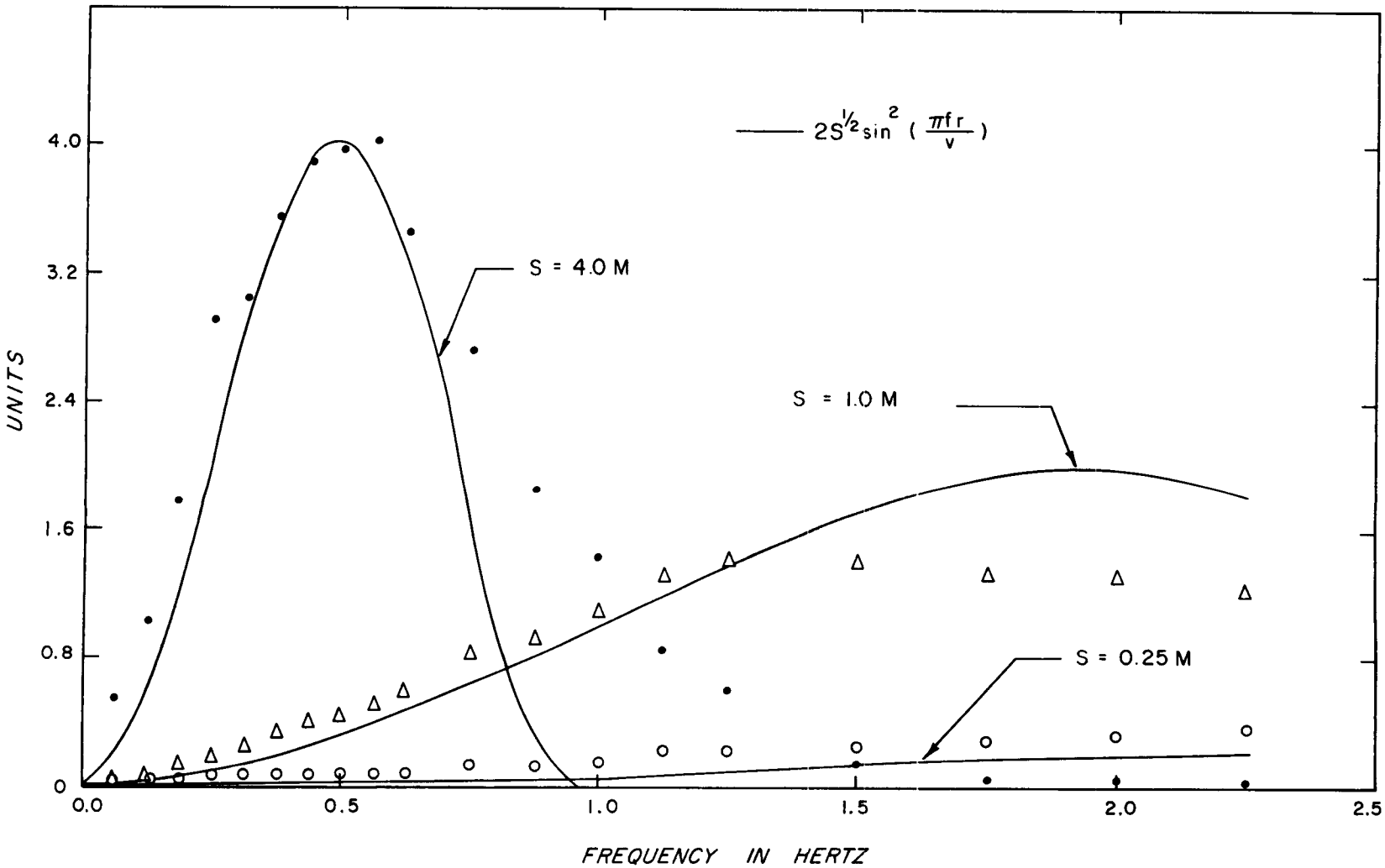

Figure 5-8. Difference Spectra of Example 2 Divided by $Kf^{-5/3}$
(Legend for this figure is on page 43)

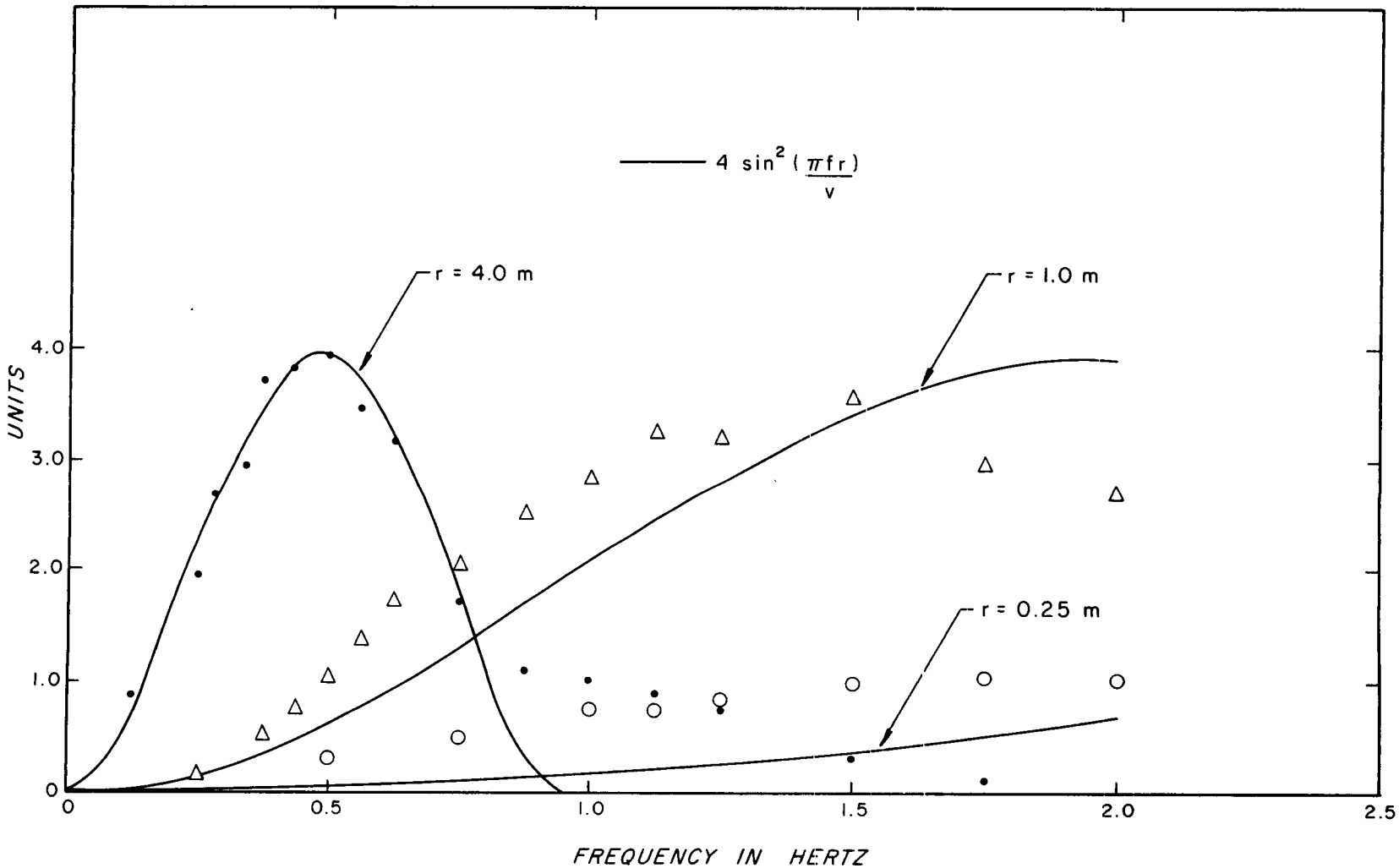

Figure 5-9. Difference Spectra of Example 2 Divided by $Kf^{-2.16}$
(Legend for this figure is on page 43)

log-log spectra, relative spectra assuming a $Kf^{-5/3}$ single unit spectra, and relative spectra assuming a $Kf^{-2.16}$ single unit spectra for example 3 are shown in Figs. 5-10, 5-11, and 5-12, respectively.

Example 4 is for a 5.0 meter in-line spacing. The log-log spectra and relative spectra are shown in Figs. 5-13 and 5-14.

The largest refractometer spacing of 10.0 meters provided data for example 5. Figure 5-15 is a plot of the log-log spectra for this example. The relative spectra follow a $2(1 - \sin x/x)$ filter function as shown in Fig. 5-16.

In example 5, the values of relative spectra at the higher frequencies are greater than predicted by about 20 per cent. Considering the total error as being in the difference data spectra results in the difference data amplitudes being in error of 10 per cent. On the other hand, assuming equal measurement error in both difference and absolute spectra leads to a reasonable 5 per cent error in amplitude measurements.

2. Box Formation with Variable Wind Conditions

a. 0.75 meter spacing. Figures 5-17 through 5-23 show the log-log spectra for examples 6 through 12, respectively. Relative spectra are shown in Figs. 5-24 through 5-30 for examples 6 through 12, respectively. In the assumed filter function, no arbitrary constants were used for the curves drawn for the relative spectra plots. The only factors introduced were the mean wind velocity and the cavity spacing.

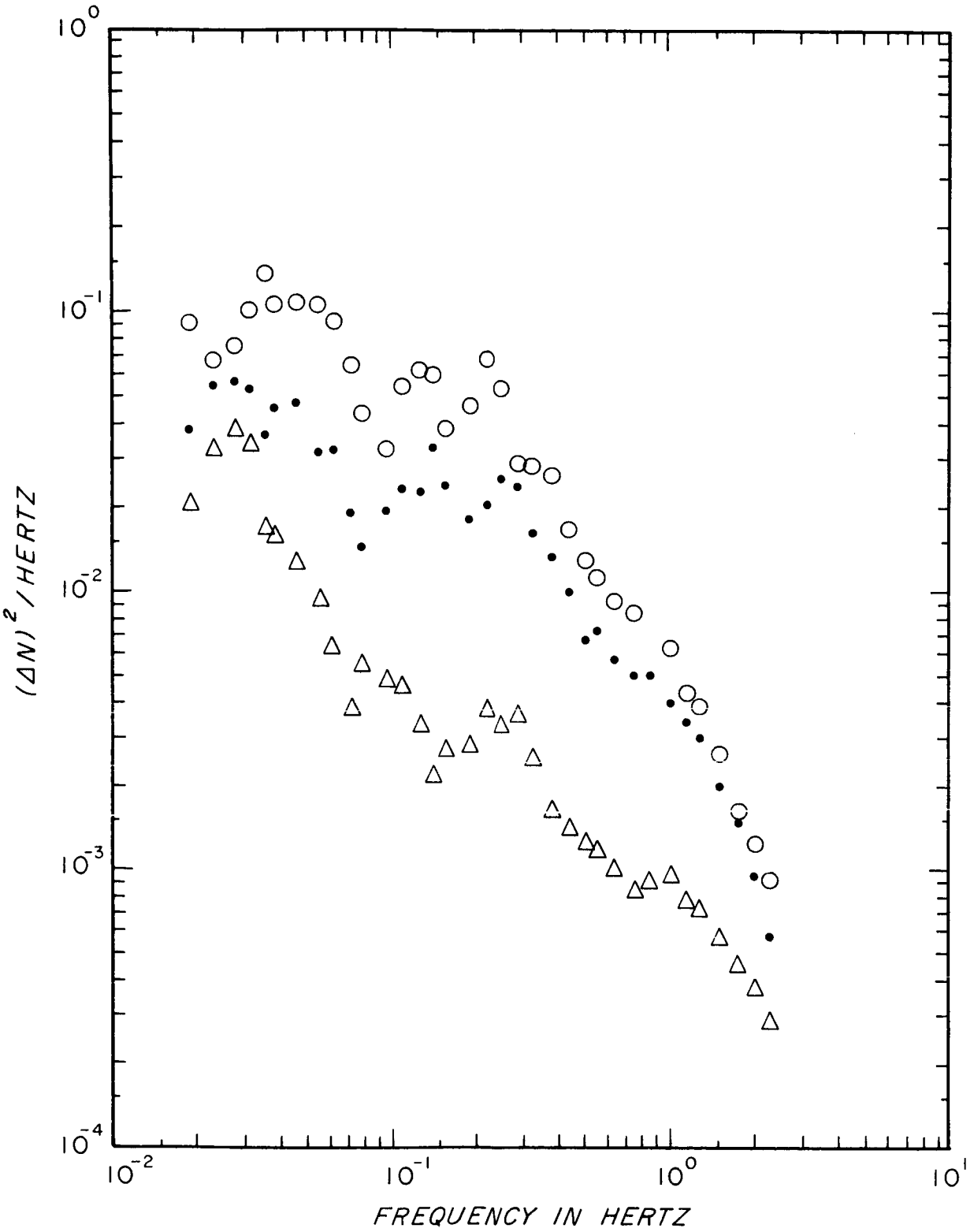

Figure 5-10 Spectra of In-Line Formation of Example 3
(Legend for this figure is on page 43)

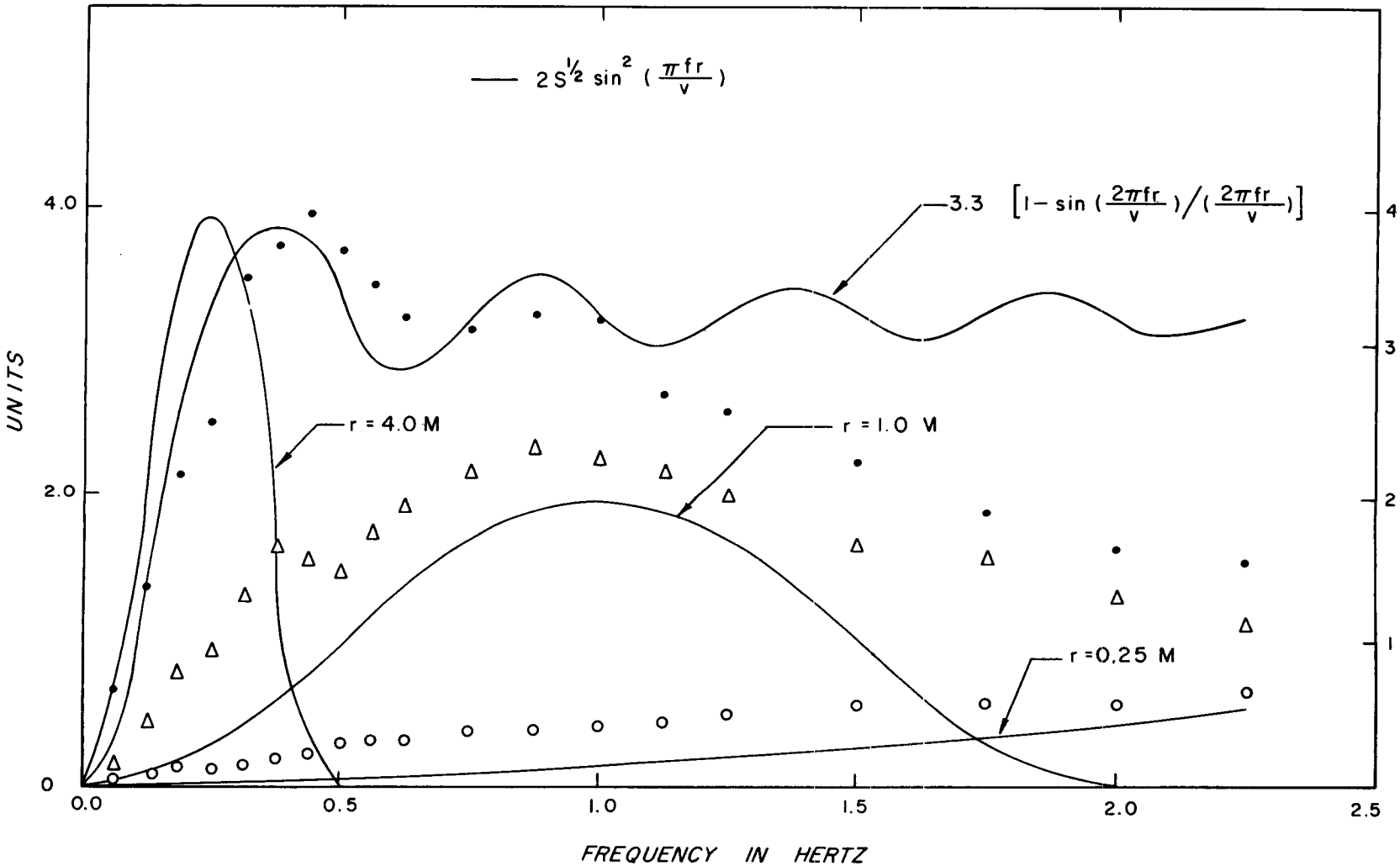

Figure 5-11. Difference Spectra of Example 3 Divided by $Kf^{-5/3}$
(Legend for this figure is on page 43)

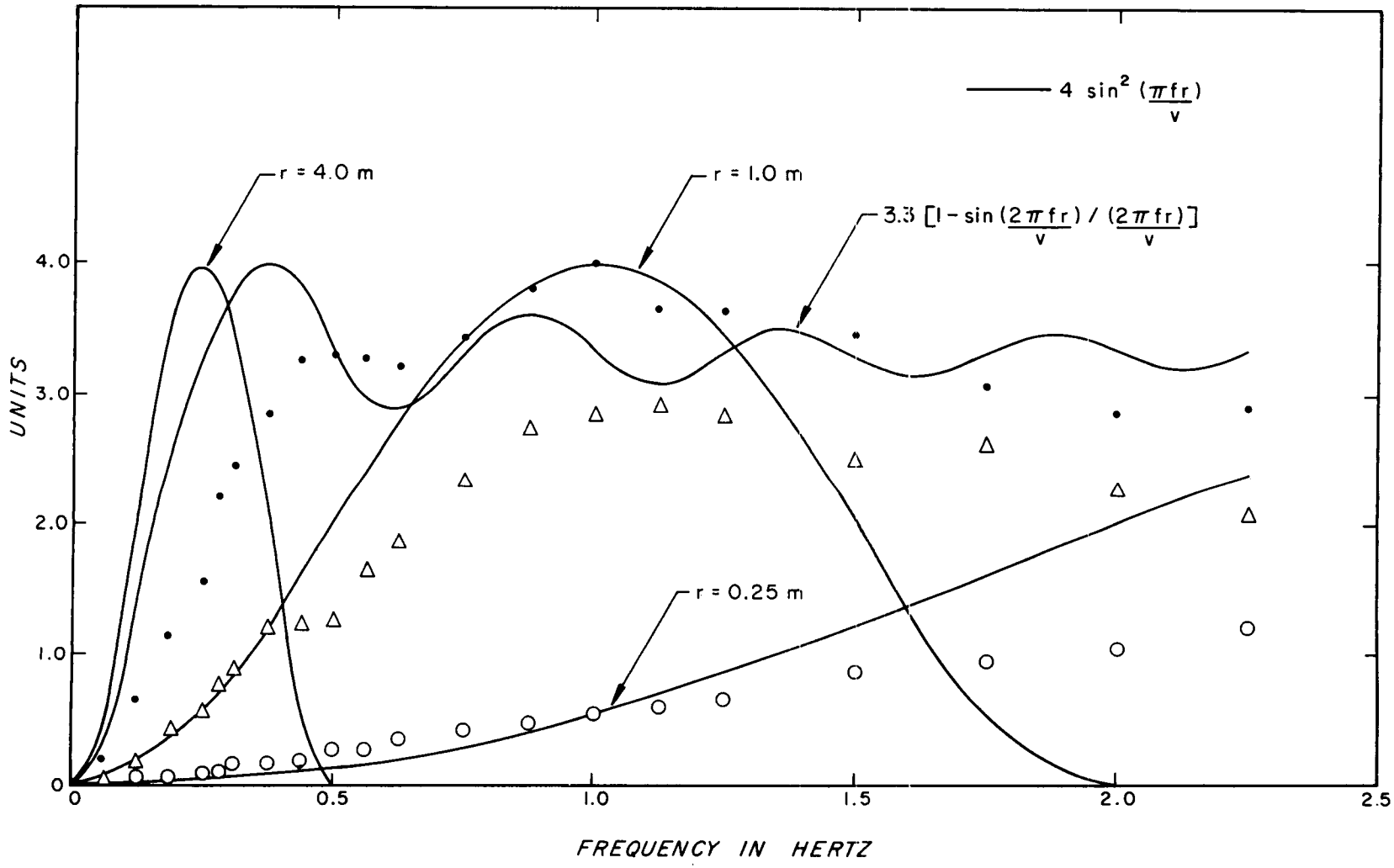

Figure 5-12. Difference Spectra of Example 3 Divided by $Kf^{-2.16}$
(Legend for this figure is on page 43)

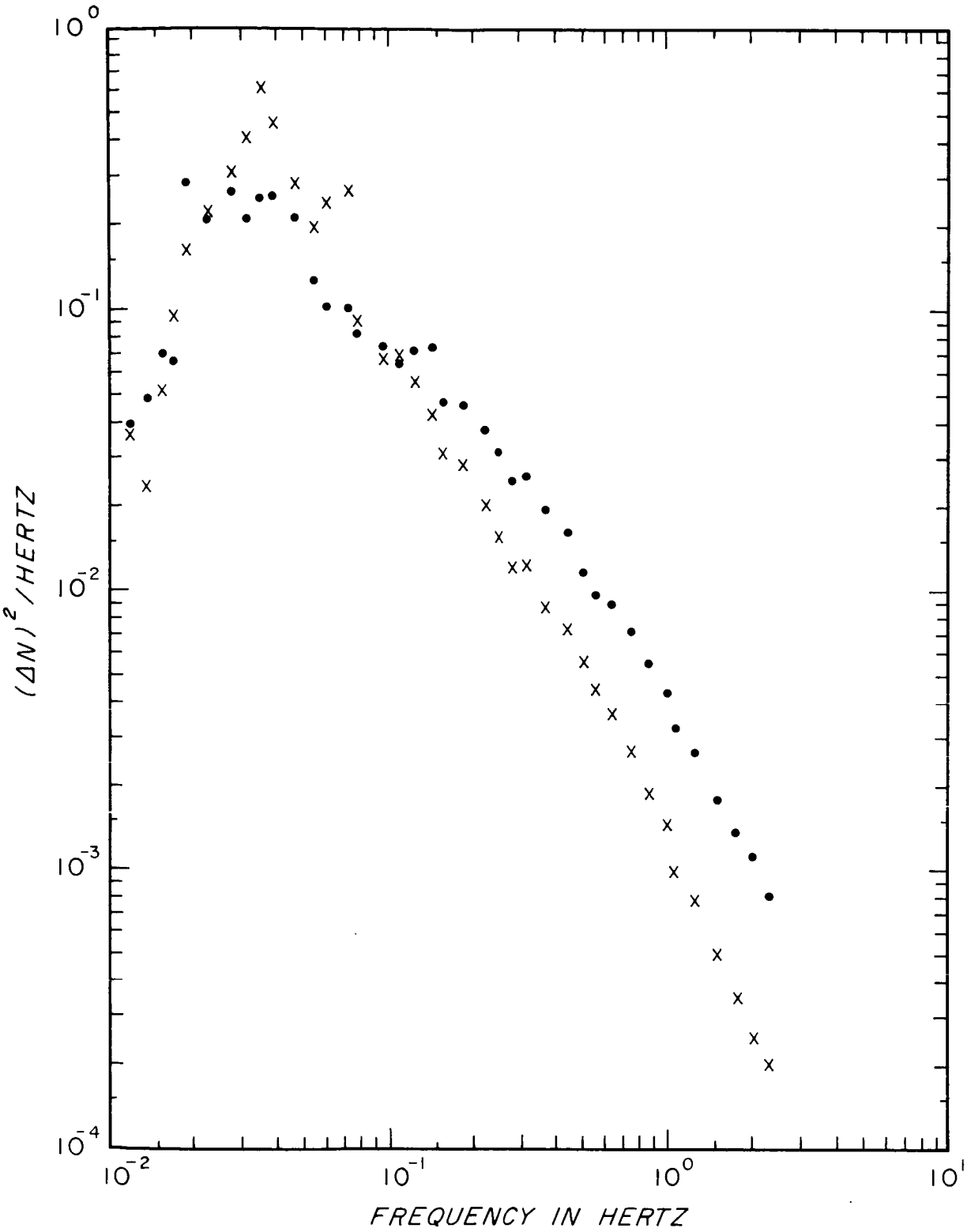

Figure 5-13. Spectra of Example 4 for 5 Meter Separation
(Legend for this figure is on page 43)

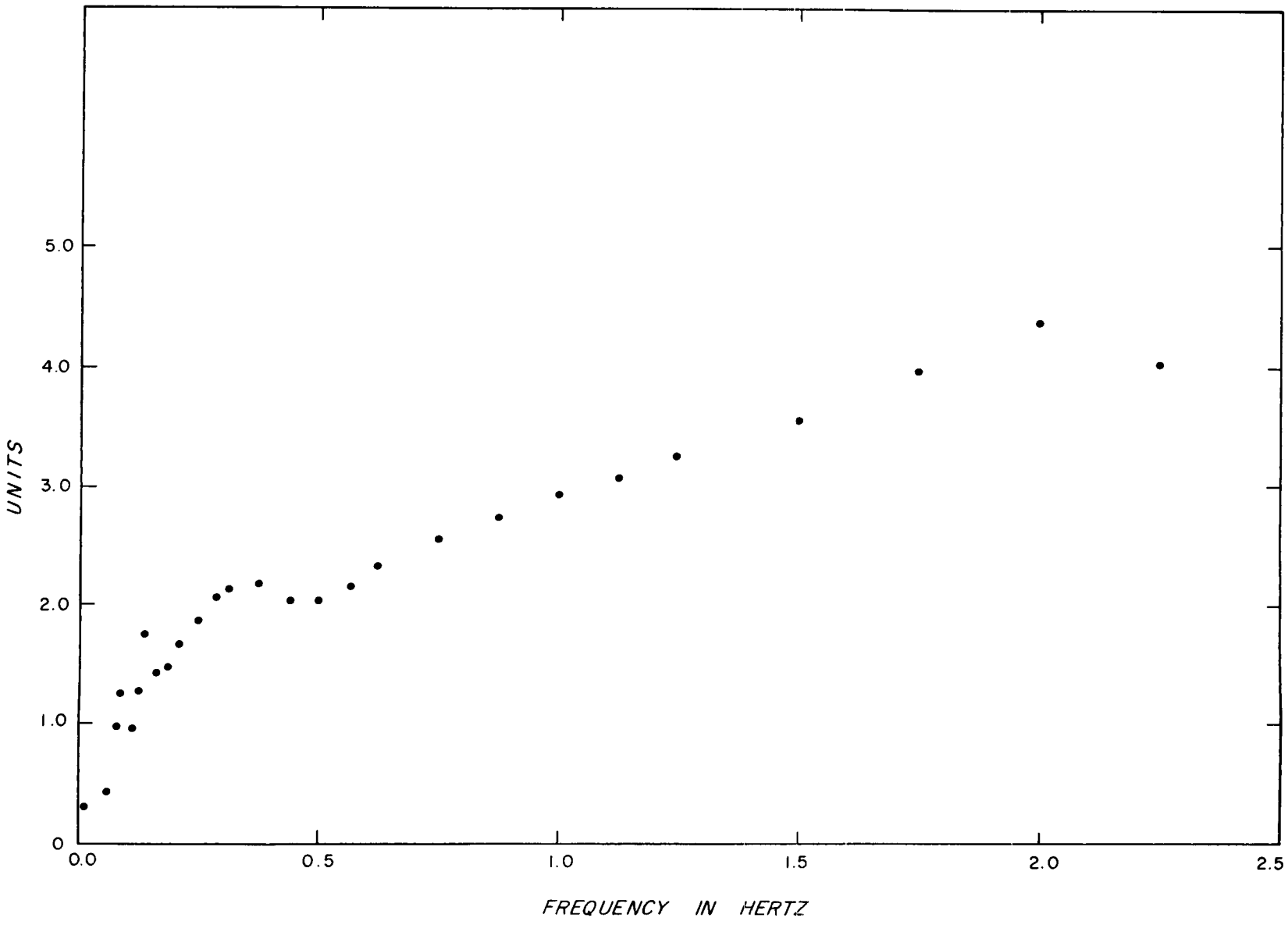

Figure 5-14. Relative Spectra of Example 4 for 5 Meter Separation
(Legend for this figure is on page 43)

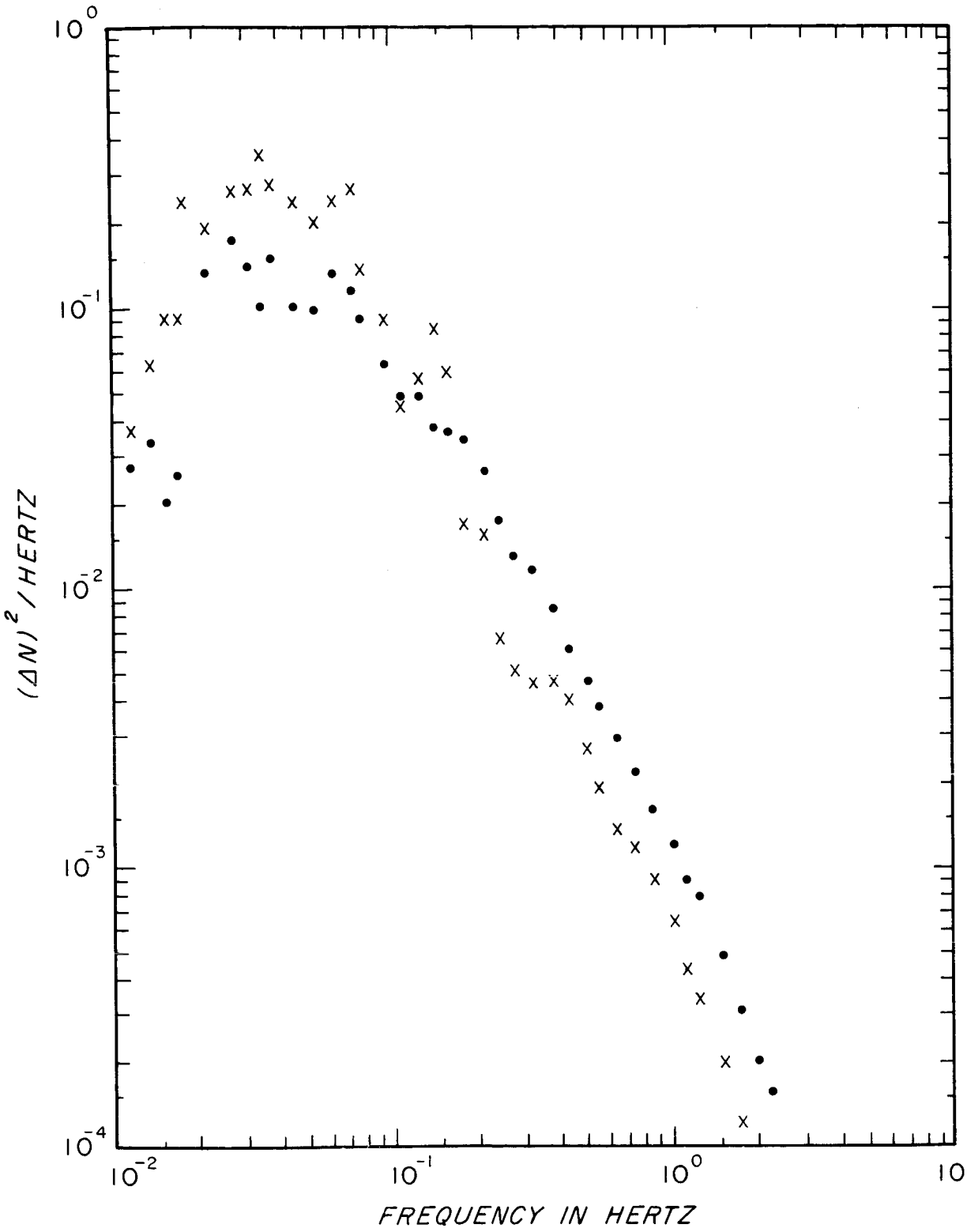

Figure 5-15. Spectra of Example 5 for 10 Meter Separation
(Legend for this figure is on page 43)

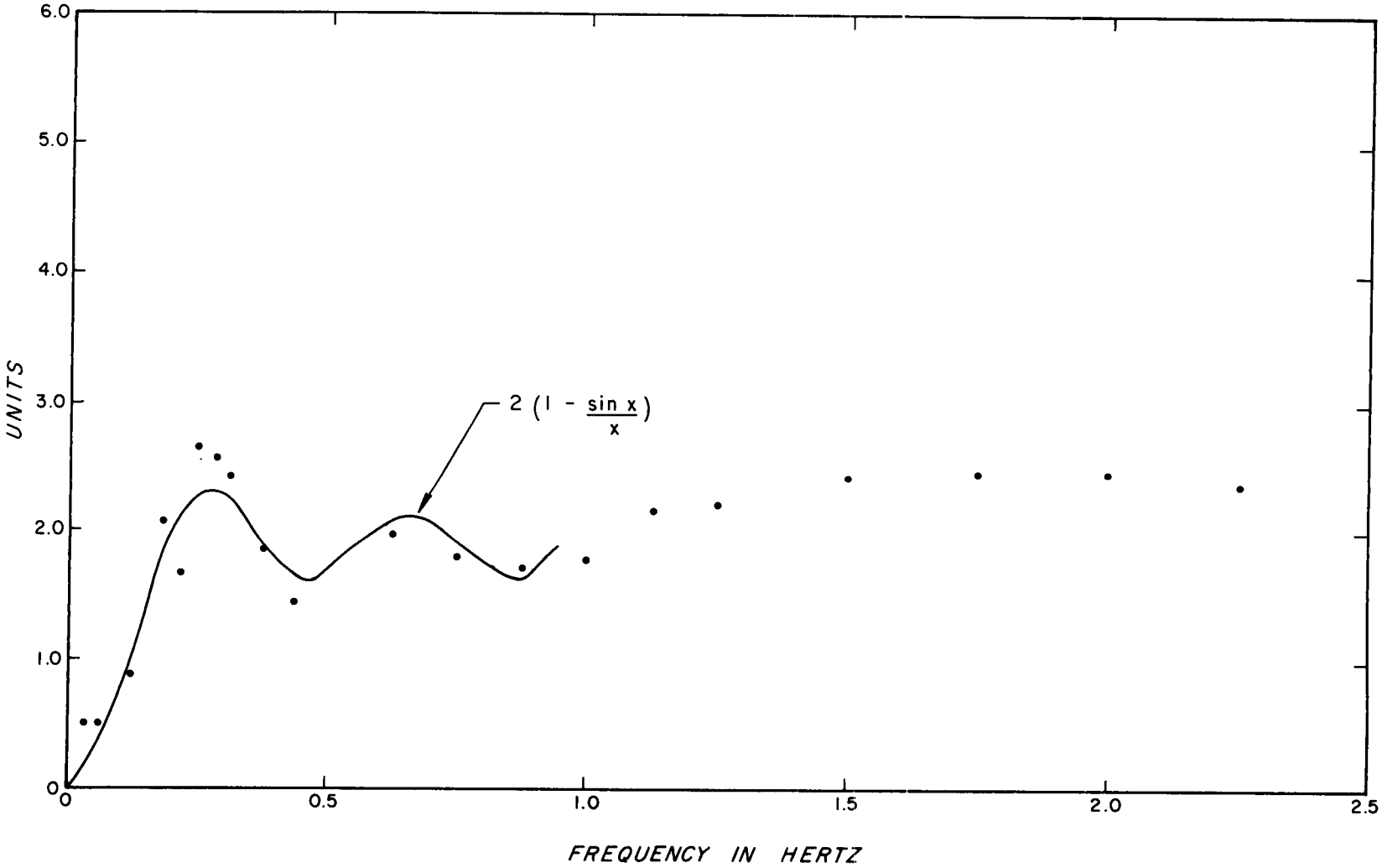

Figure 5-16. Relative Spectra of Example 5 for 10 Meter Separation
(Legend for this figure is on page 43)

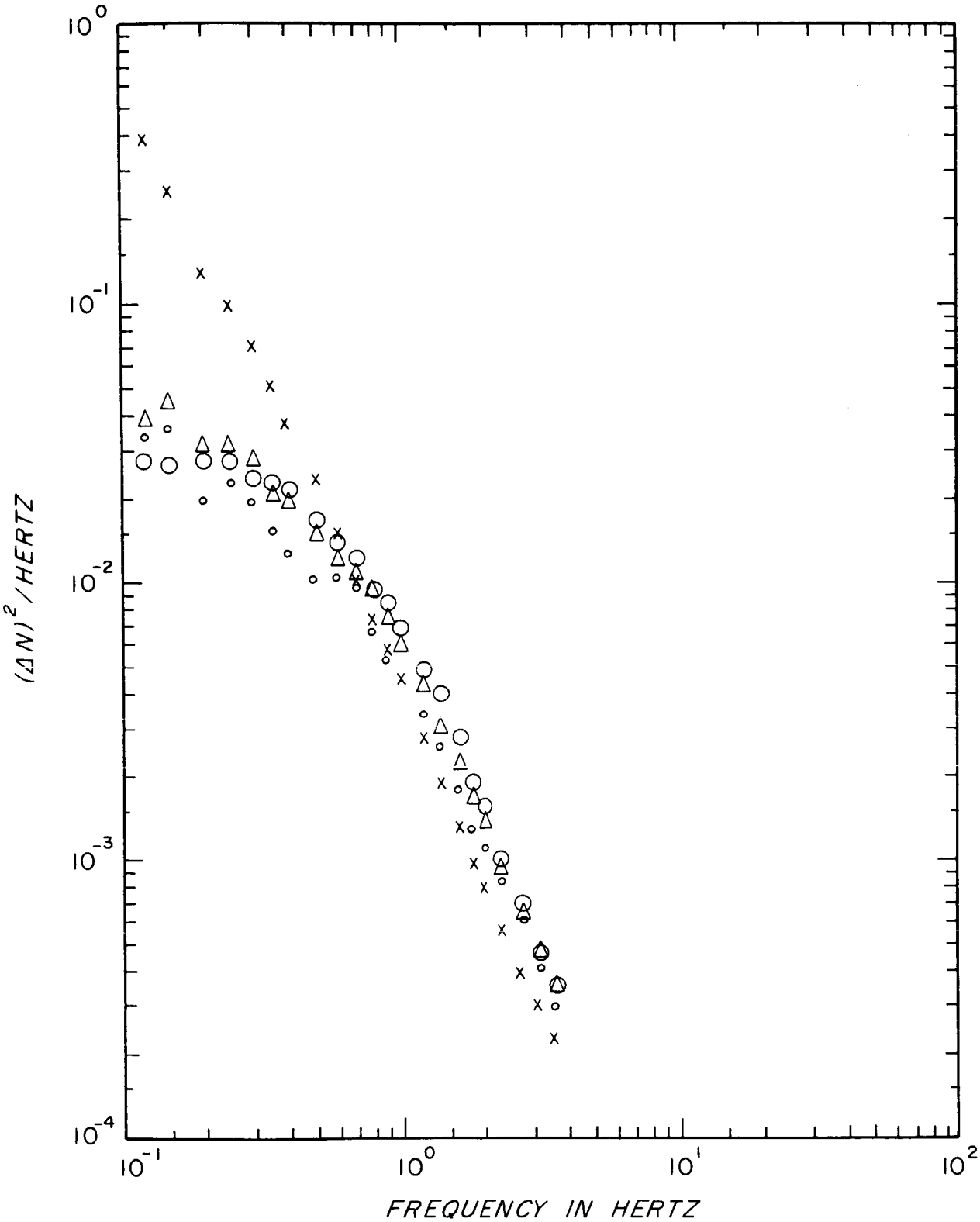

Figure 5-17. Spectra of Example 6 for 0.75 Meter Box Formation
(Legend for this figure is on page 43)

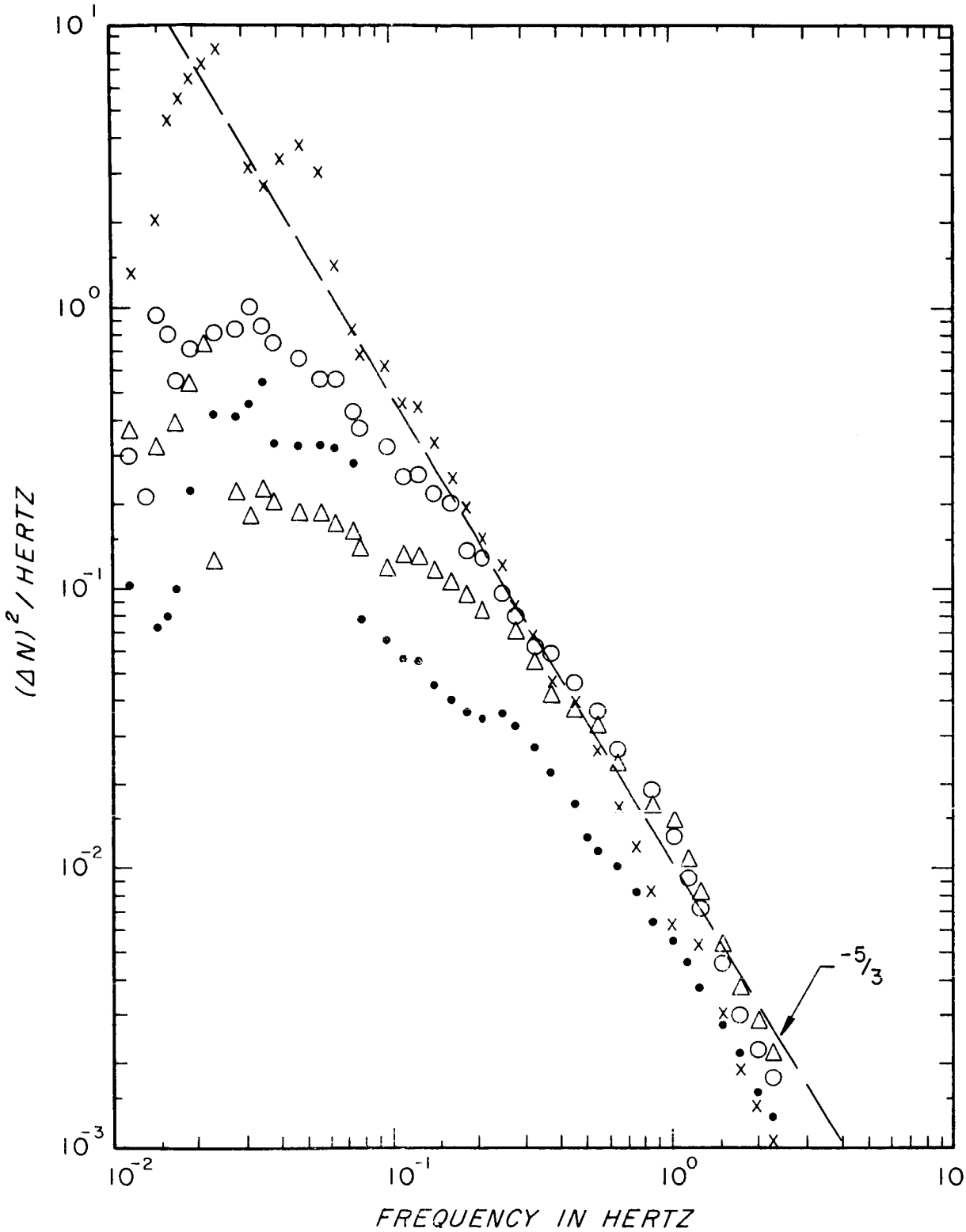

Figure 5-18. Spectra of Example 7 for 0.75 Meter Box Formation
(Legend for this figure is on page 43)

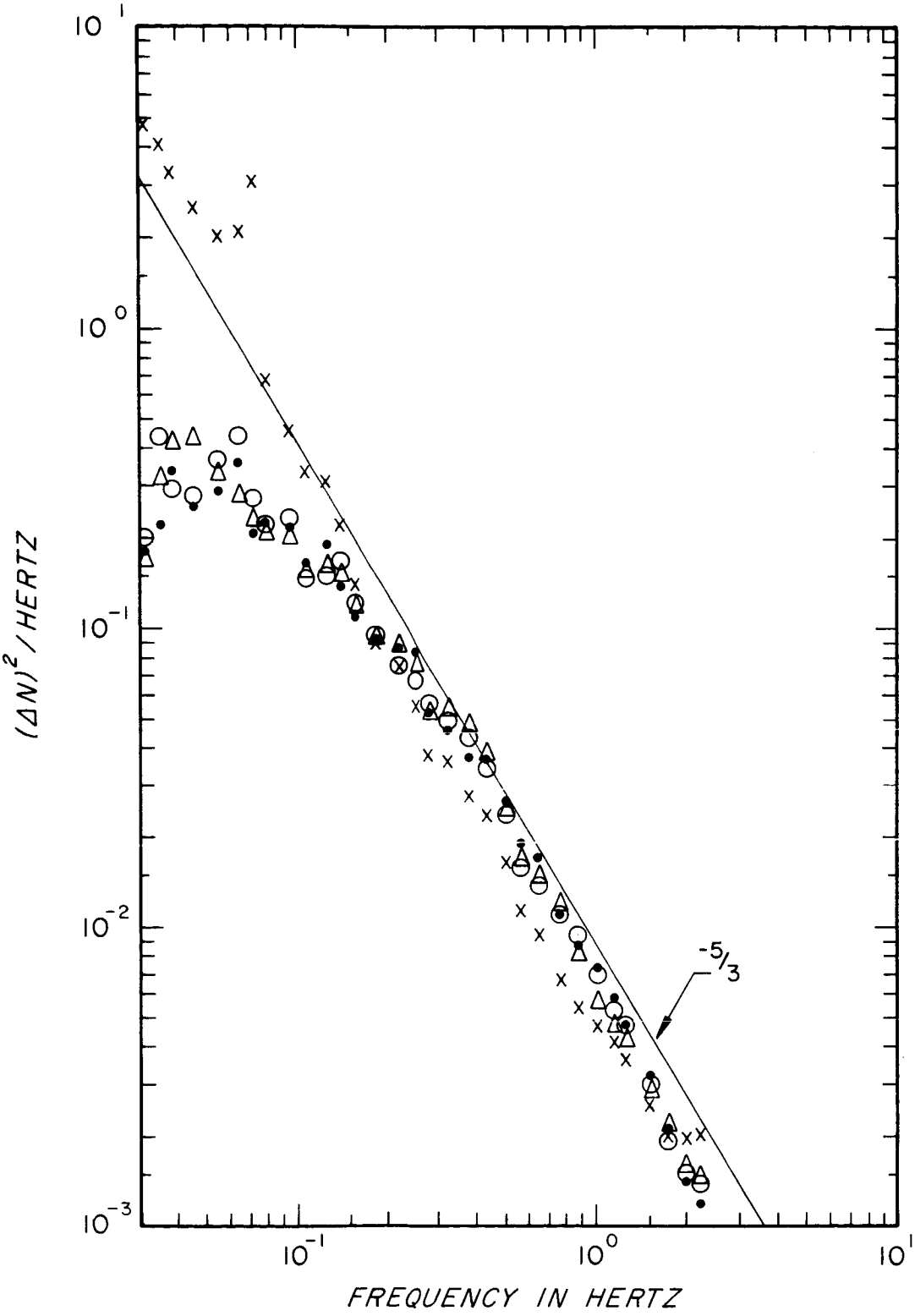

Figure 5-19. Spectra of Example 8 for 0.75 Meter Box Formation
(Legend for this figure is on page 43)

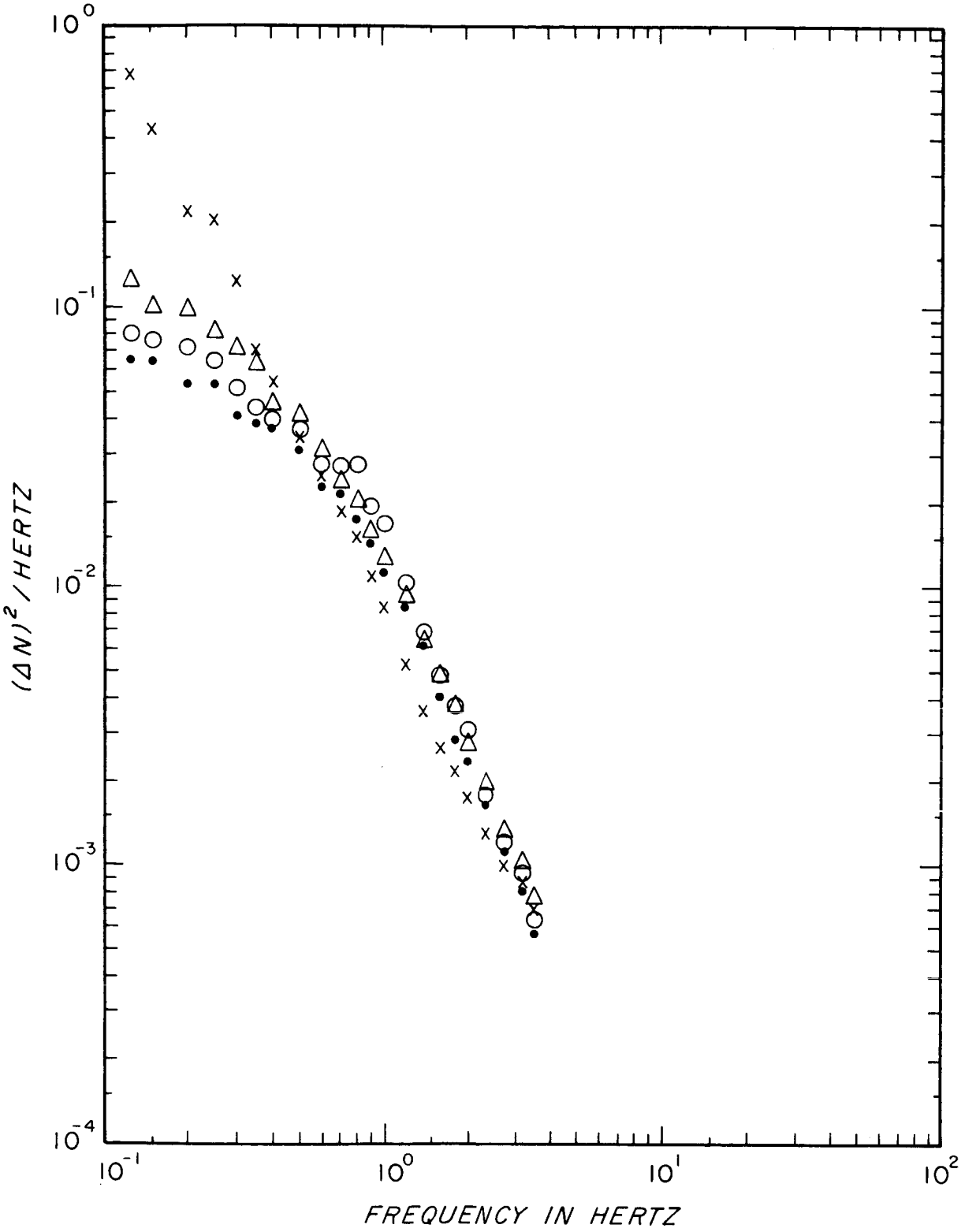

Figure 5-20. Spectra of Example 9 for 0.75 Meter Box Formation
(Legend for this figure is on page 43)

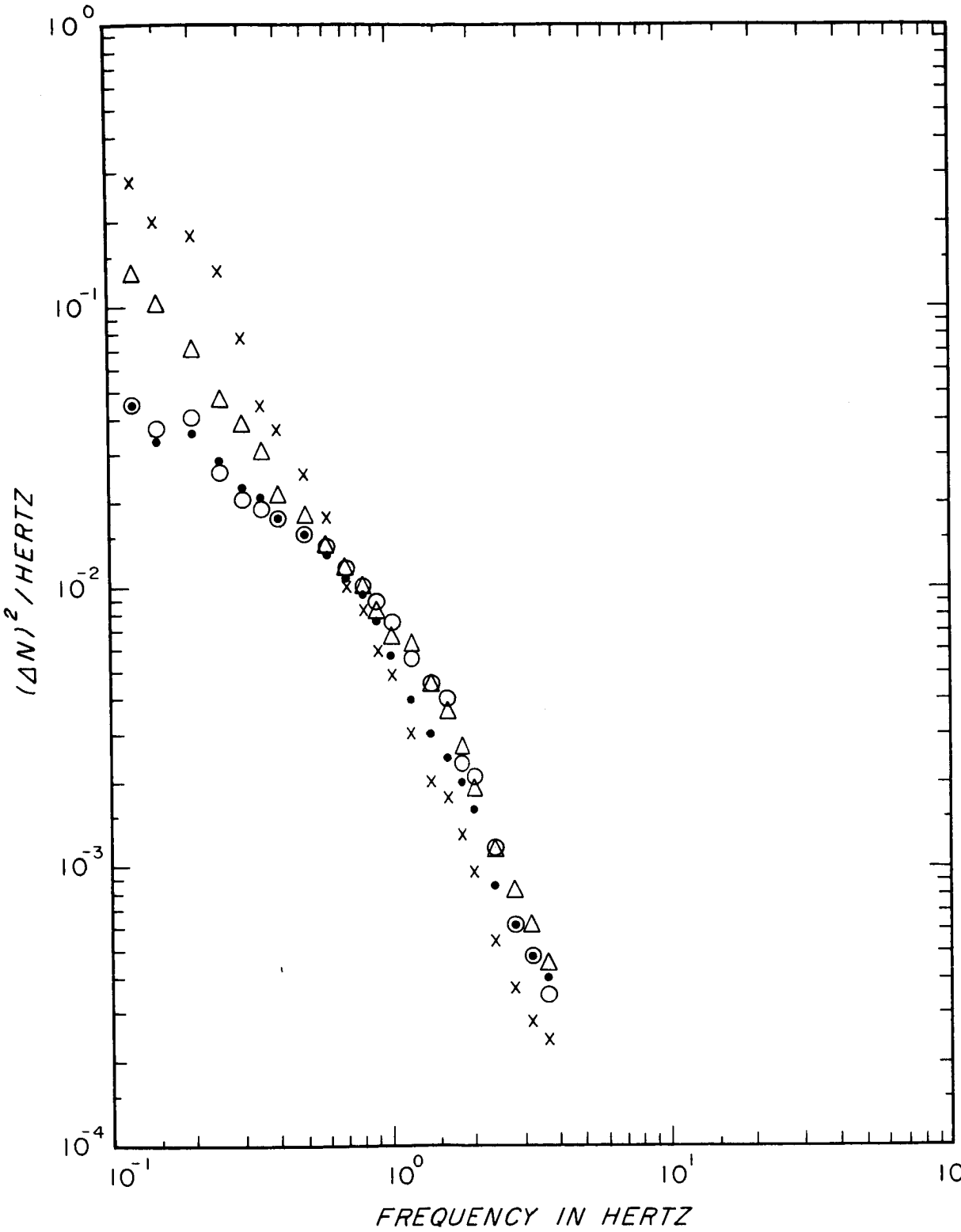

Figure 5-21. Spectra of Example 10 for 0.75 Meter Box Formation
(Legend for this figure is on page 43)

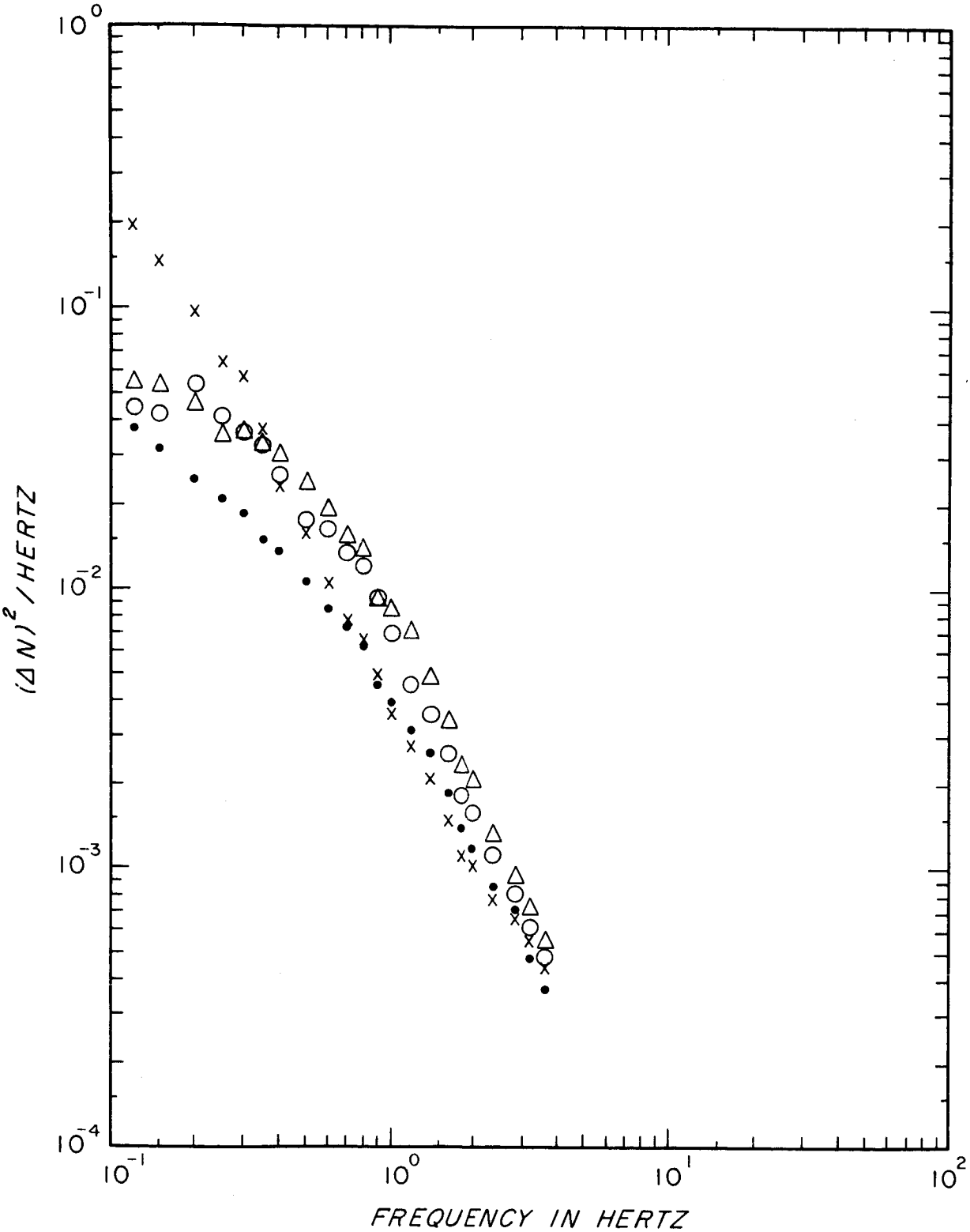

Figure 5-22. Spectra of Example 11 for 0.75 Meter Box Formation
(Legend for this figure is on page 43)

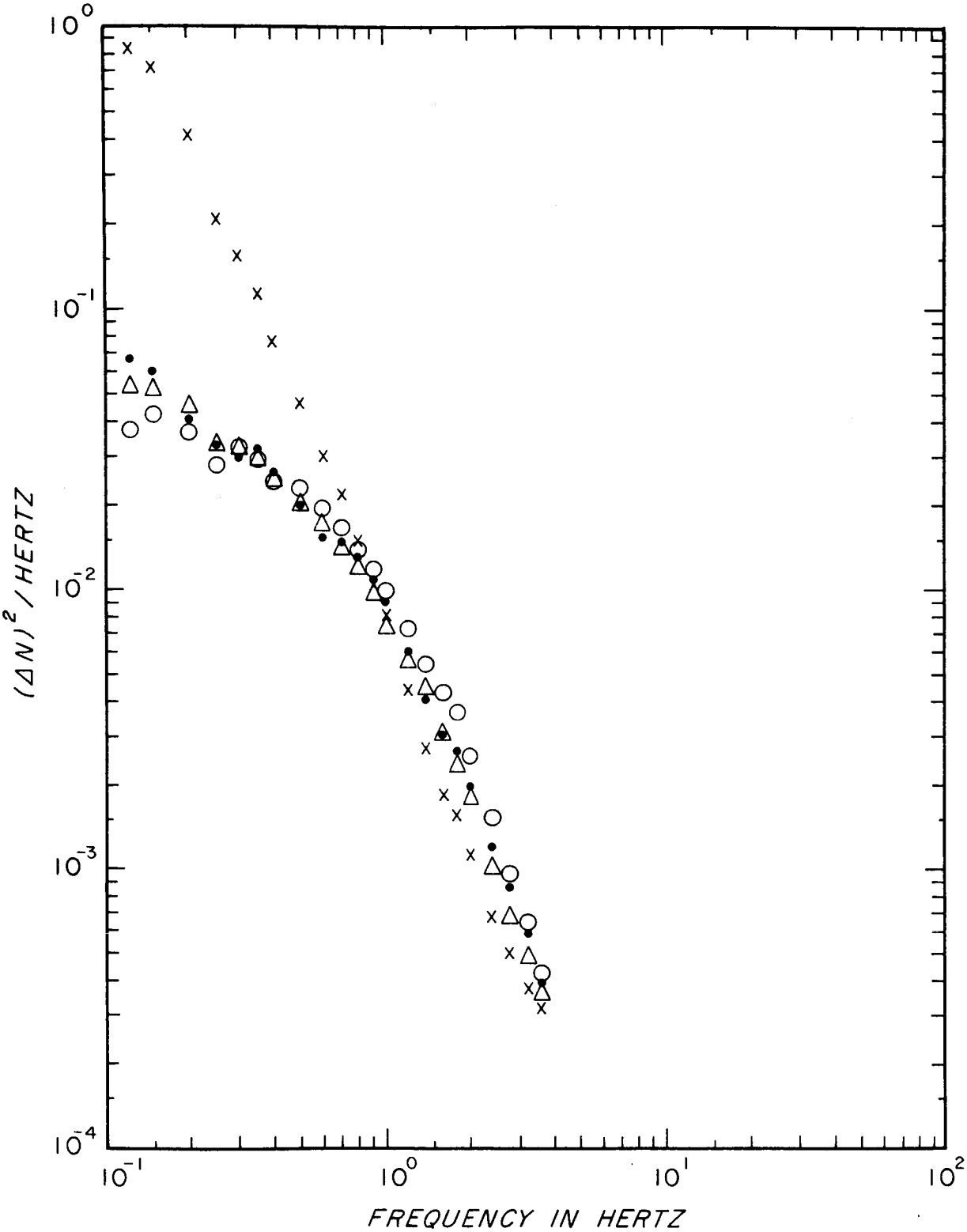

Figure 5-23. Spectra of Example 12 for 0.75 Meter Box Formation
(Legend for this figure is on page 43)

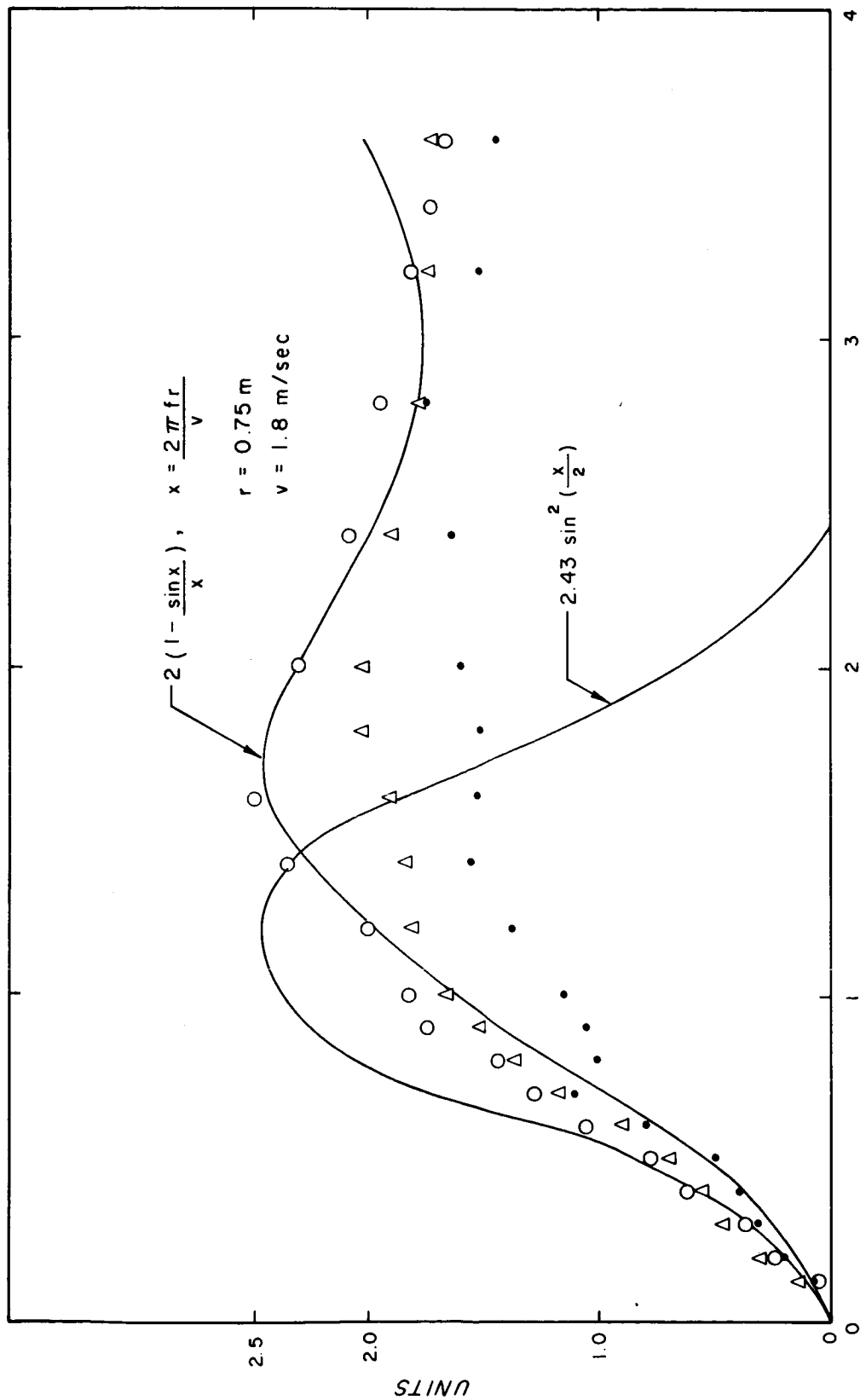

Figure 5-24. Relative Spectra of Example 6 for 0.75 Meter Box Formation (Legend for this figure is on page 43)

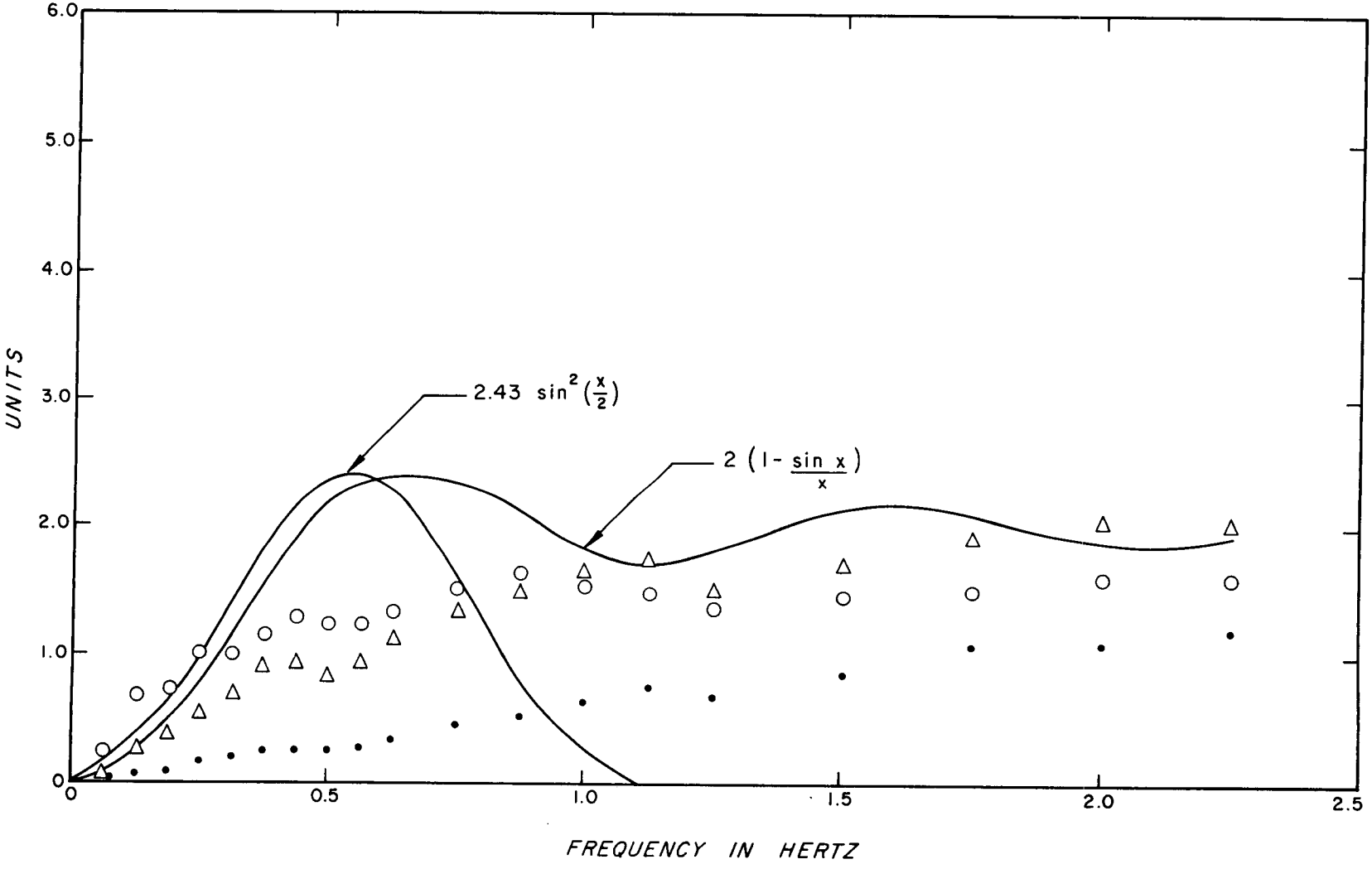

Figure 5-25. Relative Spectra of Example 7 for 0.75 Meter Box Formation (Legend for this figure is on page 43)

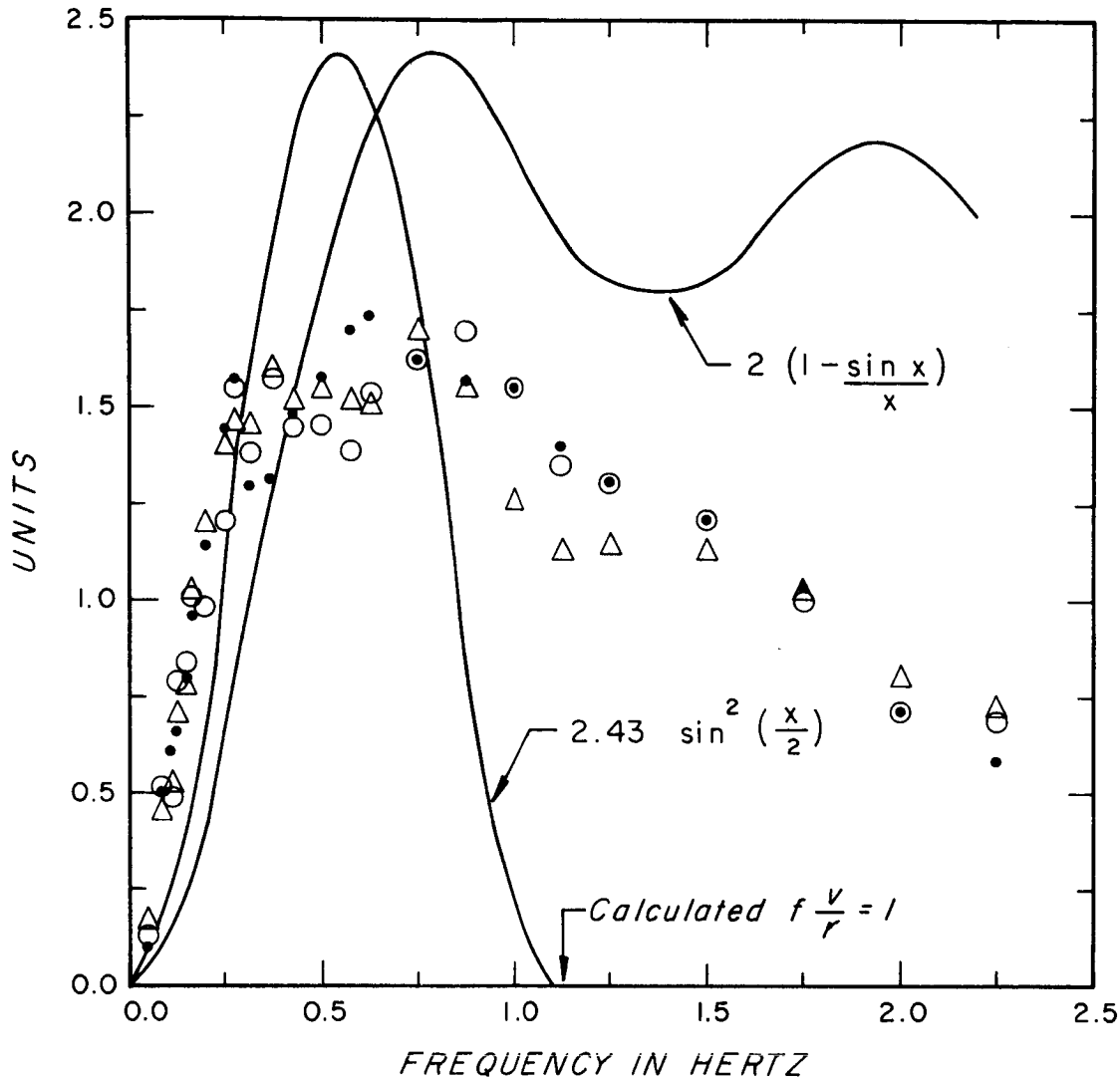

Figure 5-26. Relative Spectra of Example 8 for 0.75 Meter Box Formation (Legend for this figure is on page 43)

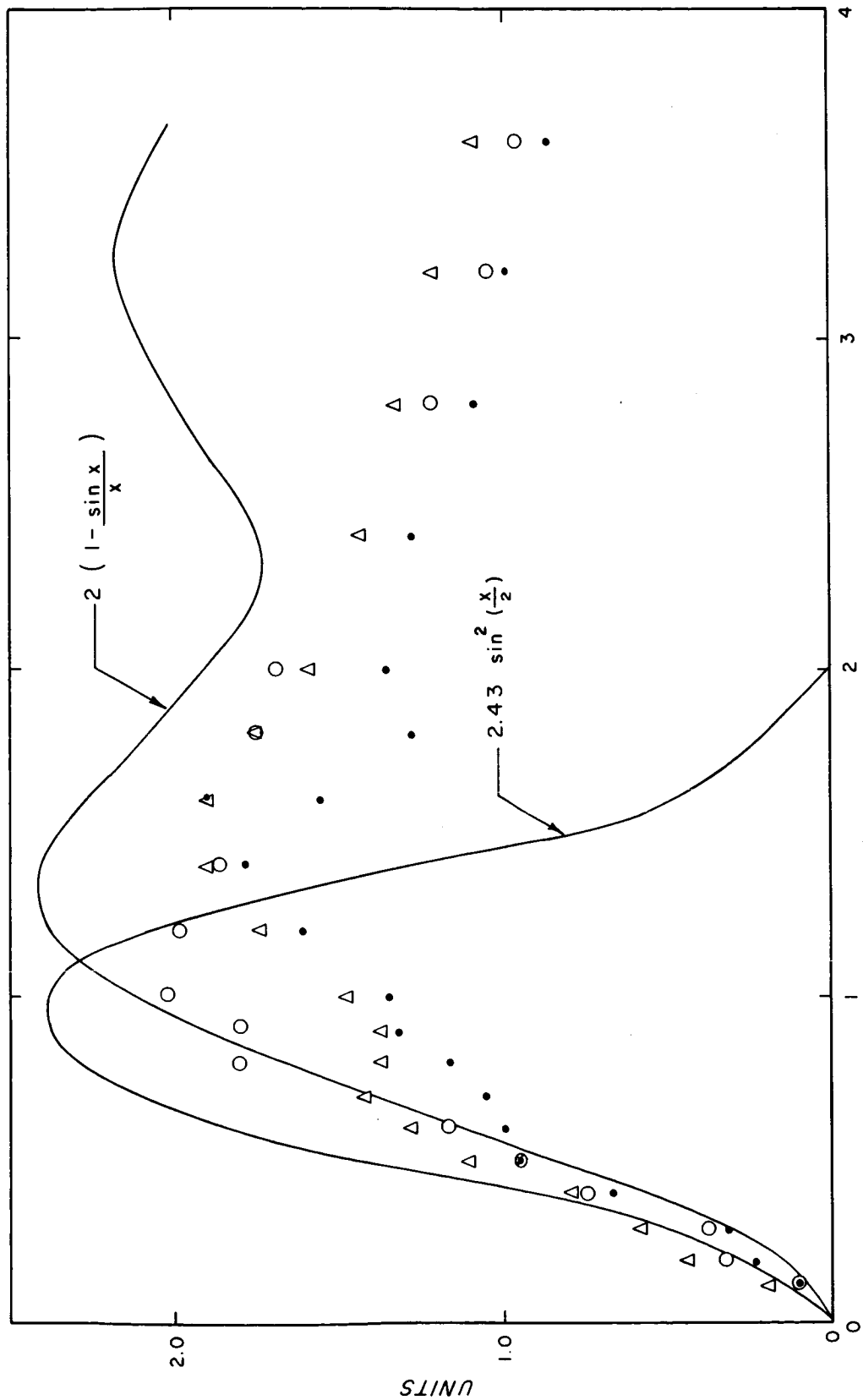

Figure 5-27. Relative Spectra of Example 9 for 0.75 Meter Box Formation (Legend for this figure is on page 43)

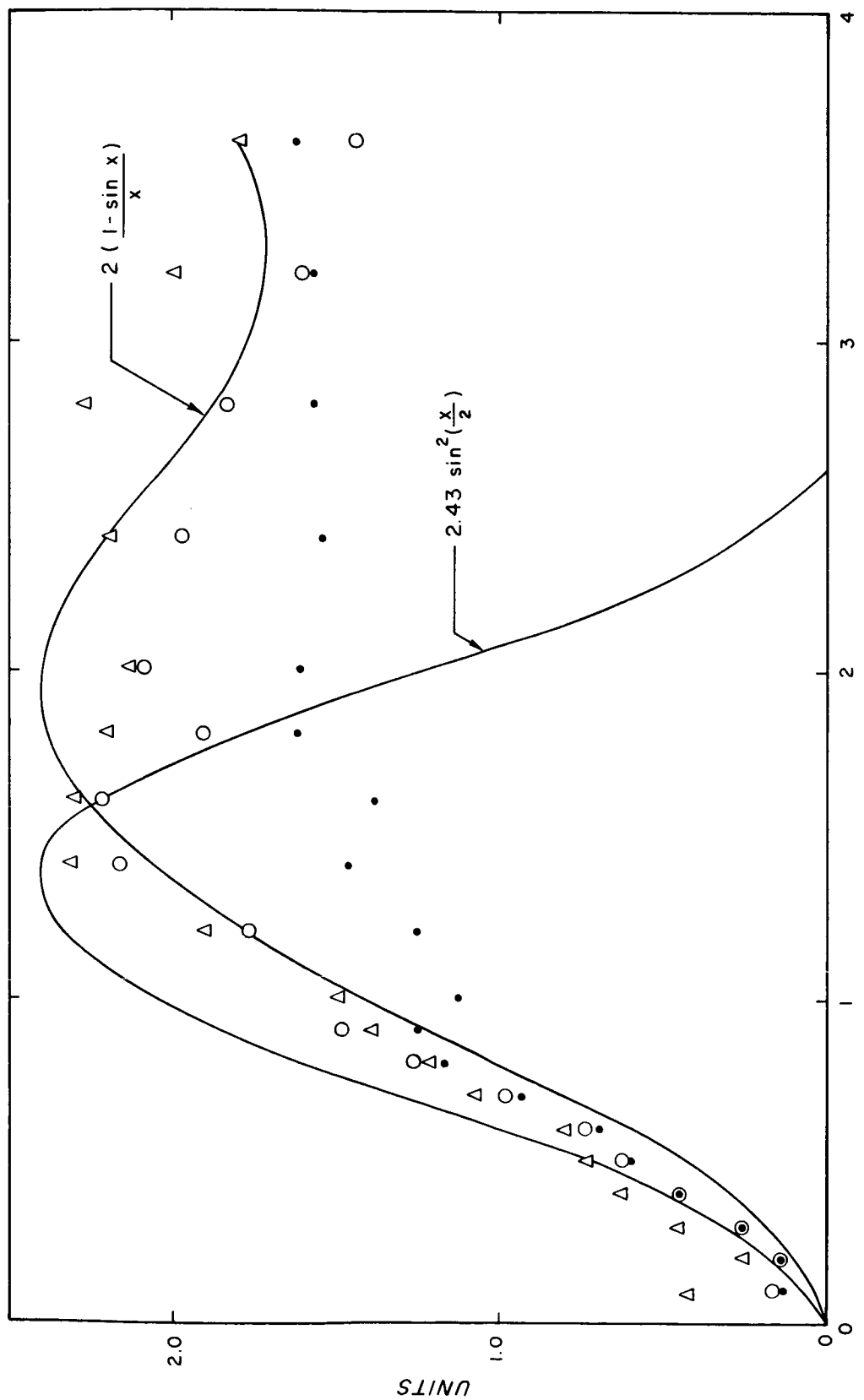

Figure 5-28. Relative Spectra of Example 10 for 0.75 Meter Box Formation (Legend for this figure is on page 43)

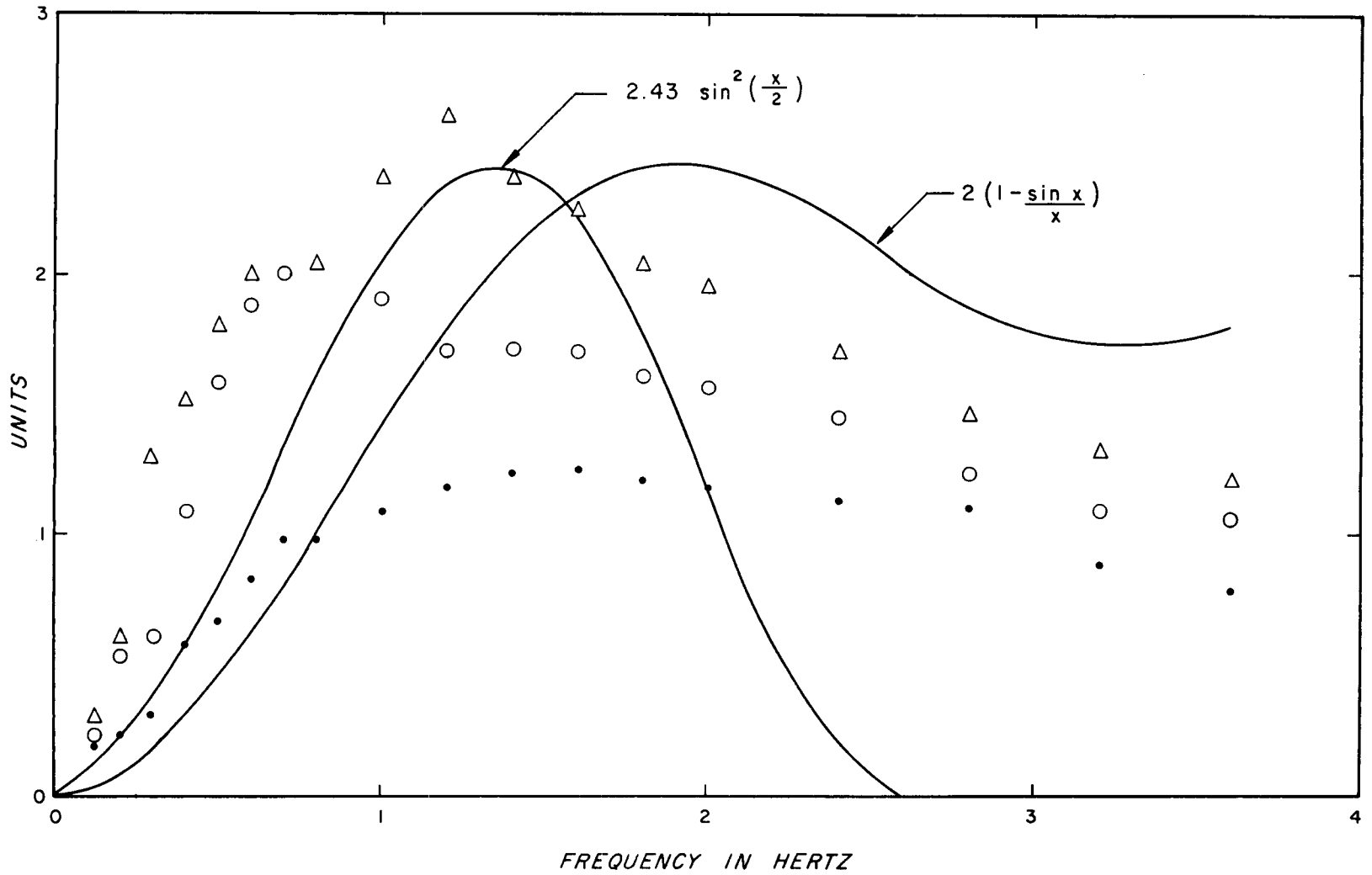

Figure 5-29. Relative Spectra of Example 11 for 0.75 Meter Box Formation (Legend for this figure is on page 43)

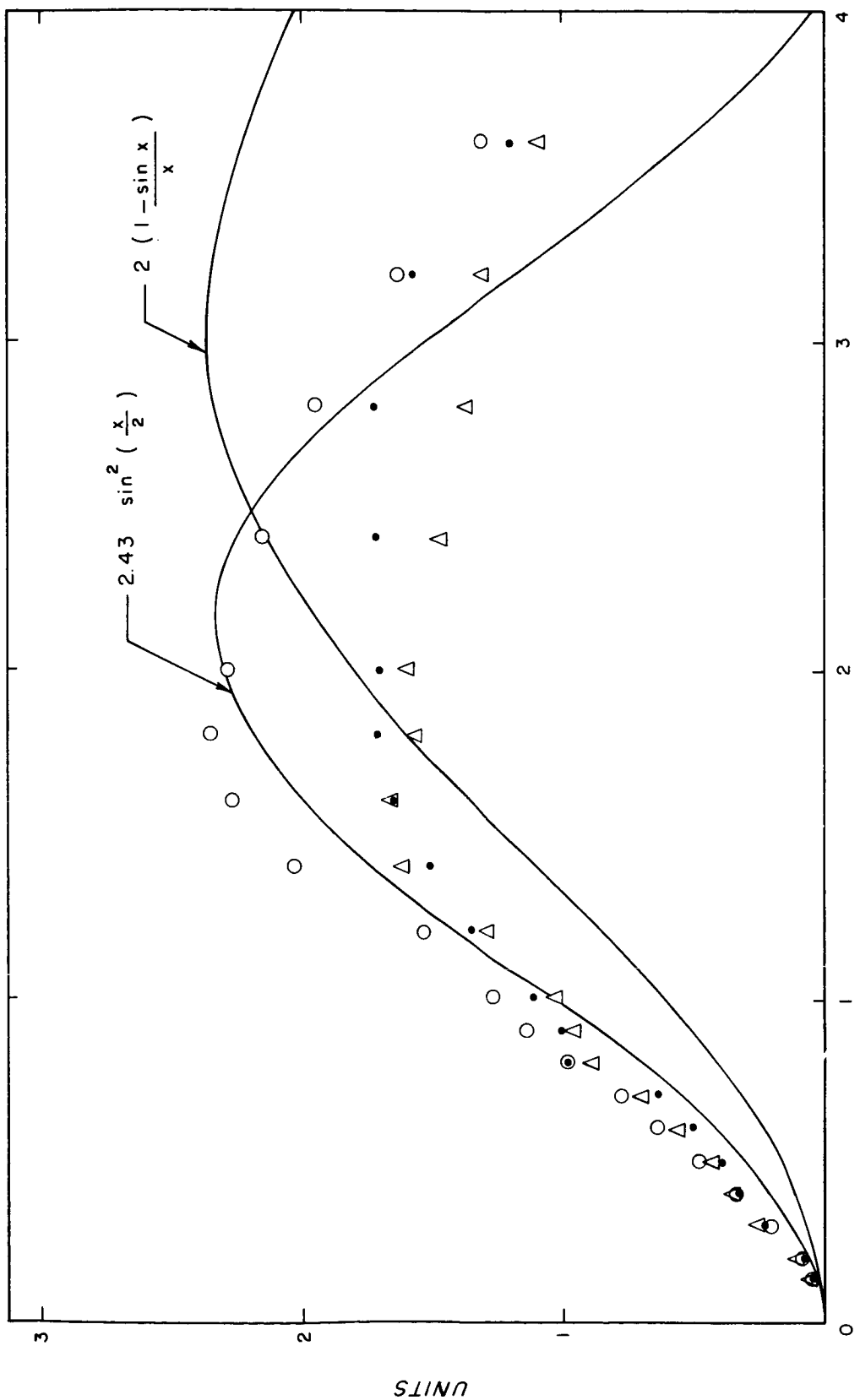

Figure 5-30. Relative Spectra of Example 12 for 0.75 Meter Box Formation (Legend for this figure is on page 43)

For the simultaneous measurements of the differences in three orthogonal directions, the normalized spectra are very similar in their overall shape. For the lower frequencies, the three spectra are of similar magnitudes in most of the cases. At the higher frequencies, the spectra of the downwind component exceed those of the crosswind component typically by 10 to 20 per cent and that of the vertical component by 15 to 25 per cent.

b. 1.8 meter spacing. Example 13 is for a 1.8 meter box formation. The log-log spectra are shown in Fig. 5-31 and the relative spectra for an assumed single unit variation of $Kf^{-5/3}$ are shown in Fig. 5-32. Figure 5-33 shows the relative spectra for an assumed single unit spectra of the form $Kf^{-2.16}$. Because of uncertainty in the mean wind speed, an arbitrary value of this velocity was used in Figs. 5-32 and 5-33 to provide a good fit with the measured data.

In addition to spectral analysis, amplitude distributions were determined for both difference and single unit refractive index data. Information about amplitude variations can be obtained from amplitude distribution plots.

C. Amplitude Distributions

1. In-Line Spacing

Amplitude distribution plots for examples 1 through 5 are shown in Figs. 5-34 through 5-38, respectively. These plots can be divided into three parts. One part extends approximately from

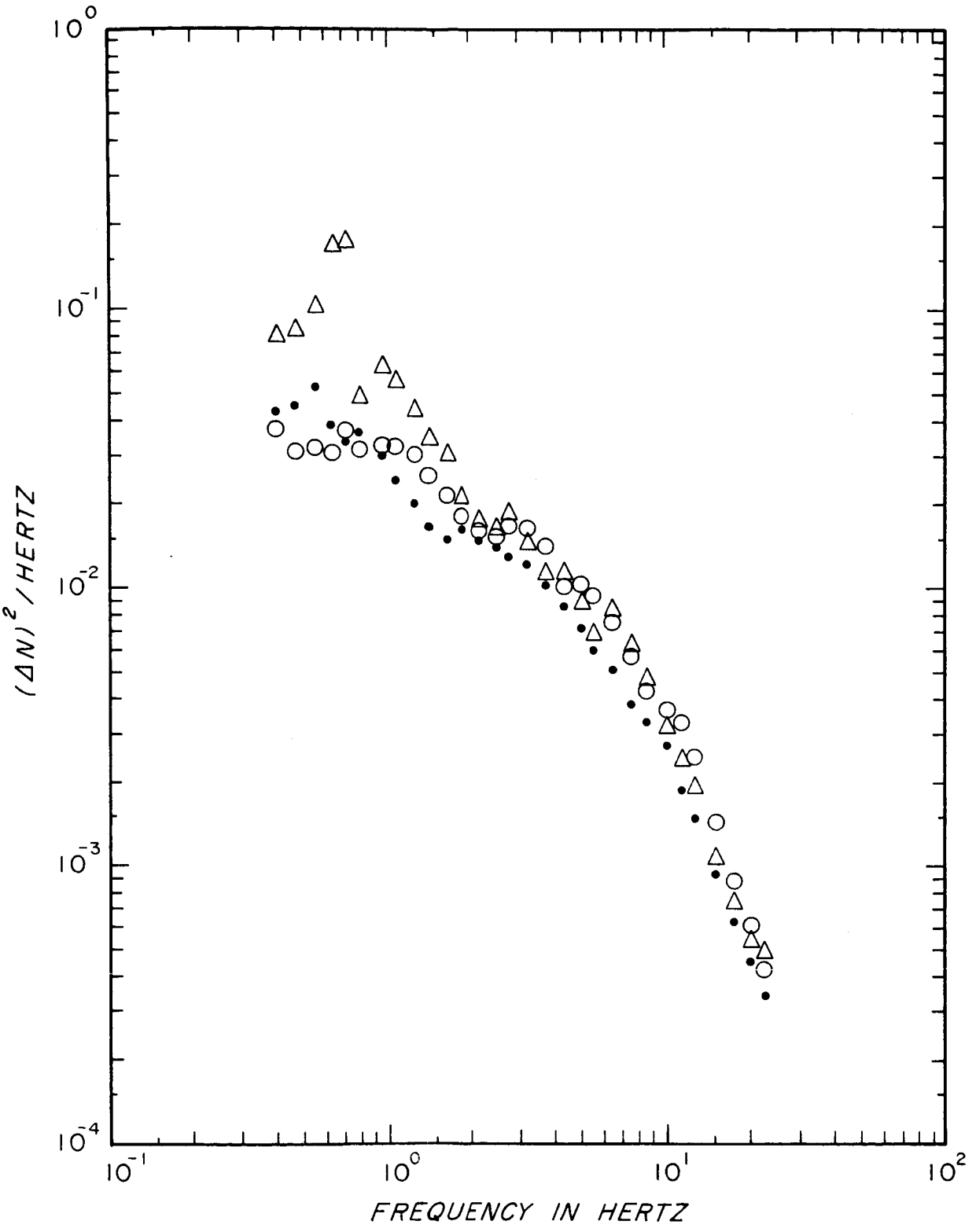

Figure 5-31. Spectra of Example 13 for 1.8 Meter Box Formation
(Legend for this figure is on page 43)

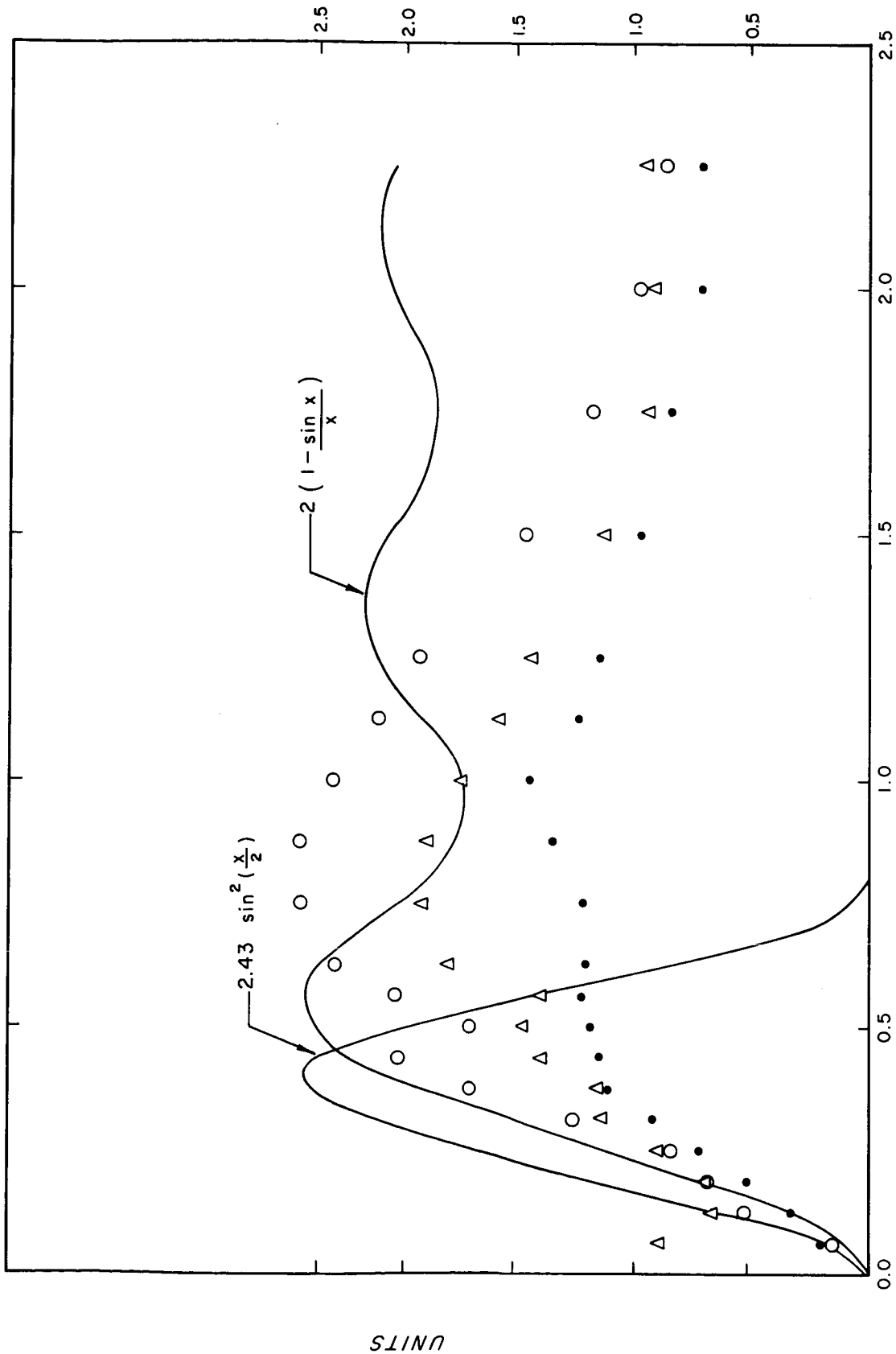

Figure 5-32. Difference Spectra of Example 13 Divided by $Kf^{-5/3}$
(Legend for this figure is on page 43)

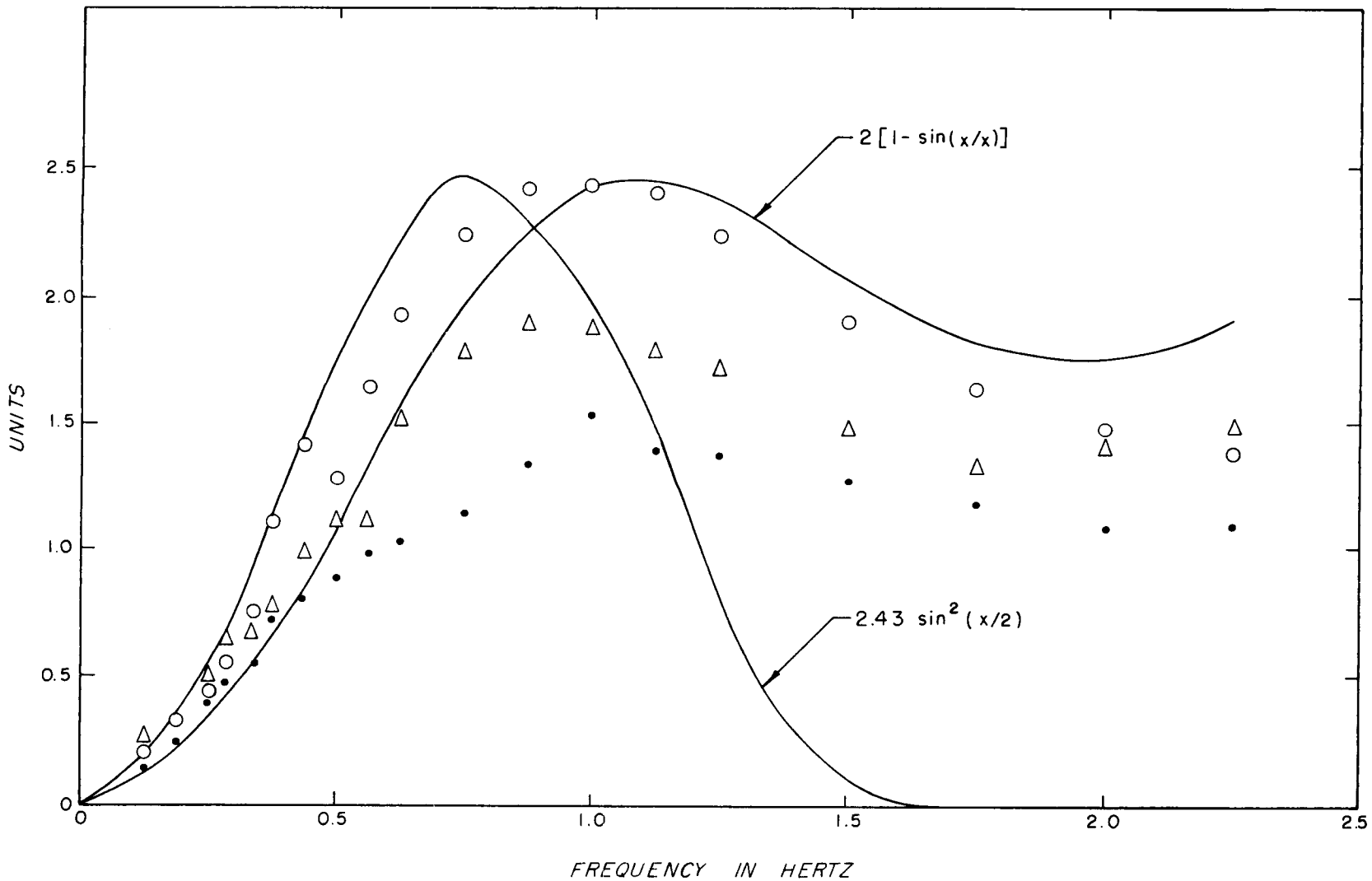

Figure 5-33. Difference Spectra of Example 13 Divided by $Kf^{-2.16}$
(Legend for this figure is on page 43)

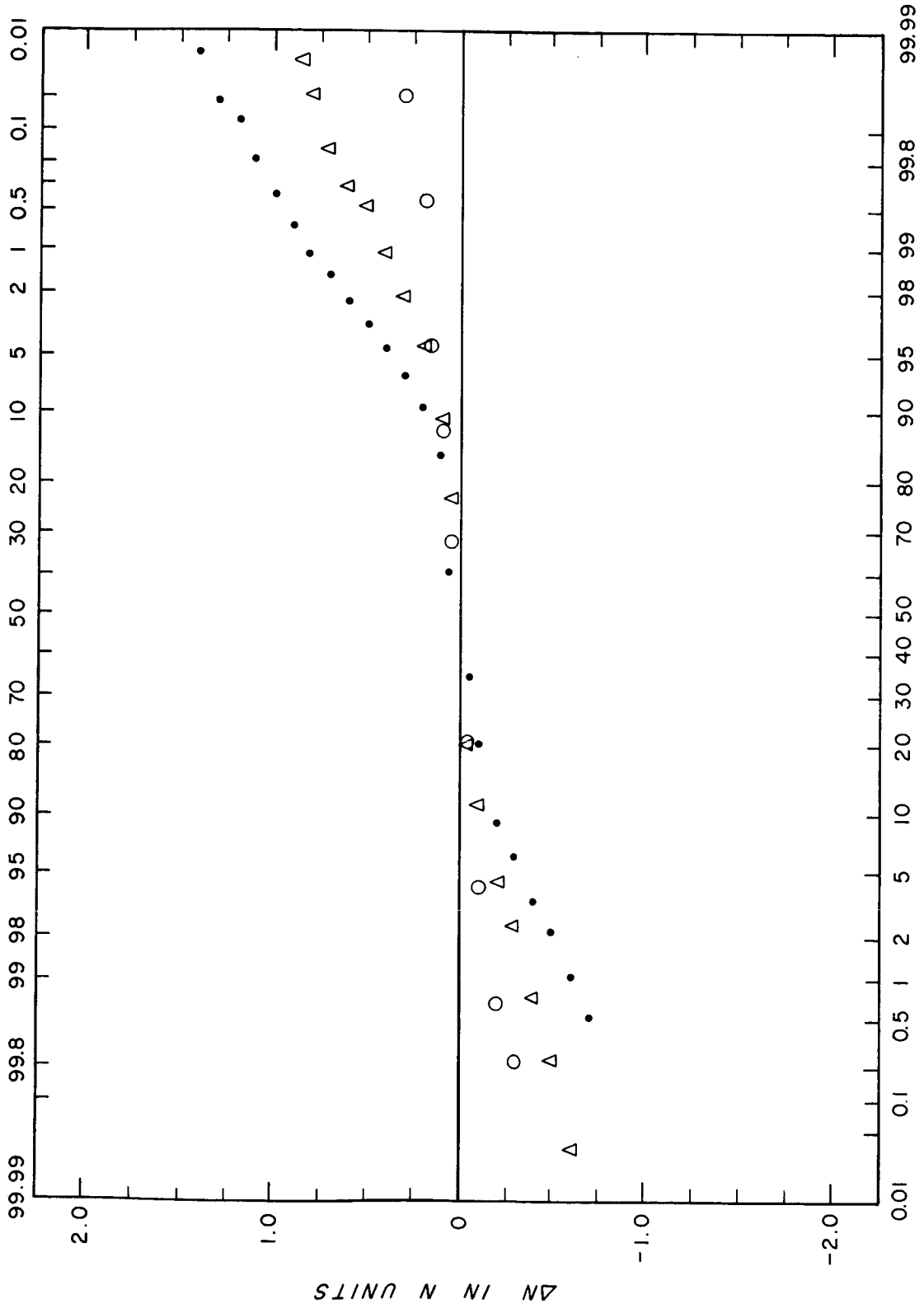

Figure 5-34. Amplitude Distribution of Example 1 for In-Line Formation (Legend for this figure is on page 43)

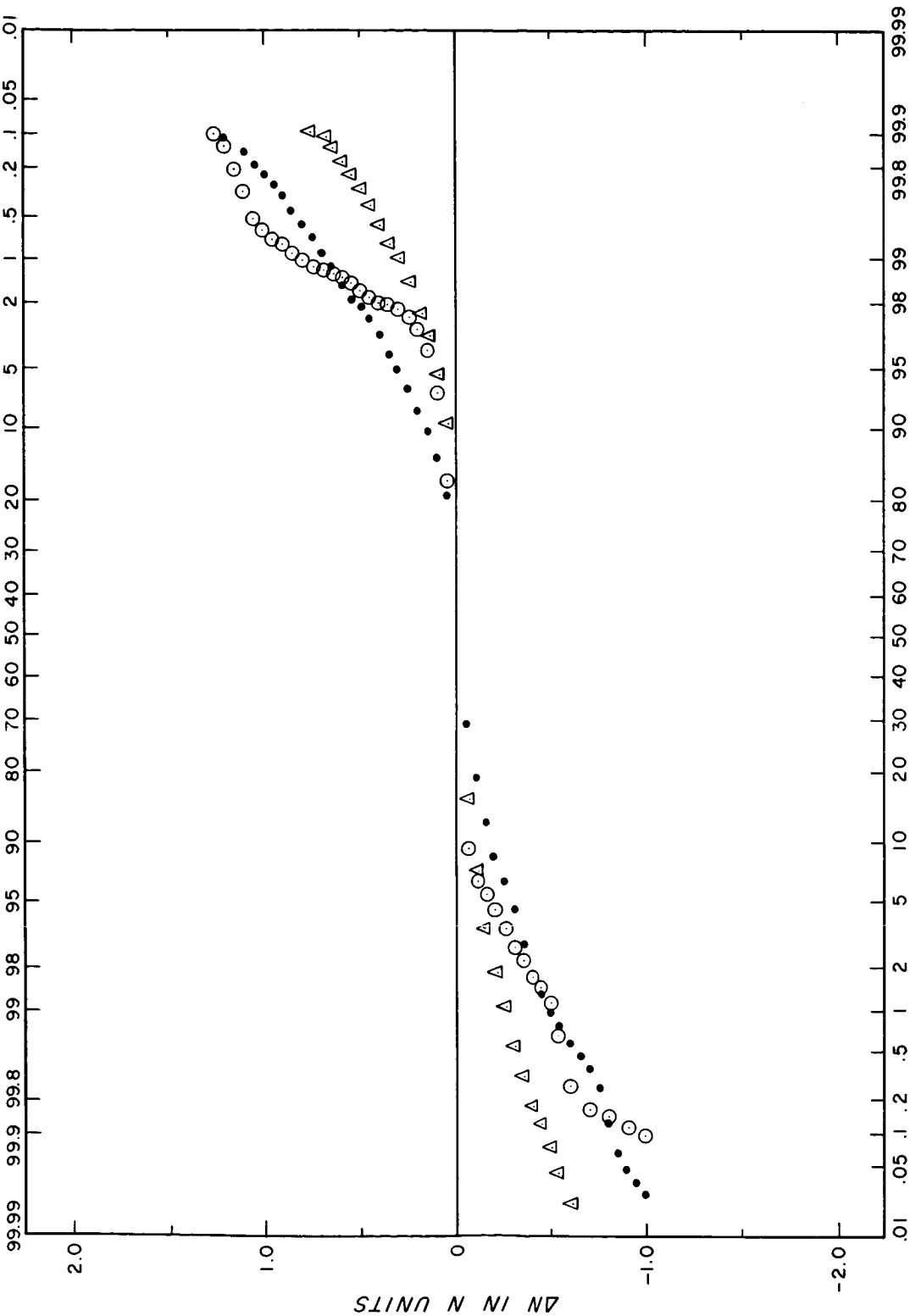

Figure 5-35. Amplitude Distribution of Example 2 for In-line Formation (Legend for this figure is on page 43)

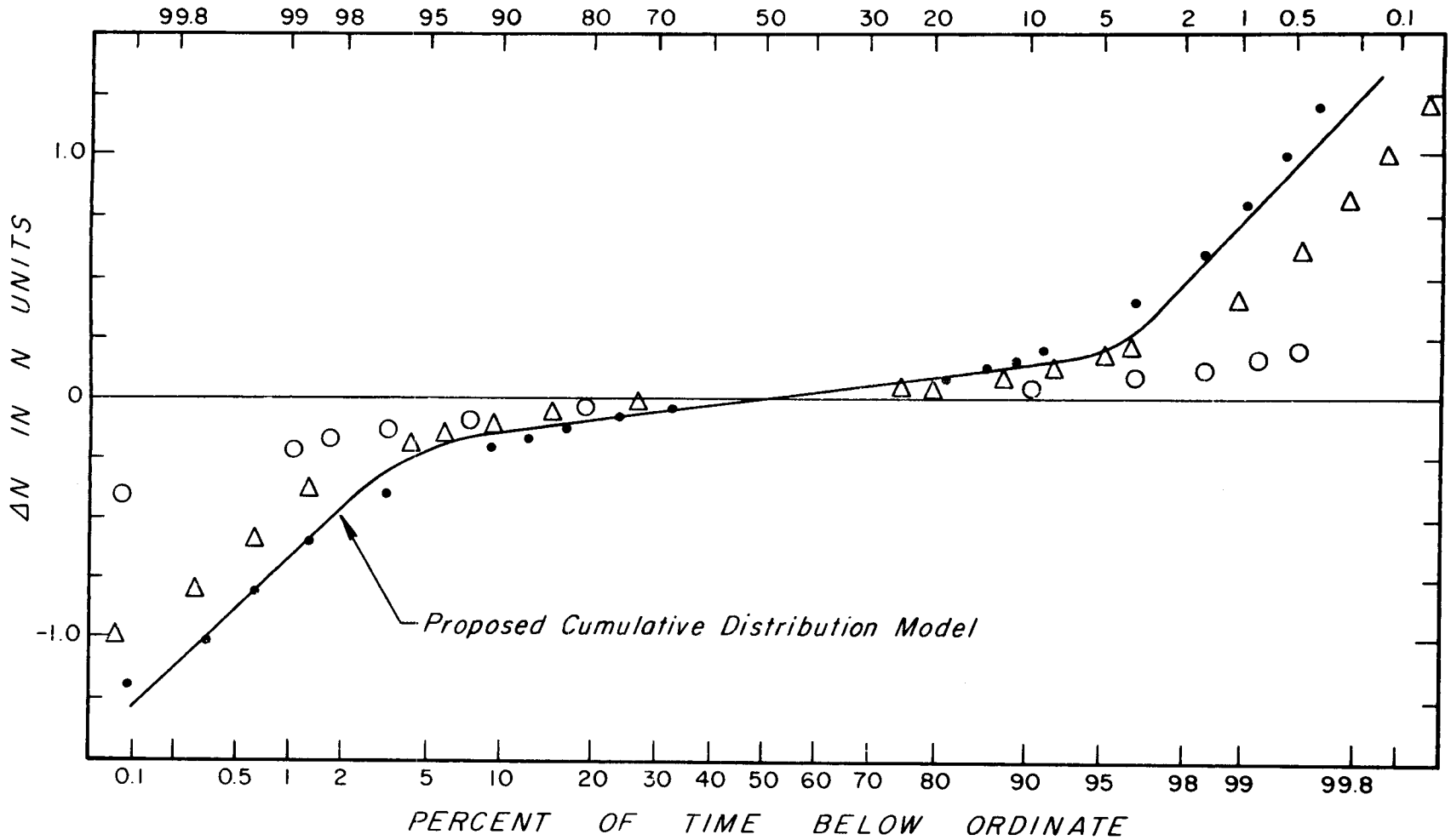

Figure 5-36. Amplitude Distribution of Example 3 for In-Line Formation (Legend for this figure is on page 43)

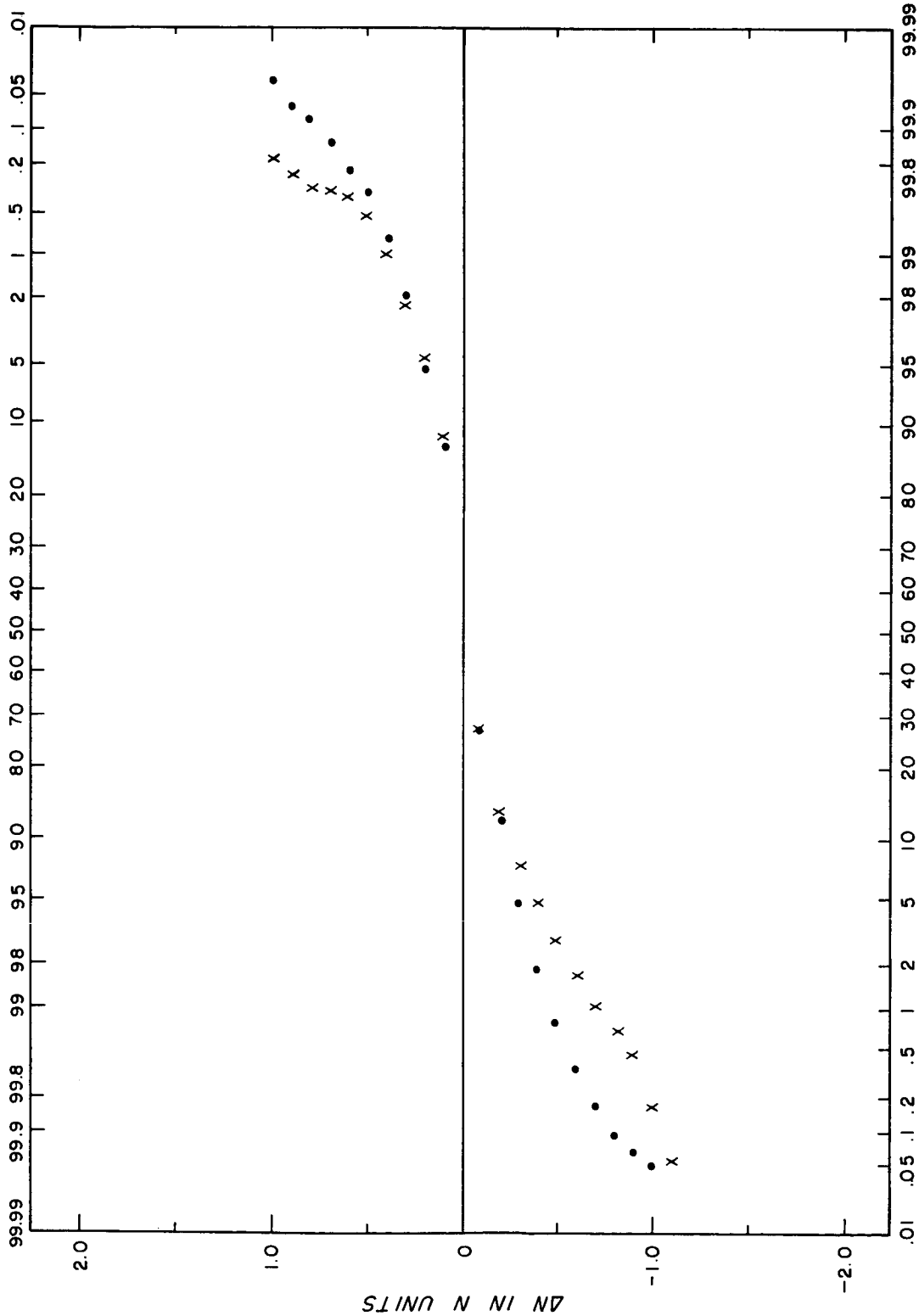

Figure 5-37. Amplitude Distribution of Example 4 for 5 Meter Separation (Legend for this figure is on page 43)

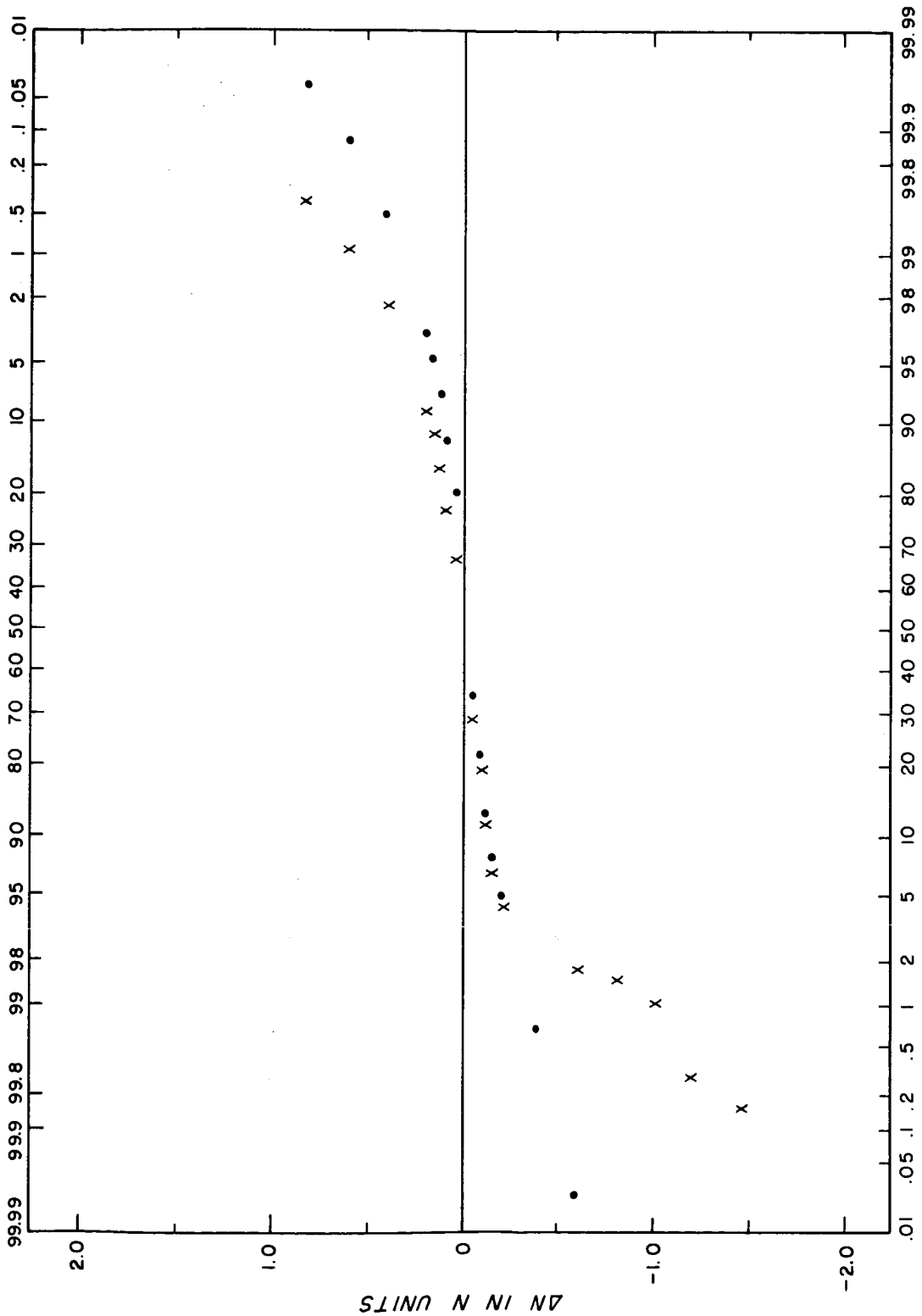

Figure 5-38. Amplitude Distribution of Example 5 for 10 Meter Separation (Legend for this figure is on page 43)

between the 5 per cent and 95 per cent points with a constant slope for each separation and the other parts consist of two end segments which are essentially straight lines with different slopes than that of the center segment. The distribution plot is approximately symmetrical about the 50 per cent probability point.

The amplitude distribution plot for the 4.0 meter spacing of example 3 was analyzed and the constants for the probability density function of eq. (4-18) were determined as follows:

$$K_1 = 0.9$$

$$K_2 = 0.05$$

$$a = 0.2$$

$$\sigma_1 = 0.1$$

$$\sigma_2 = 1.0.$$

Using these values, the function $F(\Delta N)$ of eq. (4-20) was plotted as the solid line shown in Fig. 5-36. There is very good agreement between the measured data points and the empirical mathematical model.

2. Box Formations

Amplitude distribution plots for examples 6 through 13 are shown in Figs. 5-39 through 5-46, respectively. The amplitude distribution plot for single unit refractive index variations is shown for all box formations except example 13.

The amplitude distribution for a single refractometer output as shown by the crosses in the distribution plots tends to follow

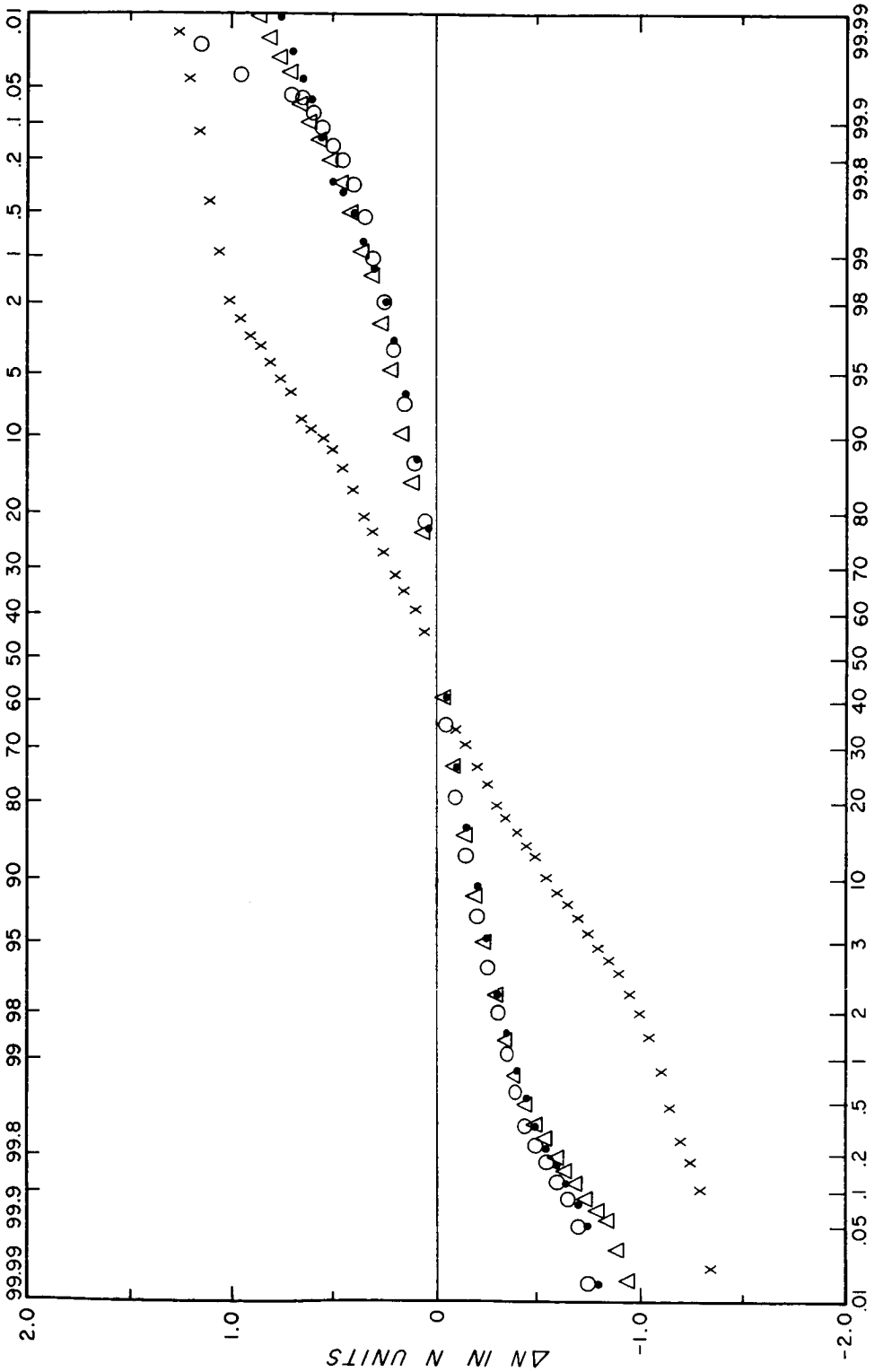

Figure 5-39. Amplitude Distribution of Example 6 for 0.75 Meter Box Formation (Legend for this figure is on page 43)

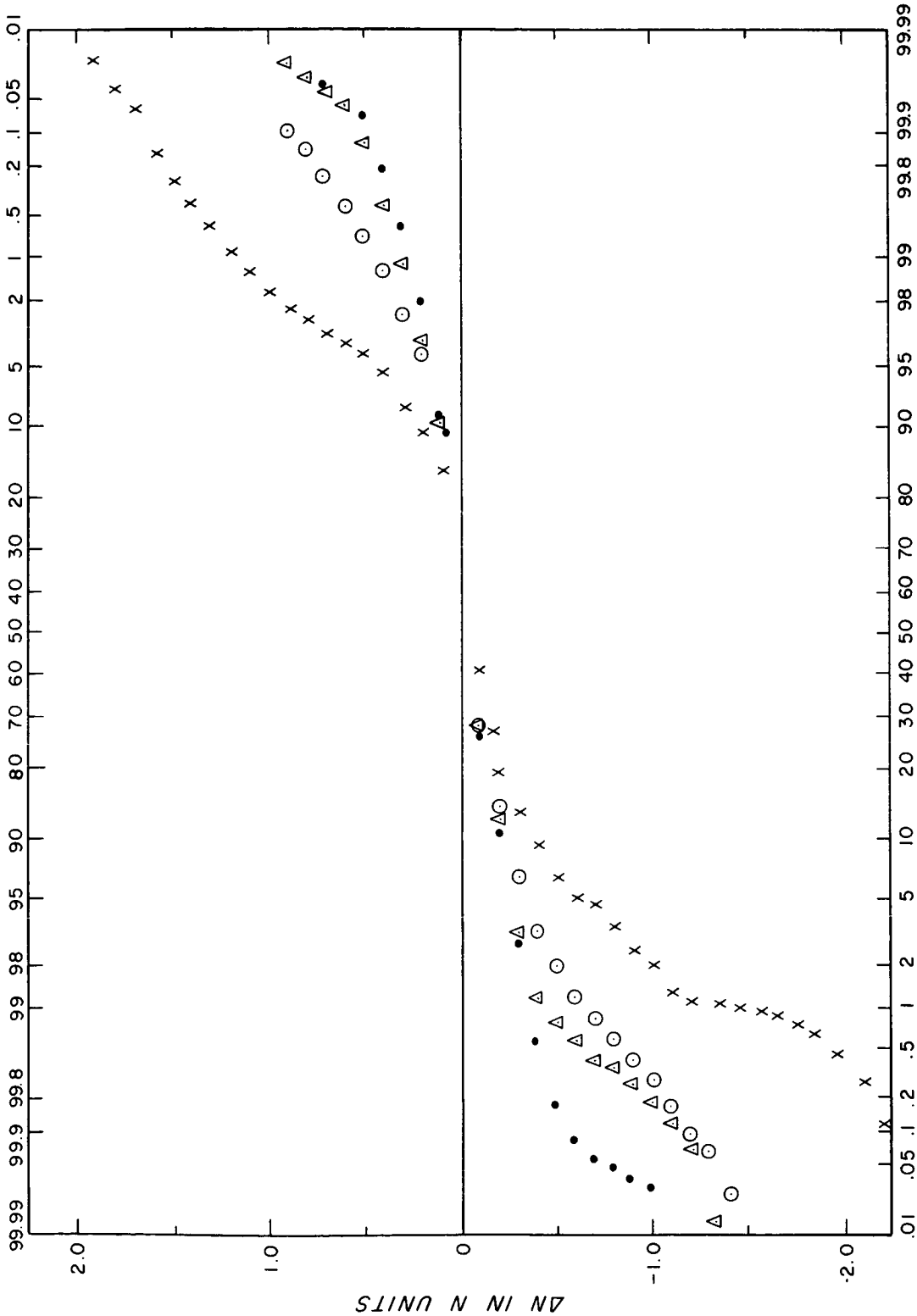

Figure 5-40. Amplitude Distribution of Example 7 for 0.75 Meter Box Formation (Legend for this figure is on page 43)

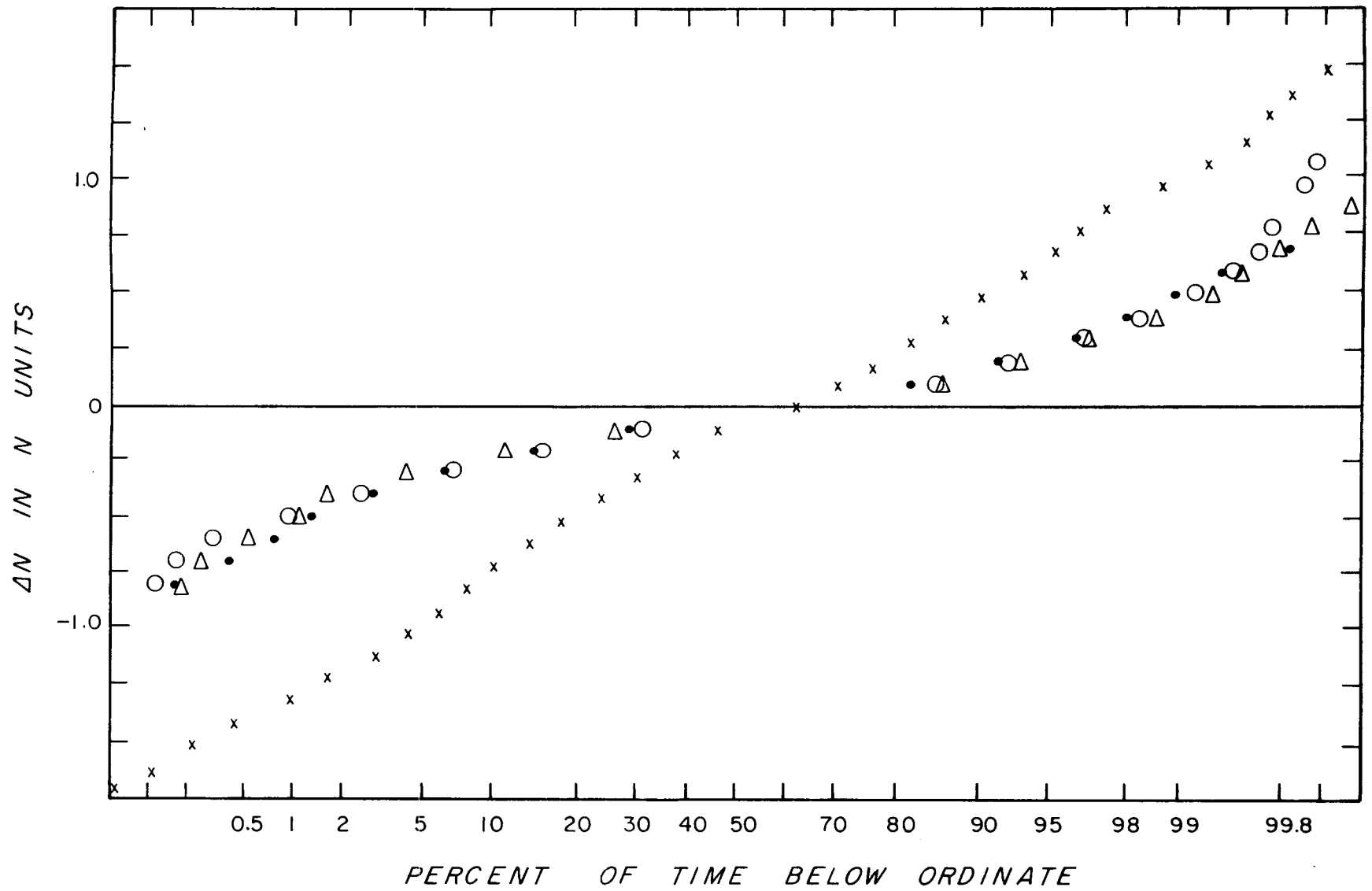

Figure 5-41. Amplitude Distribution of Example 8 for 0.75 Meter Box Formation (Legend for this figure is on page 43)

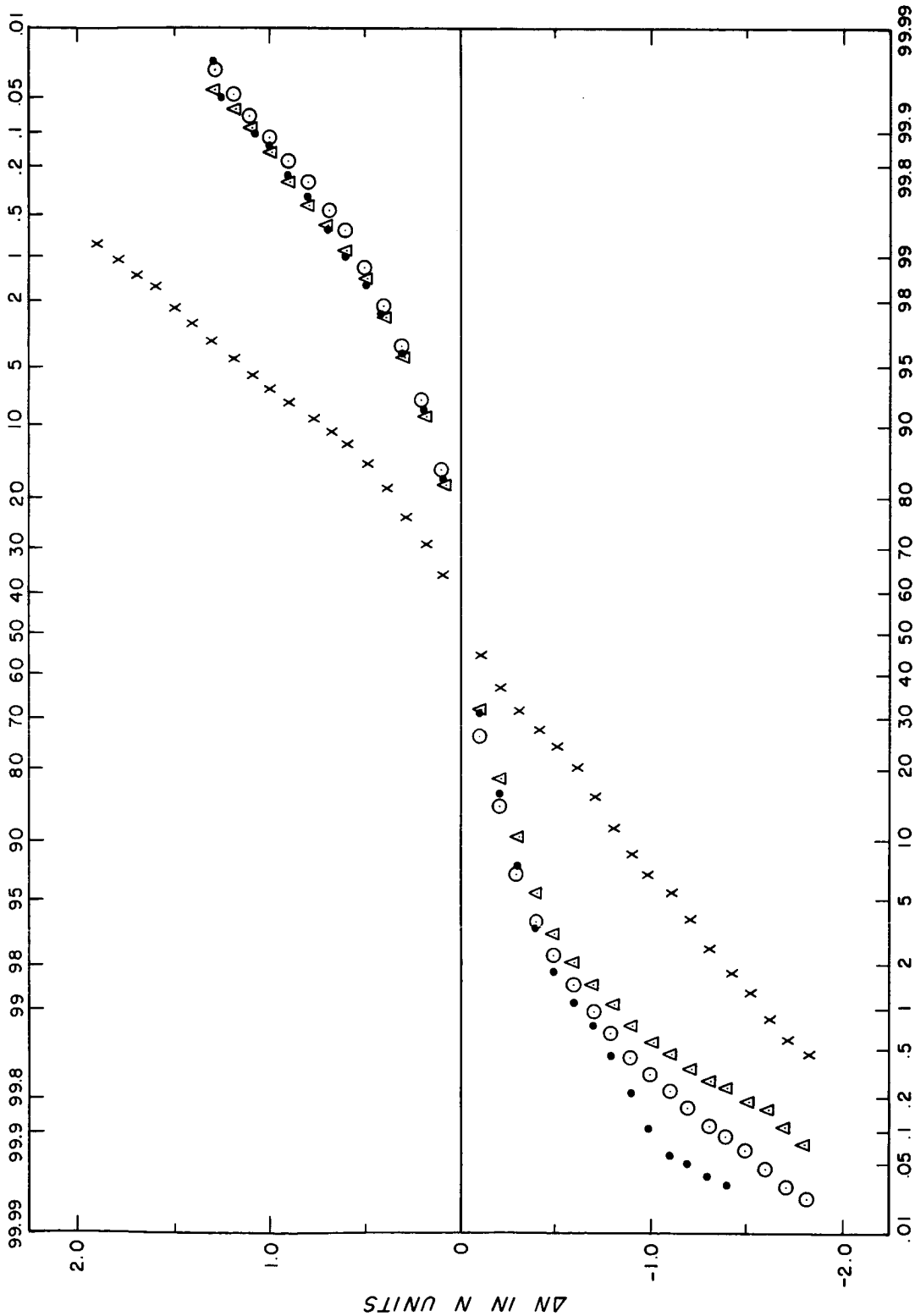

Figure 5-42. Amplitude Distribution of Example 9 for 0.75 Meter Box Formation (Legend for this figure is on page 43)

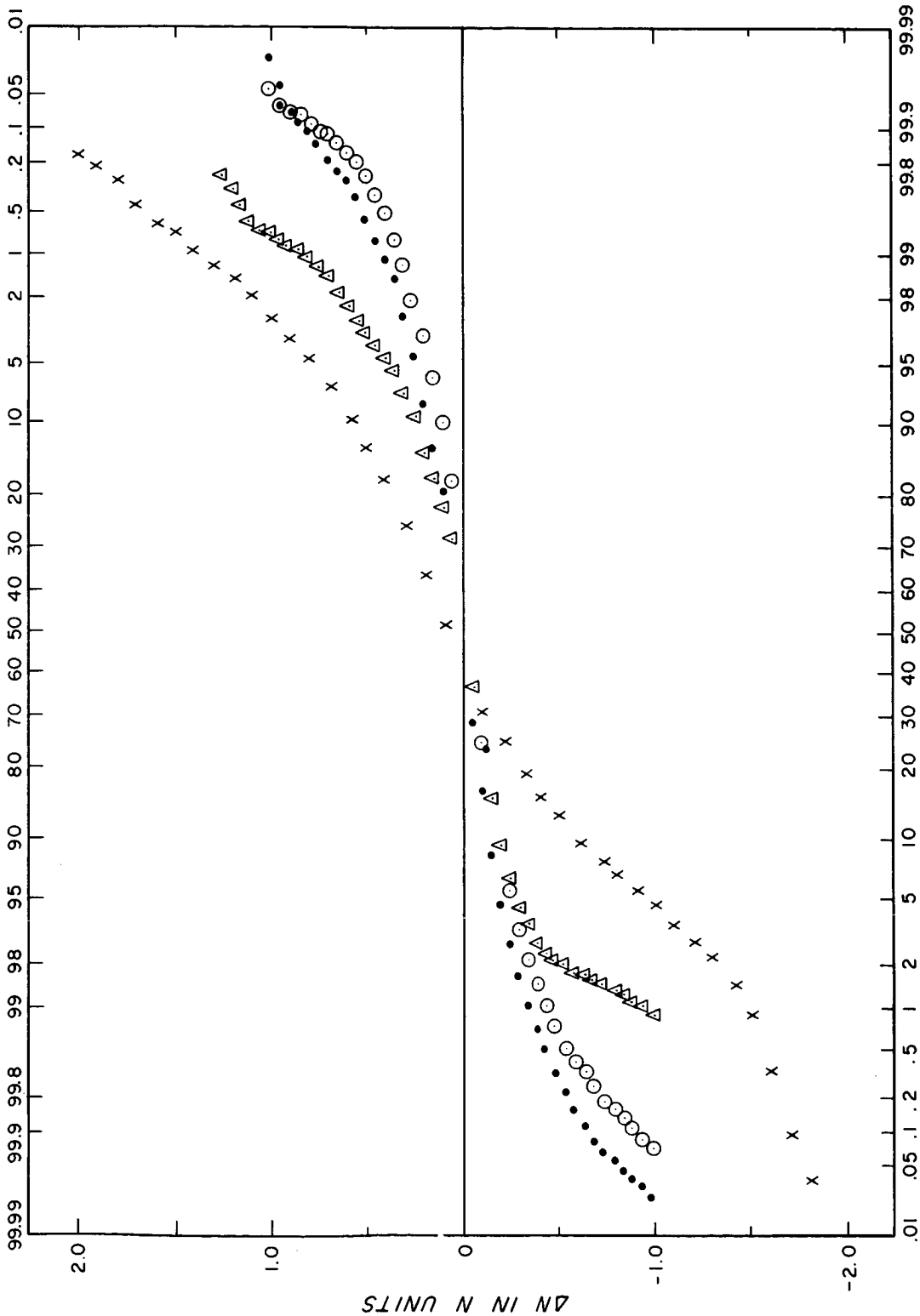

Figure 5-43. Amplitude Distribution of Example 10 for 0.75 Meter Box Formation (Legend for this figure is on page 43)

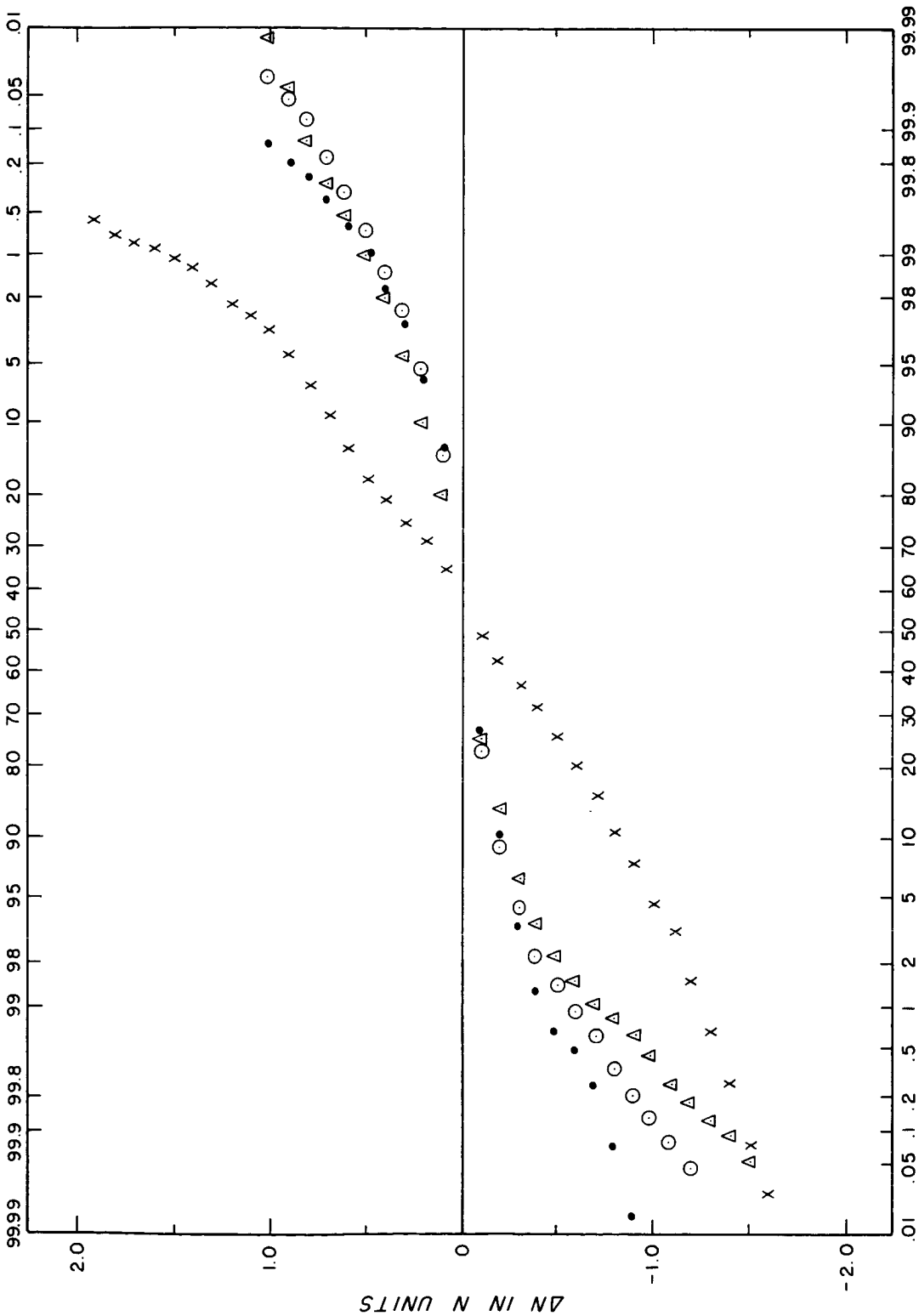

Figure 5-44. Amplitude Distribution of Example 11 for 0.75 Meter Box Formation (Legend is on page 43)

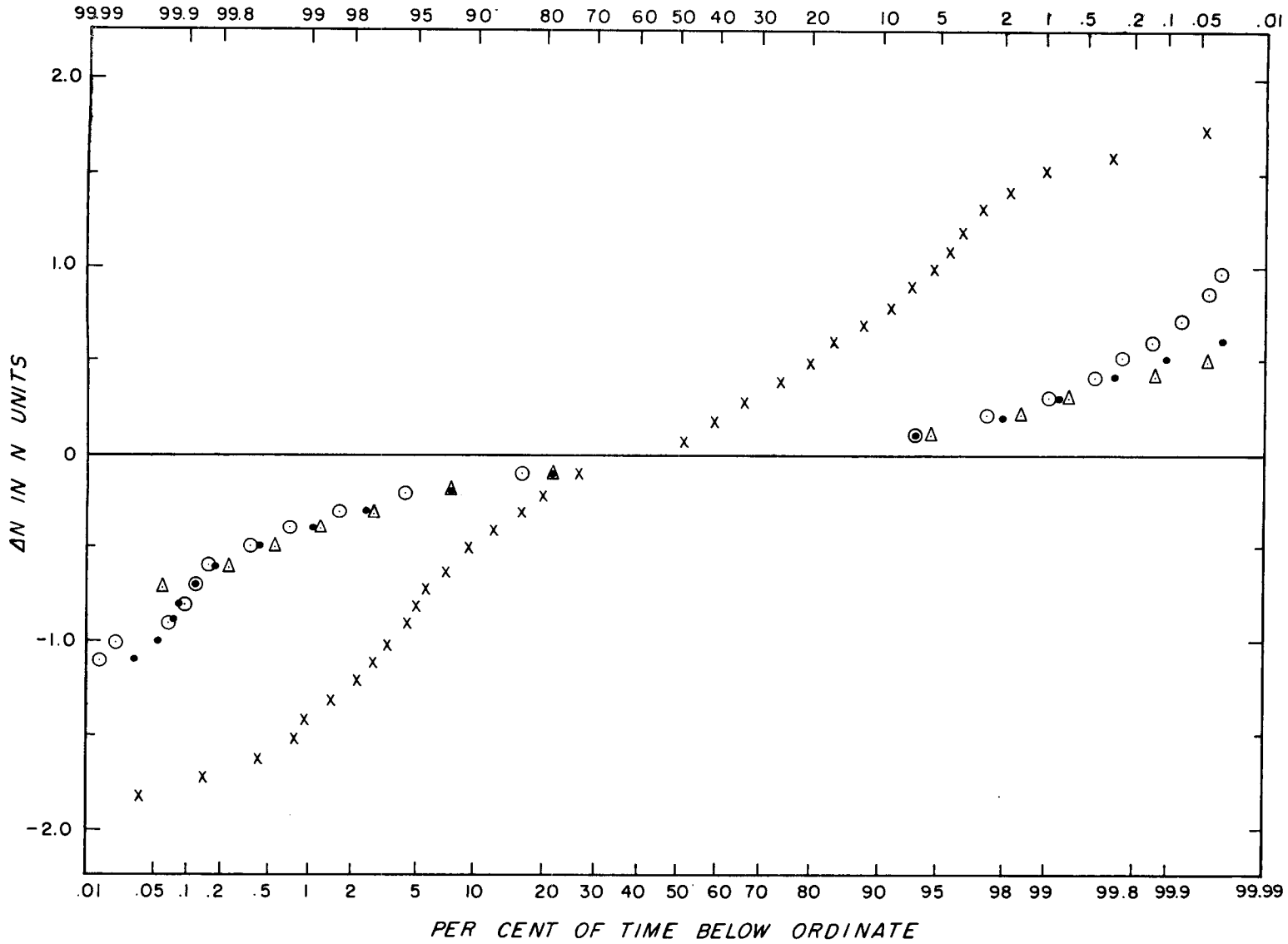

Figure 5-45. Amplitude Distribution of Example 12 for 0.75 Meter Box Formation (Legend for this figure is on page 43)

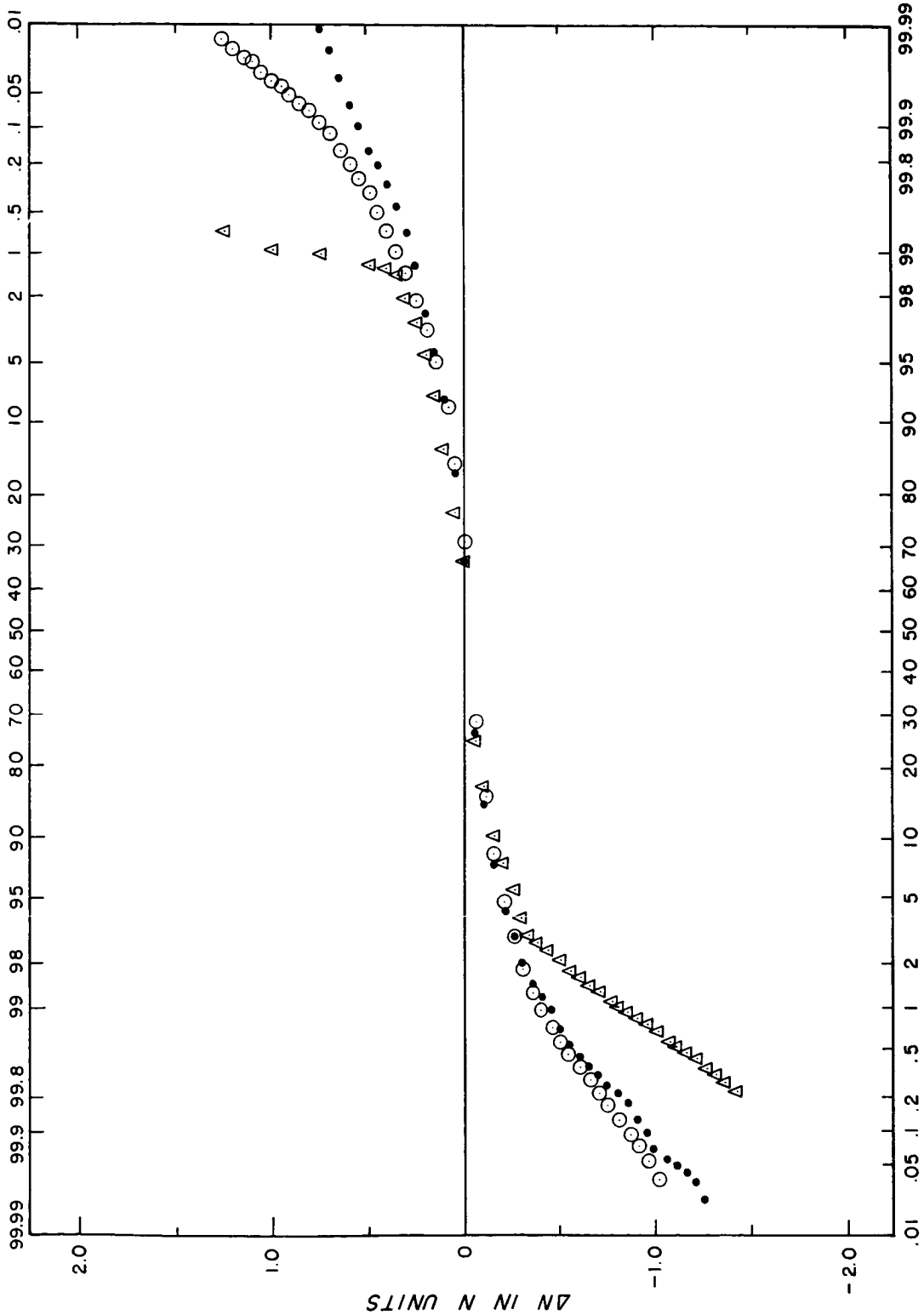

Figure 5-46. Amplitude Distribution of Example 13 for 1.8 Meter Box Formation (Legend for this figure is on page 43)

a straight line. There is some dissymmetry in the end segments below 0.2 per cent and above 99.8 per cent. Since the probability of occurrence of these amplitudes is so small, they do not seem to be statistically significant.

In most of the box formation measurements, the three differences had amplitude distributions that were approximately the same.

A digital computer was used to determine the spectra and amplitude distributions of the refractive index difference data. In so doing, the physical processes causing refractive index variations are often overlooked. In the following section, interpretations of the original data will be made from close observation of paper chart recordings.

D. Interpretation of Data by Observation

1. General

Paper chart recordings were made of the 13 sets of data investigated. Some of the chart recordings were made at a slow chart speed (25 mm/min) so that gross features of the data could be observed. Other chart recordings were made at a faster speed (2.5 mm/sec) in order to observe the variations in finer detail.

Refractive index variations are very complex in nature and no single model will hold for the many different variations observed. The type of model chosen and the refractometer spacing relative to the refractive index model determines the predicted difference variations. Rearrangement of the refractometer spacing relative to the refractive index model drastically changes the nature of the predicted variations.

2. Displacement of Single Unit Spikes

The data from a single refractometer consist of small refractive index changes (0.0 - 0.5 N) for 70 to 90 per cent of the time and larger changes (0.5 - 2.0 N) from 10 to 30 per cent of the time as noted from amplitude distributions.

The changes in the data of a single refractometer could not be characterized by any one type of variation (rectangular, sinusoidal, etc.). There would be times when variations that are approximately rectangular in form would occur and at other times such waveforms as triangular, sinusoidal, and many other types were observed.

The single refractometer data were characterized by impulsive type variations in the direction of increasing index above a slowly changing level. Also there were instances where abrupt changes in the data would occur in the direction of decreasing index. The slowly changing base line on the single refractometer data could be attributed partly to the temperature changes affecting the refractometer cavity as well as long term changes in index.

3. Duration of Single Unit Spikes

The duration of the refractive index variations of a single refractometer indicates the disturbance size. By multiplying the wind speed by the time duration of the disturbance, the approximate size of the refractive index disturbances can be determined. The single unit refractive index disturbances consist of a gross disturbance of tens of meters in size with small disturbances of tenths of meters to several meters superimposed on the gross variations.

The approximate sizes of disturbances were determined for a 78 second data segment of example 5. The number and approximate sizes of the gross disturbances noted are given below:

Number	Approximate Size
3	5 m
2	10 m
1	15 m
1	20 m
2	25 m
1	30 m
1	35 m
1	40 m

Example (a) of Fig. 5-47 indicates a disturbance size of approximately 9.0 meters and example (c) shows the disturbance to be about 4.0 meters in size.

4. Disturbance Affecting Reference Unit Only

At times the difference data variations were almost identical to the variations of the single refractometer data. This is indicative of the case where the refractive index disturbance passes the reference refractometer but does not pass the second unit. Example (c) of Fig. 5-48 shows the two horizontal difference being almost identical to the single unit variation. The disturbance size as determined from the single unit variation is approximately 1.0 meter which is comparable to the 0.75 meter refractometer spacing. If the disturbance is spherical in shape and the center of the disturbance passes the reference refractometer then the disturbance will affect only the down wind refractometer pair at the same time.

In order to observe disturbances that affect the reference unit only, the atmosphere surrounding the non-reference refractometer must be undisturbed.

5. Disturbance Affecting Non-Reference Unit Only

In section 4 conditions were described which permit observation of disturbances affecting the reference refractometer only. In order to observe disturbances affecting the non-reference unit only, the atmosphere surrounding the reference refractometer must be undisturbed.

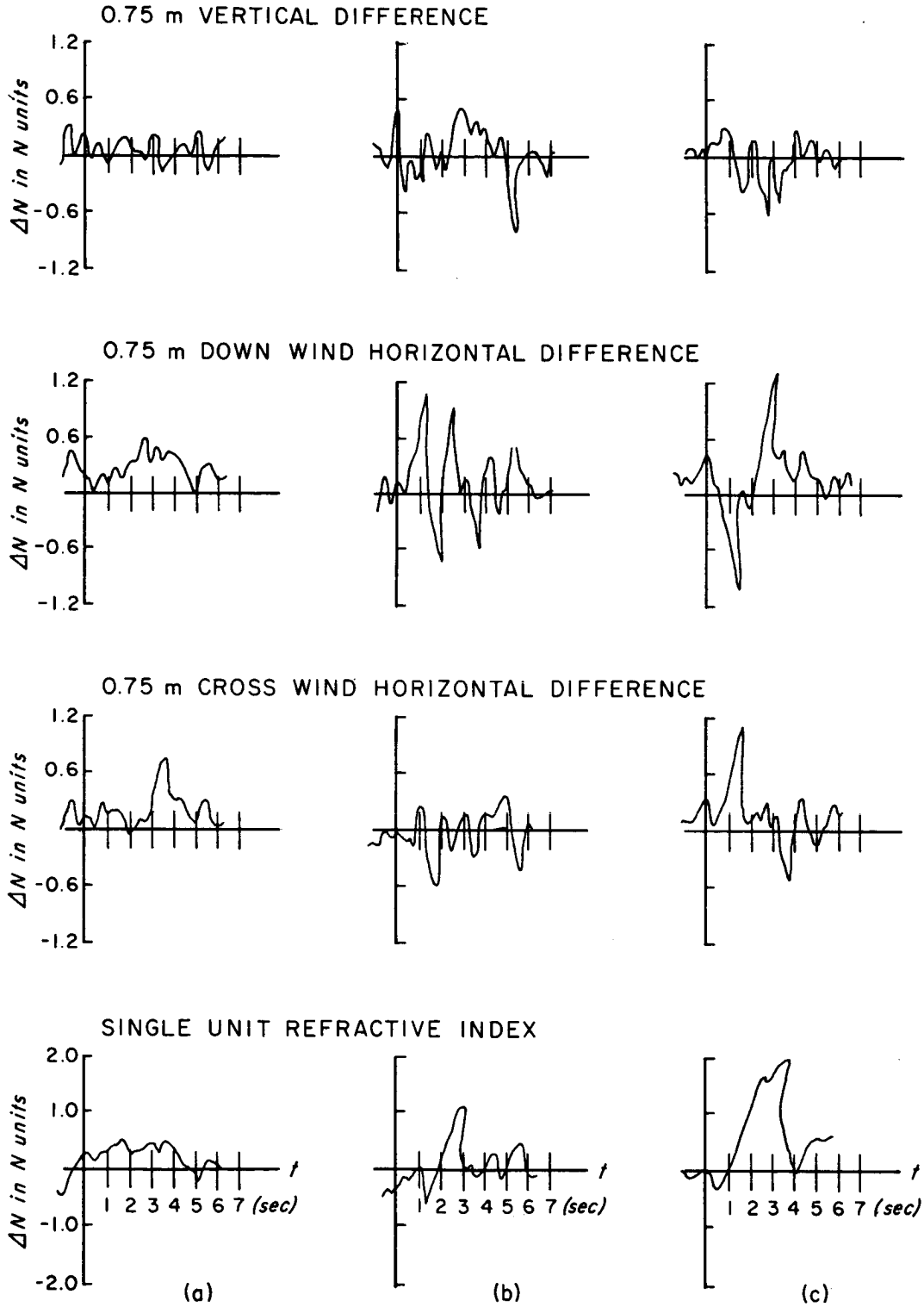

Figure 5-47. Typical Refractive Index Variations for Single Unit and for 0.75 Meter Box Formation Difference Data of Example 6

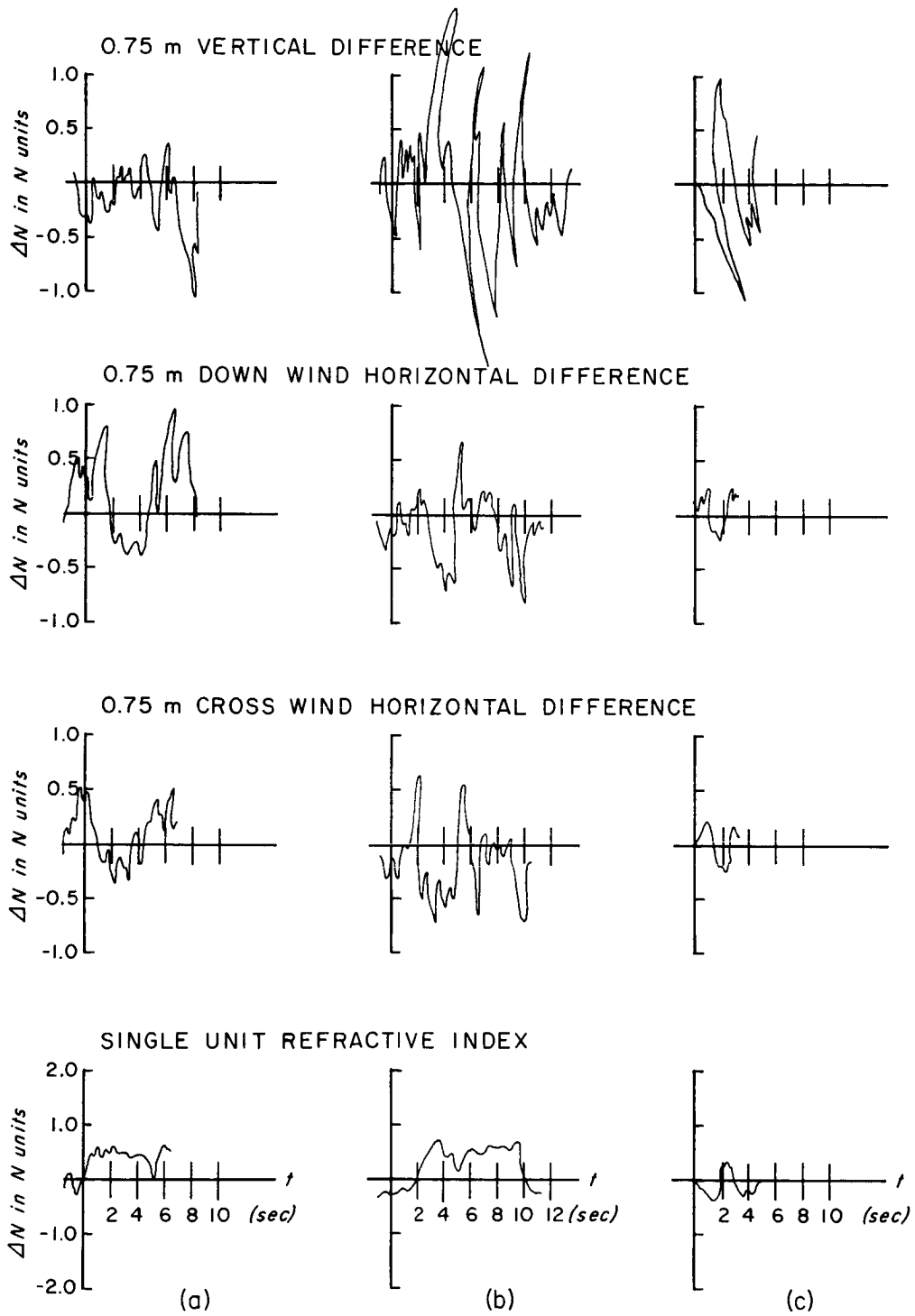

Figure 5-48. Typical Refractive Index Variations for Single Unit and for 0.75 Meter Box Formation Difference Data of Example 8

The size of the refractive index disturbance shown in example (a) of Fig. 5-49 is approximately 8.0 meters which is greater than the 5.0 meter refractometer spacing.

6. Disturbances Affecting Two Cavities in Sequence

Abrupt changes in the refractive index variations of a single unit usually had associated with it changes in refractive index differences. In some instances, the difference variations were in one direction only, while at other times changes in the refractometer data would be accompanied by changes in the difference data first in one direction and then in the opposite direction.

Disturbances which were greater in size than the refractometer spacing usually cause consecutive changes in opposite directions on the difference data. For refractive index disturbance sizes comparable to or smaller than the refractometer spacing, variations in the difference data may be in one direction only or in two directions depending upon the orientation of the refractometers with respect to the refractive index disturbances.

Example (c) of Fig. 5-47 illustrates a sharp refractive index disturbance. A 2.0 second time duration of the single unit disturbance indicates a disturbance size of about 4.0 meters. This waveform is almost rectangular with minor variations during the peak of the waveform. Since the disturbance size is more than 5.0 times the refractometer spacing, the difference data should contain spikes in both directions. The

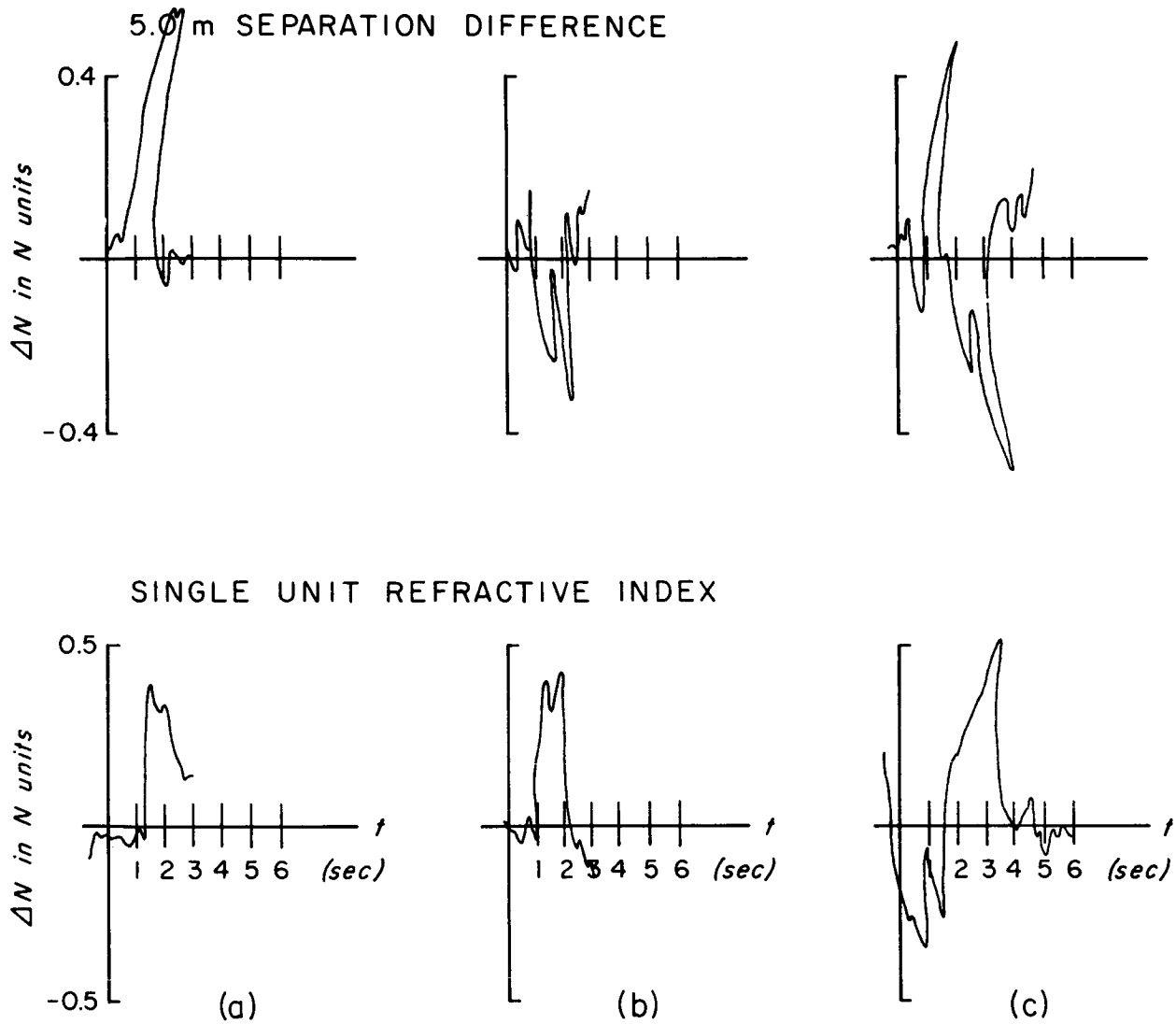

Figure 5-49. Typical Refractive Index Variations for Single Unit and for 5 Meter In-Line Difference Data of Example 4

amplitude of the down wind difference is greater than the amplitude of the cross wind difference indicating that the refractive index gradients encountered in the down wind direction are greater than those encountered in the cross wind direction.

7. Comparison of Vertical and Horizontal Difference Data

In general, the characteristics of the vertical difference data are different from those of the horizontal difference data.

A refractive index distrubance in the form of a vertical front should cause the vertical difference data to be similar to the horizontal cross wind difference data.

In example (c) of Fig. 5-47 the horizontal cross wind difference is quite different from the vertical difference. Although the disturbance size in the horizontal direction is greater than the refractometer spacing, the vertical difference data indicate that the refractive index disturbance is different in the vertical direction than in the horizontal direction. This indicates that the refractive index has a horizontal size which is greater than the vertical size.

Example (a) of Fig. 5-48 illustrates the disagreement between the horizontal and vertical differences. Both horizontal differences are very similar to the single unit data, whereas the vertical difference data show quite abrupt changes indicating a large refractive index disturbance just 0.75 meter below the undisturbed horizontal refractive index.

8. Frequency of Occurrence of Spikes on Refractive Index Difference Data

Examples 11 and 12 were analyzed for frequency of occurrence of spikes on the difference data. The spikes were counted that were between 0.5 N and 1.5 N and between -0.5 and -1.5 N. A sixty minute sample of data was broken into six ten minute segments and the spikes were counted for each segment.

The levels that are given above are quite arbitrary. It is possible that some of the spikes were not counted that were on the borderline of the set levels. The levels are above and below the average refractive index variations. This average value was slowly changing but an attempt was made to compensate for its changing value.

Also the number of positive spikes will be increased because of positive spikes that are caused by magnetic tape "dropouts." The spikes that were caused by the tape "dropouts" can hardly be distinguished from spikes due to refractive index changes. When, however, the spike occurs on all channels or is accompanied by a spike in the opposite direction, instrumentation error may be ruled out.

The number of spikes counted for two examples of refractive index difference data are given in Table 5-2. Two columns are given for each difference, one for positive spikes and one for negative spikes. An average of between 0.9 and 1.7 spikes per minute was noted for both positive and negative spikes. In example 11 a minimum number of 53

Table 5-2

Number of Spikes Noted on Refractive Index Difference Data for 10 Minute Segments and Total Time of 60 Minutes

	Vertical Difference $\Delta N > 0.5N$	Vertical Difference $\Delta N < -0.5N$	Horizontal Down Wind Difference $\Delta N > 0.5N$	Horizontal Down Wind Difference $\Delta N < -0.5N$	Horizontal Cross Wind Difference $\Delta N > 0.5N$	Horizontal Cross Wind Difference $\Delta N < -0.5N$
			Example Number 11			
	9	7	15	13	8	10
	8	10	11	10	7	8
	11	14	13	14	18	14
	8	10	9	14	15	8
	12	16	11	13	13	14
	5	12	18	16	15	11
Total	53	69	77	80	76	65
Ave. per min.	0.88	1.15	1.28	1.33	1.26	1.08
			Example Number 12			
	26	10	17	19	10	11
	18	16	20	25	11	19
	18	19	17	12	15	14
	25	15	17	20	8	15
	7	9	10	9	11	9
	10	7	6	8	7	9
Total	104	76	87	93	62	77
Ave. per min.	1.73	1.26	1.45	1.55	1.03	1.28

positive spikes was counted on the vertical difference. The maximum number of 80 negative spikes was noted on horizontal down wind difference data. The next highest number of 77 positive spikes was counted for the horizontal down wind difference data. It is to be expected that the down wind horizontal difference data contain a large number of spikes because the refractive index disturbance passes both refractometers in the down wind refractometer pair, thus causing a positive and a negative spike.

In example 12 the minimum number of 62 positive spikes was noted in the horizontal cross wind difference data. This is to be anticipated because for refractive index disturbances of sizes comparable to and smaller than the refractometer spacing, only one spike is caused by the disturbance. Also refractive index disturbances which are frontal in form would cause only a small change in the cross wind difference provided the front passes the cross wind refractometer pair simultaneously.

The maximum number of 104 positive spikes was noted on the vertical difference data for example 12. The next highest number of spikes was noted on the horizontal down wind difference data with 93 positive spikes followed by 87 negative spikes on the down wind data. The vertical difference data are greatly influenced by vertical gradients in refractive index and changes in refractive index disturbances in the vertical direction. Also the magnetic tape "dropouts" may have contributed heavily to the high count of positive spikes in the vertical difference data.

In general it was noted that the horizontal down wind difference data have the highest number of spikes and the horizontal wind difference data the lowest number, whereas the number of spikes counted on the vertical difference data varied between the number of spikes recorded on both horizontal differences.

E. Refractive Index Structure Functions

The structure function for index of refraction is given by eq. (4-23). The quantity C_n^2 is of great importance since it is independent of separation distance and dependent upon the parameters of the atmosphere and the state of turbulence in the atmosphere.

Eklund (1965, p. 70) has calculated the value of C_n^2 from 10 cm wavelength radar measurements as being of the order of $5 \times 10^{-14} (\text{cm})^{-2/3}$. Stephens and Reiter (1966, p. 39) estimate C_n^2 to be in the neighborhood of $10^{-17} (\text{cm})^{-2/3}$ in regions of clear air turbulence.

Calculations made with data taken by Walker (1960, p. 41) yield values of C_n^2 from $9 \times 10^{-14} (\text{cm})^{-2/3}$ at a 150 meter height to $2.5 \times 10^{-15} (\text{cm})^{-2/3}$ at a height of 1070 meters. These data consist of a 20 second sample length. During one run at a height of 760 meters, the first 20 seconds of data yielded a value of $7 \times 10^{-15} (\text{cm})^{-2/3}$, whereas the next 20 second of data yielded a value of $2 \times 10^{-14} (\text{cm})^{-2/3}$, greater by more than a factor of 2.

The structure function for the index of refraction as derived from the probability density function of eq. (4-18) is given by eq. (4-25). Using the constant evaluated for the 4-meter separation of example 3, the contributions to the structure function are as follows:

From center section

$$D_n(400) \cong 10^{-14}$$

From end sections

$$D_n(400) \cong 10^{-13}.$$

The spikes in the difference data dominate the end sections in the amplitude distribution plots. Thus, it is noted that the spikes make a contribution to the structure function for this sample approximately ten times that of the continuum. In the single point refractive index sample, however, the effect of the spike on the rms value would be insignificant.

The original data for example 3 are shown in Fig. 5-2. A plot of $D_n(r)$ as a function of r for the samples of the original data designated as "a", "b" and "c" in Fig. 5-2 is shown in Fig. 5-50. In addition, $D_n(r)$ is plotted for an entire hour of data for the same spacings during a period when the atmospheric refractive index was less disturbed.

For comparison, eq. (4-23) is plotted for C_n^2 in units of $(cm)^{-2/3}$ of 10^{-14}, 10^{-15}, and 10^{-16}.

It is noted from Fig. 5-50 that $D_n(r)$ is greater by a factor of 10 during the time intervals "a" and "b" when numerous spikes were present as compared to the time interval "c" when no spikes were present.

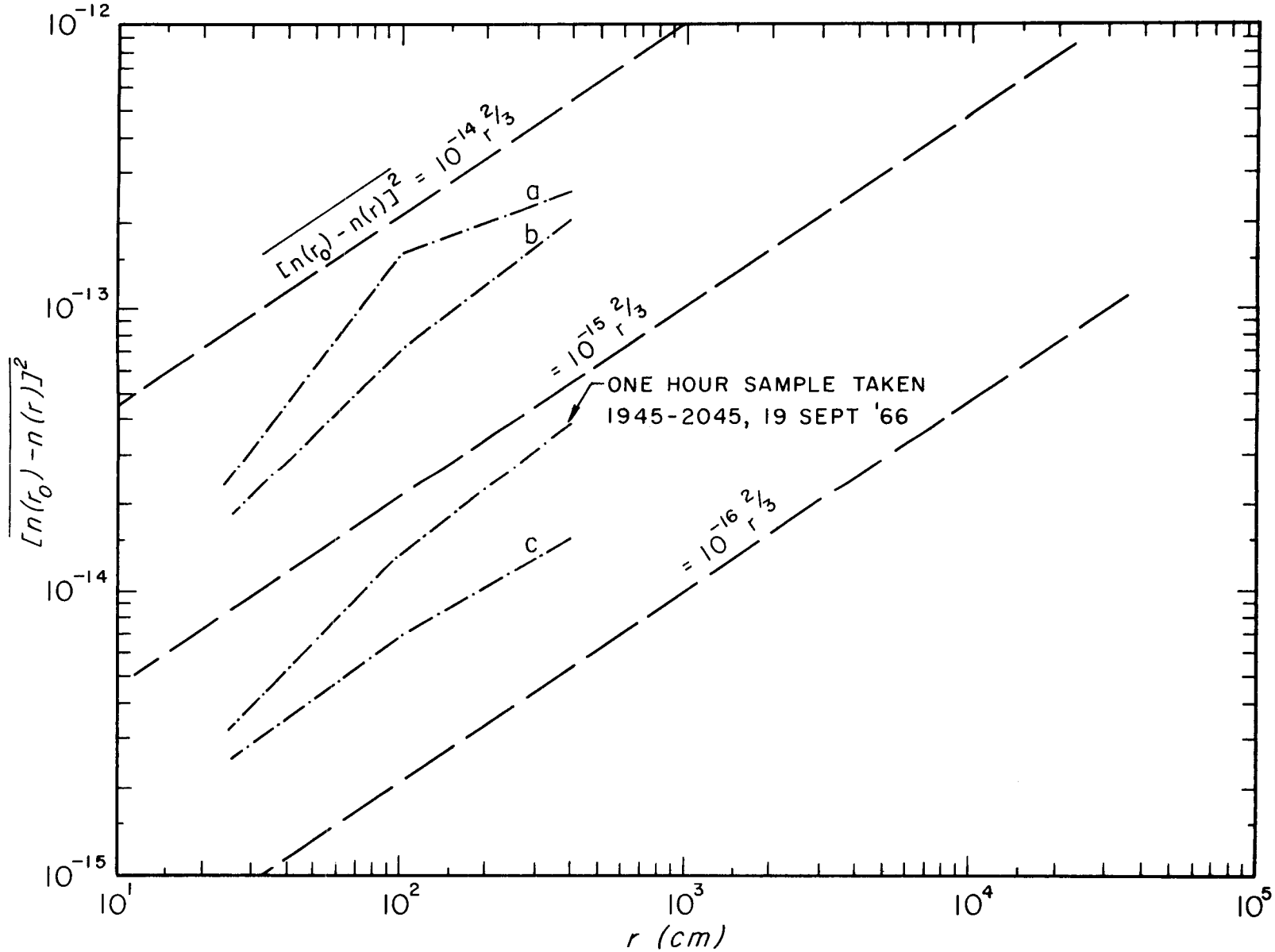

Figure 5-50. One Dimensional Structure Functions Plotted for Three 5 Minute Sections of Data as Shown in Fig. 5-2 and a One hour Sample at a Different Time

As noted in Fig. 5-50, the slope of the measured structure function is greater than 2/3 for small values of r (10 - 40 cm). This increase in slope is caused in part by the filtering action of the refractometer cavity (see Appendix C).

VI. SUMMARY AND CONCLUSIONS

The variations of refractive index are very complex in nature and examination of these variations in great detail is difficult due to the filtering effect of present day measuring techniques. In addition, the longer wavelength data tends to obscure the characteristics of the fine scale variations. By measuring differences in refractive index rather than index variation itself, the effects of the longer wavelength data are minimized. This is the primary advantage in studying the results of refractive index difference tests.

Refractive index difference measurements indicate two types of mechanism causing the fluctuations present in the data.

An estimate may be made of the extent of the anomalies causing the disturbances by a study of the response of a single cavity to a disturbance. If the disturbance moves past the detector with the prevailing wind speed, the linear dimension in the direction of the wind will be the wind speed times the duration of the impulse.

For the single refractometer data discussed in this study, the spikes continue typically for 2 seconds with a wind speed of 2 meters per second. This would predict a size of about four meters for the disturbance.

In the original data for the in-line spacing shown in Fig. 5-2, the amplitude of the spikes is less for the 1 meter separation than for the

4 meter and much less for the 0.25 meter than for 1 meter. This indicates that the disturbance arrives at the second refractometer for the smaller separations before it has passed the first unit. Frequently, a spike in one direction is followed immediately by a spike in the opposite sense. This is interpreted as the movement of the abrupt disturbance past one unit and then past the other. Also this result can be viewed as the difference signal being the differentiated single unit signal.

The most obvious suggestion for the cause of the spikes in the refractive index is enhancement of water vapor in patches. There is no immediate explanation of the cause of this clustering since the relative humidity was considerably less than conditions conducive to condensation. The amount of the enhancement will be only a few per cent of the total water vapor content.

The influence of the spikes on the rms value of a given time sample for single point refractive index data is small since the long term variations obscure the abrupt changes. The spikes are much more evident on the difference data which removes the long-period large-intensity changes. The spikes on the difference data are shortened in time duration since cutoff starts when the blob reaches the second sampling cavity and not when it has moved away from the first cavity. In the box formation, the occurrence of the spikes between various pairs of cavities differ by a small amount.

In most examples reported, the relative spectra were roughly approximated by $2(1 - \sin x/x)$ filter function. Only in one example did the relative spectra tend to follow a $4 \sin^2(\frac{x}{2})$ form. In all cases the behavior of the relative spectra at low frequencies was similar. The behavior of the relative spectra at high frequencies was affected by the filtering effect of the sampling cavity.

The amplitude distribution plots were similar in their general shape. Examination of amplitude probability distribution indicates one set of characteristics between approximately 5 per cent and 95 per cent points and another set of characteristics outside of these limits.

The quantity C_n^2 for the index of refraction structure function was determined for refractive index differences. Values calculated from data taken during this study compare favorably with those currently reported. The structure function has a value approximately ten times greater for data containing spikes over that of the continuum.

A significant contribution to the study of structure functions of index of refraction would be made by determining the height dependence of C_n^2.

APPENDIX A

Computer Program Used for Determining Refractive Index Power Spectra

A listing of the program used to compute power spectra for the refractive index data is included in this appendix. The program consists of a main program and three sub-programs.

The main program is primarily a control program with input-output commands. Also the channel scale factors are entered into the computer under control of the main program.

Basically the computer calculates a Fourier series analysis of 40 data points by computing the sine and cosine coefficients at specific frequency intervals. These coefficients are computed over a four octave frequency range with four points computed between each octave of frequency. The computed frequency components are determined by the sampling rate. A sampling rate of 16 samples per second results in the sine and cosine coefficients being computed for frequencies from 3.6 Hz to 4 octaves below 3.6 Hz.

"ARRAY" is the sub-program that computes the values of sin $(2\pi f)$ and cos $(2\pi f)$, where f is the frequency at which point the spectrum is being computed.

"N PUT" is the sub-program that controls the digitizing of the analog refractive index data. The program is written for four data

channels. Data is stored in a 40 x 4 array with a 20 x 4 array being used to store incoming data whereas the data in the remaining 20 x 4 array is being transferred into the next sub-program "COMP."

The sub-program "COMP" uses the results from sub-program "ARRAY" and data from the sub-program "N PUT" to compute the power spectra. The execution time that this program requires determines the sampling rate of the recorded analog data. Included in this sub-program is a program that compensates for the effect of the alias filters.

```
*     PROGRAM FOR REAL TIME POWER SPECTRA
      DIMENSION PR(16,41),NPR(10),JDATA(1600),IDATA(160),CO(95),SI(95),A(4)
  100 FORMAT(//$        FREQUENCY          PWR CH1          PWR CH 2          $
     1$PWR CH 3          PWR CH 4$)
  109 FORMAT ($ACCEPT A(1) THRU A(NCHAN)$)
  110 FORMAT (4F20.9)
  101 FORMAT($ACCEPT NO. OF DATA PTS., NO. OF DECIMATIONS, NCHAN,$
     1 $NSKIP, ΔT, ALIAS FILTER BREAK$)
  102 FORMAT(4I10,2F10.0)
  103 FORMAT(1P5E16.3 )
  106 FORMAT($START DATA$)
  107 FORMAT($NO. OF SPECTRA$)
  108 FORMAT(10I6)
      CALL ARRAY(CO,SI)
      TYPE 101
      ACCEPT 102,NT,NDEC,NCHAN,NSKIP,DT,FD
      NF = 5*(NDEC+1)
      TYPE 109
      ACCEPT 110, (A(I), I=1,NCHAN)
      TYPE 106
      PAUSE
      CALL NPUT(IDATA,20,ICOUNT,NSKIP)
      CALL COMP(NT,NDEC,PR,CO,SI,IDATA,JDATA,ICOUNT,NPR,FD,DT,NCHAN)
      TYPE 107
      TYPE 108,(NPR(I),I=1,NDEC+1)
      DO 29 J=1,NCHAN
   29 A(J) = ( A(J)/(204.7*5.0))**2
      DO 19 I=1,NF
      DO 19 J=1,NCHAN
      K = J*(10 -J) -8
   19 PR(J,I) = A(J)*PR(K,I)
  104 FORMAT(/$TAPE NUMBER    SAMPLING RATE    ALIAS FILTER    SAMPLE$
     1$ LENGTH MIN    DATE$)
  105 FORMAT($
  111 FORMAT($ACCEPT TAPE NO.,RATE,ALIAS FILTER,SAMPLE LENGTH,DATE$)
      TYPE 111
      ACCEPT 105
      TYPE 104
      TYPE 105
      PUNCH 104
      PUNCH 105
      PUNCH 100
      PUNCH 103,(CO(I),(PR(J,I),J=1,NCHAN),I=1,NF)
      CALL EXIT
      END
```

```
      SUBROUTINE ARRAY(CO,SI)
      DIMENSION CO(95),SI(95)
      PI = 3.14159265359
      P = .05*PI
      JX = 0
      DO 5 I=1,5
      Q = (10-I)*P
      DO 5 J = 1,19
      JX =  JX+1
      T = .5-.5*COS(J*P)
      R = J*Q
      CO(JX) = COS(R)*T
    5 SI(JX) = SIN(R)*T
      RETURN
      END



      SUBROUTINE COMP(NT,NDEC,PR,CO,SI,IDATA,JDATA,ICOUNT,NPR,FD,DT,NCHAN)
      DIMENSION IDATA(40,4),JDATA(160),INUM(10),NPR(2),CO(95),
     1 SI(95),AF(19),BF(19),CF(2),GT(40),PR(16)
  100 FORMAT($DATA CLOBBERED:  DECREASE NDEC OR SAMPLE RATE$)
      NDEC1 = NDEC + 1
      NFS = 80*NDEC1
      NSP = (NT-20)/20
      JCOUNT = 2
      IG = 1
      DO 1 I = 1,NFS
    1 PR(I) = 0.0
      DO 2 I=1,NDEC1
      INUM(I) = 0
    2 NPR(I) = 0
    3 IF(ICOUNT-1) 3,4,8
    4 DO 5 J=1,NCHAN
      IH = (J-1)*40
      DO 5 I=1,20
      IH = IH+1
    5 JDATA(IH) = IDATA(I,J)
      DO 20 II = 1,NSP
    7 IF(ICOUNT-JCOUNT)7,9,8
    8 TYPE 100
      PAUSE
    9 IG = 22-IG
      IG2 = IG+19
      DO 10 J = 1,NCHAN
      IH = 40*J-20
      DO 10 I=IG,IG2
      IH = IH+1
   10 JDATA(IH) = IDATA(I,J)
      IF(ICOUNT-JCOUNT)12,12,8
   12 JCOUNT = JCOUNT + 1
```

```
      MI = 1
        INUM[1] = 40
   13 M8 = [MI-1]*80
        M6 = 2*M8
        DO 110 IJ = 1,NCHAN
        IT = 2*IJ-1-2*NCHAN
        IFIR = [IJ-1]*40 + M6
        ILAS = IFIR + 40
        DO 105 I=1,19
        ID1 = JDATA[I+IFIR]
        ID2 = JDATA[ILAS-I]
        AF[I] = ID1-ID2
  105   BF[I] = ID1+ID2
        CF[1] = JDATA[IFIR+20]
        CF[2] = -JDATA[IFIR+20]
        IB = 1
        JK = 0
        DO 110 I=1,5
        IB = 3-IB
        IT = IT+8
        A = 0.0
        B = 0.0
        DO 108 J = 1,19
        JK = JK+1
        A = AF[J]*SI[JK]+A
  108   B = BF[J]*CO[JK]+B
        GT[IT] = CF[IB]+B
  110   GT[IT+1] = A
        JK = M8
        LX = [MI-1]*5
        DO 125 K=1,5
        LX = LX + 1
        I2 = 8*K-1
        L = 1
        DO 120 I = I2-2*[NCHAN-1],I2,2
        AF[L] = GT[I]**2+GT[I+1]**2
        L = L+1
        IF[I-I2] 118,120,120
  118   DO 119 J=I+2,I2,2
        AF[L] = GT[I]*GT[J]+GT[I+1]*GT[J+1]
        AF[L+1] = GT[I]*GT[J+1]-GT[I+1]*GT[J]
  119   L = L+2
  120   CONTINUE
        DO 125 I = 1,16
        JK = JK+1
        PR[JK] = AF[I] + PR[JK]
  125   CONTINUE
        NPR[MI] = NPR[MI] + 1
        IF[MI-NDEC1] 14,15,15
   14   KFIR = INUM[MI+1]+160
        DO 210 J = 1,NCHAN
        IFIR = M6+[J-1]*40
```

```
      JFIR = IFIR+KFIR
      DO 210 I=IFIR+1,IFIR+19,2
      JFIR = JFIR+1
  210 JDATA[JFIR] = [JDATA[I]+4*JDATA[I+1]+8*JDATA[I+2]+10*JDATA[I+3]
     1 +8*JDATA[I+4]+4*JDATA[I+5]+JDATA[I+6]]/9
   15 DO 18 J=1,NCHAN
      M9 = M6+40*J-39
      DO 18 I=M9,M9+19
   18 JDATA[I] = JDATA[I+20]
      INUM[MI] = INUM[MI]-20
      IF[MI-NDEC1]19,20,20
   19 MI = MI + 1
      INUM[MI] = INUM[MI]+10
      IF[INUM[MI]-40]20,13,13
   20 CONTINUE
      JK = 0
      PI = 3.14159265359
      A = DT
      B = .025/DT
      C = COS[.125*PI]
      S = COS[.375*PI]
      DO 22 I=1,NDEC1
      DO 21 J=1,5
      JK = JK+1
      CO[JK] = B*[10-J]
   21 SI[JK] = A/[7.5*NPR[I]]*[[[FD**2-CO[JK]**2]**2-4.0*[CO[JK]*FD]
     1**2*C*S]**2+[2.0*CO[JK]*FD*[C+S]*[FD**2-CO[JK]**2]]**2]/FD**8
      A = 2.*A
   22 B = B*.5
      NF = JK
      A = .1125*PI
      DO 23 I=1,NDEC
      IG = I*5+1
      XK = A/CO[IG]
      DO 23 J=IG,NF
      B=XK*CO[J]
   23 SI[J] = [3.0*SIN[B]**2/[SIN[3.*B]*SIN[2.*B]]]**4*SI[J]
      JK = 0
      DO 25 I=1,NF
      DO 25 J = 1,16
      JK = JK+1
   25 PR[JK] = SI[I]*PR[JK]
      RETURN
      END
```

```
      SUBPROGRAM NPUT

XSD   OPD 010000000
$NPUT PZE
      BRM 201SYS
      XSD IDATA
      XSD ICNT
      XSD KEY
      XSD NSKIP
      BRM 202SYS
      STX HOLDX
      LDX JUMP
      EAX CNVRT
      STX 0200
      CLB
      STB *KEY
      LDA *ICNT
      LSH 00001
      STA ITEMP
      CNA
      STA RESET
      LDA IDATA
      ADD N1
      LDX N4
SET   STA LOC+4,2
      ADD ITEMP
      BRX SET
      LDA ONE
      STA NKEY
      STA INDEX
      LDA *ICNT
      SUB ONE
      STA ICNT2
      STA I
      LDX HOLDX
      EOM 020002
      BRR NPUT
CNVRT PZE
      STA HOLDA
      MIN INDEX
      LDA INDEX
      SKG *NSKIP
      BRU GOBAK+2
      STB HOLDB
      STX HOLDX
      LDA ONE
      STA INDEX
      LDX N4
      EOM 030070
      POT ZERO
LOOP  SKS 030000
```

```
        BRU $-1
        EOM 030060
        PIN ITEMP
        EOM 030001,2
        MIN LOC+4,2
        LDA ITEMP
        RSH 0014
        STA *LOC+4,2
        BRX LOOP
        SKR I
        BRU GOBAK
        LDA ICNT2
        STA I
        MIN *KEY
        LDA NKEY
        CNA
        STA NKEY
        SKA PLUS
        BRU GOBAK
        LDA RESET
        ADM LOC
        ADM LOC+1
        ADM LOC+2
        ADM LOC+3
GOBAK   LDX HOLDX
        LDB HOLDB
        LDA HOLDA
        BRU *CNVRT
        HLT 235SYS
IDATA   RES 2
ICNT    RES 2
KEY     RES 2
NSKIP   RES 2
NKEY    RES 2
ICNT2   RES 1
ITEMP   RES 1
LOC     RES 4
INDEX   RES 1
HOLDX   RES 1
HOLDA   RES 1
HOLDB   RES 1
I       RES 1
RESET   RES 1
N4      DATA -4
N1      DATA -1
ZERO    DATA 0
ONE     DATA 1
JUMP    DATA 04300000
PLUS    DATA 040000000
        END
```

APPENDIX B

Computer Program Used for Determining Amplitude Distributions

A listing of the program used to determine amplitude distributions is included in this appendix. The sub-program "N PUT" is used to digitize the data before the amplitude distribution analysis is made. The execution time required for this program allows a sampling rate of up to 125 samples per second to be used for each of the four channels.

The program was written to divide the total signal excursion into 100 intervals. Scale factors are entered in the computer under control of the main program. These scale factors allow greater utilization of the program because of the different levels of variations encountered during the data taking process. Also amplitude scale factors for each of the four channels are inserted into the computer under control of the main program.

```
    PROGRAM FOR AMPLITUDE DISTRIBUTIONS
    DIMENSION AD[ 5,-60/60 ], IDATA[ 40,4 ],D[4],A[4],S[4],FM[4],AVE[4],T[4],SM[4]
100 FORMAT [ 10F8.3 ]
101 FORMAT [//$       ΔN      AD1      AD2      AD3      AD4       ΔN      AD1$
   1$      AD2      AD3      AD4$/]
102 FORMAT [ 8F10.4 ]
103 FORMAT [$ REDUCE SAMPLING RATE$]
104 FORMAT [$ ACCEPT TOTAL NO. OF DATA POINTS, NSKIP, SCALE FACTOR B$]
105 FORMAT [ 2I20,F10.5]
106 FORMAT [$START DATA$]
107 FORMAT [ 4F20.10 ]
108 FORMAT [$ACCEPT A[1] THRU A[4]$]
109 FORMAT[//$        FM1        SM1        FM2        SM2        FM3        SM3$
    1$        FM4        SM4$/]
    TYPE 104
    ACCEPT 105, NT,NSKIP,B
    TYPE 108
    ACCEPT 107, [ A[I], I = 1,4 ]
    DO 35 J = 1,4
    SM[J]=0.0
    S[J] = 0.0
    AVE[J]=0.00
    T[J]=0.0
    FM[J] = 0.0
 35 A[J] = A[J]*B/[204.7*5.]
    NTH = NT/20
    DO 6 J=-60,60
    DO 6 I = 2,5
  6 AD[I,J] = 0.0
    JCOUNT = 1
    COUNT = 0.0
    TYPE 106
    PAUSE
    CALL NPUT[IDATA,20,KEY,NSKIP]
    DO 15 K=1,NTH
  3 IF[KEY -JCOUNT] 3,4,5
  5 TYPE 103
  4 JCOUNT = JCOUNT + 1
    IS = [K/2]*2-K
    IC = 20*IS
    IL = 21+IC
    IH= 40+ IC
    DO 15 I = IL,IH
    COUNT=COUNT + 1.0
    DO 15 J= 1,4
    JK=J+1
    D[J]=IDATA[I,J]
    D[J] = D[J]*A[J]
    T[J]=T[J] +D[J]
    AVE[J]=T[J]/COUNT
    D[J]=D[J] - AVE[J]
    JN=D[J]
 15 AD[JK,JN]=AD[JK,JN] +1.0
```

```
    DO 41 I=-50,50
    C=I
    DO 41 J=1,4
    JK=J+1
    SM[J]=SM[J] + C*C*AD[JK,I]
 41 FM[J]=FM[J] + C*AD[JK,I]
    DO 51 I= -50,50
    DO 51 J=1,4
    JK=J+1
    M=FM[J]/COUNT
    N=I-M
    S[J] = S[J] + AD[JK,N]
 51 AD[JK,N]= S[J]*100./COUNT
    DO 61 I=-60,60
    E=I
 61 AD[1,I]=E/B
    DO 71 J=1,4
    GM=FM[J]/COUNT
    TM=SM[J]/COUNT
     SM[J]=[TM -GM*GM]/[B*B]
 71 FM[J]=GM/B
121 FORMAT[/$TAPE NUMBER    SAMPLING RATE    ALIAS FILTER    SAMPLE $
   1$ LENGTH MIN    DATE$]
122 FORMAT[$                                                        $]
111 FORMAT[$ACCEPT TAPE NO.,RATE,ALIAS FILTER,SAMPLE LENGTH,DATE$]
    TYPE 111
    ACCEPT 122
    TYPE 121
    TYPE 122
    PUNCH TAPE 121
    PUNCH TAPE 122
    PUNCH TAPE 109
    PUNCH TAPE 102, [FM[J],SM[J],J=1,4]
    PUNCH TAPE 101
    PUNCH TAPE 100,[[[ AD[I,J], I=1,5],[ AD[I,J+50], I=1,5 ], J= -50,0 ]]
    CALL EXIT
    END
```

APPENDIX C

Relative Response of a Refractometer Cavity

The resonant frequency of an electromagnetic cavity varies inversely with the square root of the permittivity of the medium inside the cavity with a constant permeability.

The electric field in the r direction (based on a cylindrical coordinate system) for the cavities used in this experiment can be expressed as

$$\bar{E}_o = \frac{V}{r \ell n (\frac{r_b}{r_a})} \sin(\frac{\pi z}{2L}) \bar{a}_r , \qquad \text{(C-1)}$$

where

- V is the voltage difference between the inner rod of radius r_a and outer cylinder of radius r_b
- r is the radial distance from the cavity axis
- L is the length of the cavity
- z is the distance along the cavity axis toward the open circuited end of the cavity
- $\bar{a}_r$ is the unit vector in the r direction.

For changes in permittivity only, first order perturbation theory shows that the change in resonant frequency, $\Delta\omega$, of a cavity is given by

$$\Delta\omega = -\frac{\omega_o}{4U} \int_V \Delta\epsilon \, \bar{E}_o^* \cdot \bar{E} \, dV , \qquad \text{(C-2)}$$

where ω_o is the resonant frequency of the cavity corresponding to ϵ_o (permittivity of free space)

$\Delta\epsilon$ is the change in permittivity

$\bar{E}_o^*$ is the complex conjugate of the electric field associated with ϵ_o

$\bar{E}$ is the electric field in the perturbed region of the cavity

U is the total average energy stored in the cavity.

The total average energy stored in the cavity is twice the average energy stored in the electric field, U_e, where

$$U_e = \frac{\epsilon_o}{2} \int_V \bar{E}_o^* \cdot \bar{E}_o \, dV, \tag{C-3}$$

and

$$U = 2U_e = \epsilon_o \int_V \bar{E}_o^* \cdot \bar{E}_o \, dV. \tag{C-4}$$

After substitution of the values for the electric field and the limits of integration, equation (C-4) becomes

$$U = \epsilon_o \int_0^L \int_0^{2\pi} \int_{r_a}^{r_b} \left| \frac{V}{r \ln(\frac{r_b}{r_a})} \right|^2 \sin^2(\frac{\pi z}{2L}) \, r \, dr \, d\theta \, dz. \tag{C-5}$$

Integration of equation (C-5) for the total average stored energy gives

$$U = \frac{\pi \epsilon_o V^2 L}{\ln(\frac{r_b}{r_a})}. \tag{C-6}$$

The dielectric constant, K (relative to free space), is related to refractive index, n, by

$$K = n^2. \tag{C-7}$$

For small changes in refractive index the dielectric constant can be related to these changes as

$$\begin{aligned} K - 1 &= (n + 1)(n - 1), \\ &= 2(n - 1). \end{aligned} \tag{C-8}$$

Equation (C-8) can be expressed as

$$K - 1 = 2N', \tag{C-9}$$

where

$$N' = n - 1, \tag{C-10}$$

the change in refractive index.

The change in permittivity of the perturbed medium with permittivity ϵ_1 can be expressed as

$$\Delta\epsilon = \dot{\epsilon}_1 - \epsilon_o = K\epsilon_o - \epsilon_o = \epsilon_o(K - 1). \tag{C-11}$$

Equation (C-11) becomes

$$\Delta\epsilon = 2\epsilon_o N' \tag{C-12}$$

after substituting equation (C-9) for K - 1.

In order to determine the response of the cavity as a function of wavenumber k, the change in refractive index is assumed to have the following form:

$$N' = A \sin(kz + \alpha), \tag{C-13}$$

where A is the amplitude of the variation

k is the wavenumber of the variation ($k = \frac{2\pi}{\lambda}$, where λ is the wavelength of the variation)

α is the phase angle associated with the variation.

The change in permittivity can be expressed as

$$\Delta\epsilon = 2\epsilon_o A \sin(kz + \alpha). \tag{C-14}$$

By substituting equation (C-14) into equation (C-2), changes in $\Delta\omega$ can be expressed as

$$\Delta\omega(k, \alpha) = -\frac{\omega_o}{4U} \int_V 2\epsilon_o A \sin(kz + \alpha)\, \bar{E}_o^* \cdot \bar{E}\, dv. \tag{C-15}$$

Assuming that the perturbation is small and that the electric field in the perturbed region is equal to the electric field in the unperturbed region, equation (C-15) becomes

$$\Delta\omega(k, \alpha) = -\frac{\omega_o 2\epsilon_o A}{4U}\left[\frac{V}{\ell n(\frac{r_b}{r_a})}\right]^2 \int_o^L \int_o^{2\pi} \int_{r_a}^{r_b} \sin(kz + \alpha) \sin^2(\frac{\pi z}{2L}) \frac{dr}{r} d\theta dz. \tag{C-16}$$

Integration of equation (C-16) with respect to dr and $d\theta$ gives

$$\Delta\omega(k, \alpha) = -\frac{\omega_o 2\epsilon_o A V^2 2\pi}{4U\, \ell n(\frac{r_b}{r_a})} \int_o^L \sin(kz + \alpha) \sin^2(\frac{\pi z}{2L})\, dz. \tag{C-17}$$

After substituting in the value for U, equation (C-17) becomes

$$\Delta\omega(k, a) = -\frac{\omega_o A}{L} \int_o^L \sin(kz + a) \sin^2(\frac{\pi z}{2L})\, dz. \qquad \text{(C-18)}$$

Integration of equation (C-18) gives

$$\Delta\omega(k, a) = -\omega_o A \left\{ \sin a \sin(kL) \left[\frac{1}{kL} + \frac{kL}{(kL)^2 - \pi^2} \right] \right.$$

$$\left. + \cos a \left[\frac{(1 - \cos(kL))}{kL} - \frac{kL(1 + \cos(kL))}{(kL)^2 - \pi^2} \right] \right\}. \qquad \text{(C-19)}$$

The maximum response occurs when $k = 0$ and $a = \frac{\pi}{2}$. This value of $\Delta\omega(0, \frac{\pi}{2})$ will be used as a reference for the relative response.

The response of the cavity $H_c(k, a)$ can be expressed as

$$H_c(k, a) = \frac{\Delta\omega(k, a)}{\Delta\omega(0, \frac{\pi}{2})} = \sin a\, I(k) + \cos a\, Q(k), \qquad \text{(C-20)}$$

where

$$I(k) = \sin(kL) \left[\frac{1}{kL} + \frac{kL}{(kL)^2 - \pi^2} \right], \qquad \text{(C-21)}$$

and

$$Q(k) = \frac{1 - \cos(kL)}{kL} - \frac{kL(1 + \cos kL)}{(kL)^2 - \pi^2}. \qquad \text{(C-22)}$$

Equation (C-20) can be expressed in terms of amplitude and phase components as

$$H_c(k, a) = R(k) \sin(a + \beta), \qquad \text{(C-23)}$$

where

$$R(k) = \left\{ [I(k)]^2 + [Q(k)]^2 \right\}^{\frac{1}{2}} \tag{C-24}$$

and

$$\beta = \tan^{-1}\left[\frac{Q(k)}{I(k)}\right]. \tag{C-25}$$

The term R(k) is the amplitude component of the cavity response. Since both spectra and structure function calculations depend on the square of the amplitude component, the relative response, $H_r(k)$, will be expressed by

$$H_r(k) = [R(k)]^2. \tag{C-26}$$

The relative response of the cavity as given by equation (C-26) is plotted in Fig. C-1 as a function of wavenumber k. At the cavity wavenumber, the relative response is approximately 0.2 times the relative response at zero wavenumber.

From this discussion it is apparent that the sampling cavity greatly influences the measured spectra and structure functions for wavenumbers comparable to and greater than the cavity wavenumber.

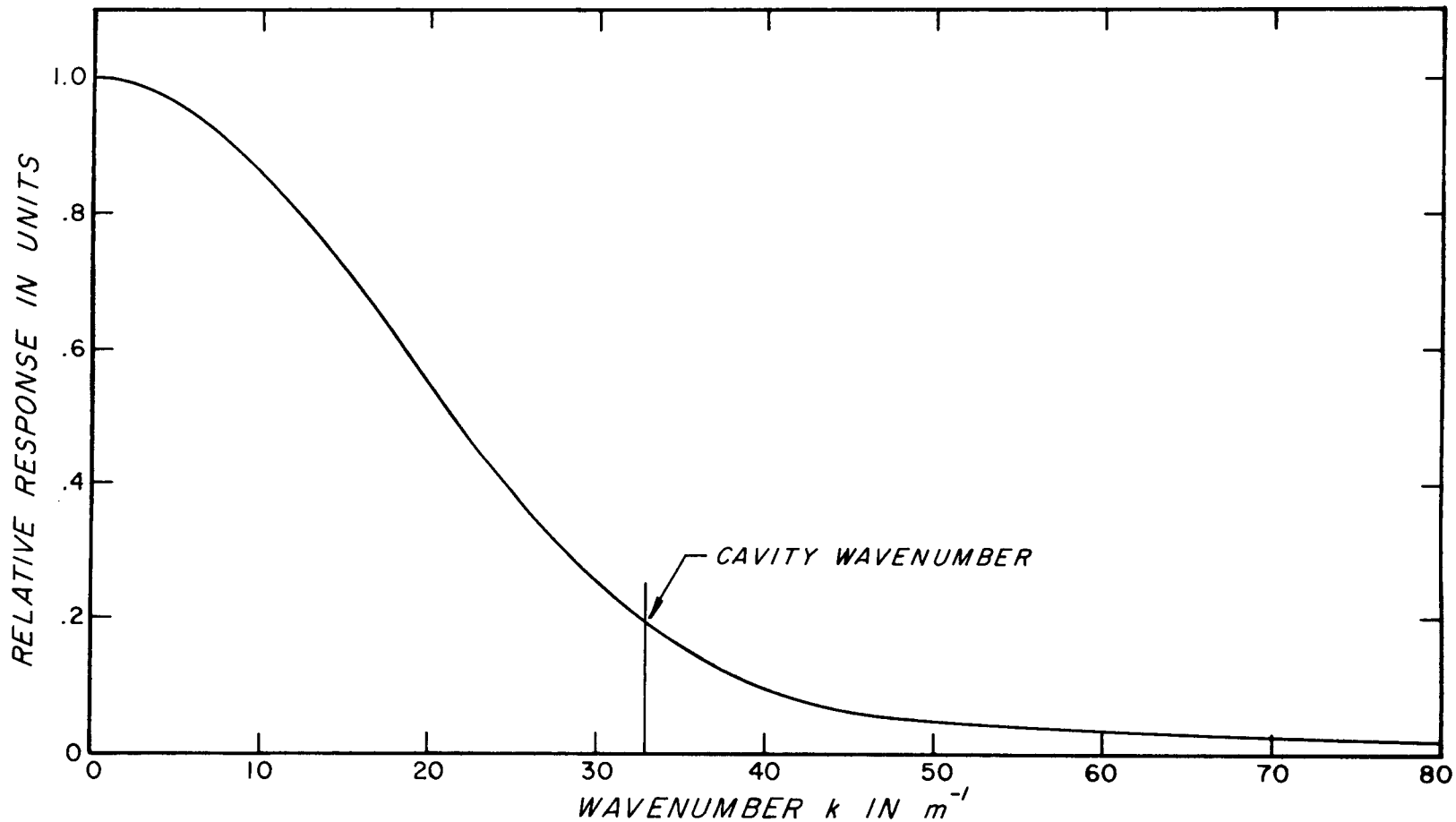

Figure C-1. Response Curve of a 0.75/4 Meter Coaxial Cavity

BIBLIOGRAPHY

Anderson, T. W., (1958), An Introduction to Multivariate Statistical Analysis, John Wiley & Sons, New York, New York.

Batchelor, G. K., (1956), The Theory of Homogeneous Turbulence, Cambridge University Press, London, England.

Deam, A. P., (1962), "Radiosonde for Atmospheric Refractive Index Measurements," Review of Scientific Instruments, Volume 33, Number 4, April.

Debye, P., (1929), Polar Molecules, Dover Publications, New York, New York.

Du Castel, F., (1966), Tropospheric Radiowave Propagation Beyond the Horizon, Pergamon Press, New York, New York.

EERL, (1960), "Operating Manual, MX-2718(XH-1) AMQ Refractometer," Electrical Engineering Research Laboratory, The University of Texas, Austin, Texas, Contract AF 33(600)-40545.

Eklund, F., (1965), Progress in Radio Science, 1960-1963, Volume II, Radio and Troposphere, edited by F. Du Castel, Elsevier Publishing Company, Amsterdam, London, New York.

Gossard, E. E., (1960), "Power Sepctra of Temperature, Humidity, and Refractive Index from Aircraft and Tethered Balloon Measurements," Institute of Radio Engineers Transaction AP-8.

Lane, J. A., (1964), "Small-Scale Irregularities of the Radio Refractive Index of the Troposphere," Nature, Volume 204, Number 4957.

Meyer, H. K., (1963), "The Troposphere," Meteorological and Astronomical Influences on Radiowave Propagation, Proceedings of Papers read at the NATO Advanced Study Institute, Corfu, 1961, edited by B. Landmark, The MacMillan Company, New York, New York.

Norton, K. A., (1964), "Effects of Tropospheric Refraction in Earth-Space Links," Proceedings of the Second Tropospheric Refraction Effects Technical Review Meeting, The Mitre Corporation, ESD-TDR-64-103, Volume I, March.

Straiton, A. W., (1964), "Measurement of the Radio Refractive Index of the Atmosphere," Advances in Radio Research, Volume I, edited by J. A. Saxton, Academic Press, New York, New York.

Straiton, A. W., Deam, A. P., Walker, G. B., (1962), "Spectra of Radio Refractive Index Between Ground Level and 5000 Feet Above Ground," Institute of Radio Engineers Transaction AP-10, Number 6, November.

Tatarski, V. I., (1961), Wave Propagation in a Turbulent Medium, (Translated by R. A. Silverman), McGraw-Hill Book Company, Inc., New York, New York.

Walker, G. B., (1960), "Single and Dual Cavity Measurements of Ground and Airborne Index of Refraction Fluctuations at 400 Mcps," Electrical Engineering Research Laboratory, The University of Texas, Report Number 6-38, Contract AF19(604)-2249.

ADDENDUM

Part of the material in this report was submitted for publication as a paper in Radio Science. The comments of one of the reviewers in accepting the paper for publication indicate that a theoretical treatment was incorrectly applied.

The paper was concerned with the filtering action on refractive index spectra at a point in space caused by the use of differences in the refractive index between two points.

In this report, two theoretical models of filter functions associated with difference measurements were suggested to provide a background against which measured difference data could be compared.

One of these models was for the case of a steady wind blowing in the direction of the line between the refractometer and represented an extreme in stability.

The second model was for the case of random wind direction. For this case, the three-dimensional correlation utilized by Tatarski [p. 14] was used to obtain a filter function as shown in equation (4-17), page 35. The reviewer for the paper containing this treatment pointed out that the use of the one-dimensional correlation function would reduce the second model to the same form as the first.

It is agreed that the second model incorrectly used the three-dimensional Tatarski function and that the general form of the random wind direction would be the same as for the constant wind in the direction

of the line between the refractometers. For a variable wind speed, however, the filter function would be the sum of a number of sine waves with different periods. This summation could take a wide variety of forms but the asymptote of the filter function would approach two for large frequencies. Curves similar to the model designated for the random wind direction case can be synthesized by summing the spectra associated with a range of wind speeds.

Thus, the model filter function shown in figures 5-11, 12, 14, 16, 24, 25, 26, 27, 28, 29, 30, 32, and 33 as $2[1 - \frac{\sin(2\pi fr/v)}{2\pi fr/v)}$ may be considered as an arbitrary example of a random wind speed situation.

Therefore, please disregard the treatment of the Tatarski model on pages 32, 34, 35, and 36.

Also, regard the reference curve in figures 5-11, 12, 14, 16, 24, 25, 26, 27, 28, 29, 30, 32, and 33 as a particular example of variable wind speed rather than variable wind direction.